The Evolution of Protoplanetary Disks Due to the Gravity of Protoplanets

Taku Takeuchi

Department of Astronomical Science, School of Mathematical and Physical Science,
The Graduate University for Advanced Studies

November, 30, 1995

ABSTRACT

We study the evolution of a protoplanetary disk due to tidal interactions between the disk itself and an embedded protoplanet. In particular, the following two processes are analyzed in detail: (1) Solutions for the propagation of density waves excited by the gravity of the protoplanet and their subsequent viscous damping are obtained within the context of the WKB approximation. The angular momentum carried by these waves and the torque exerted on the disk through the damping of the waves are obtained. (2) The evolution of the disk arising from angular momentum transfer by the density waves is simultaneously computed by solving the hydrodynamical equations in an infinitesimally thin and non-self-gravitating disk with a Keplerian rotation law.

The propagation distance (or damping length) of the waves can be quite large in disks with low viscosity. Indeed, we find that with a viscosity parameter, $\alpha \lesssim 10^{-3}$, $m = 2$ waves can reach the inner edge of the disk, whereas for $\alpha \lesssim 10^{-4}$, $m \sim (r\Omega/c)_p \sim 20$ waves can reach the inner edge as well. In disks with such small values for the viscosity, the gap size is determined by the damping length of the waves. The gap size becomes wider as the disk viscosity is decreased. When the viscosity becomes small enough to allow the waves to propagate to the inner region near the stellar surface, the removal of the inner disk ensues. We find that a Jupiter mass protoplanet facilitates the removal of the inner disk if $\alpha \lesssim 3 \times 10^{-4}$, and that the time scale for this depletion is 10^5 years. Furthermore, inner disk depletion can be detected from the infrared spectrum of T Tauri stars surrounded by protoplanetary disks. We determine the conditions for the gap formation in terms of relations between the masses of the protoplanets and the properties of the protoplanetary disks.

We apply our results to the gap sizes derived from recent observations of the disks around the pre-main-sequence binary stars, GW Ori and GG Tau. We infer that $\alpha \sim 10^{-2}$ in the disks around GW Ori and GG Tau.

Contents

1 Introduction **1**

1.1 Purpose of this work 1

1.2 Tidal interaction between the protoplanet and the protoplanetary disk . . . 3

1.3 Observational evidences for the gap formation 9

2 Formulation and numerical method **12**

2.1 Basic equations 12

2.2 Numerical method 16

2.3 Boundary condition 17

2.4 Disk model 19

3 Results **21**

3.1 Estimation of gap size 21

3.2 Protoplanet's torque 26

3.3 Gap size 32

3.4 Effects of orbital migration 42

3.5 Calculation for various models 46

4 Application **69**

4.1 Spectral evolution of the protoplanetary disks 69

4.2 Application for binary T Tauri stars 76

4.2.1 GW Ori 76

4.2.2 GG Tau 78

4.3 Application for proto-Jupiter 79

5 Discussion **81**

5.1 Waves in the disk with finite thickness 81

5.1.1 Unperturbed disk 81

5.1.2 Perturbation equations 83

5.1.3 Solution for vertical direction 85

5.1.4 WKB solution for radial direction 87

5.1.5 Angular momentum flux 89

5.1.6 Wave refraction toward vertical direction 95

5.2 Effects of the self-gravity of the protoplanetary disks 96

6 Summary **98**

A Transport of angular momentum 100

Chapter 1

Introduction

1.1. Purpose of this work

Stars surrounded by planets are believed to arise from the gravitational collapse of molecular cloud cores (e.g. Shu, Adams & Lizano 1987). Because molecular cloud cores rotate slowly (Goodman et al. 1993), a flattened disk revolving about the central star should form naturally. The presence of circumstellar disks around pre-main-sequence stars has been confirmed by recent infrared observations (e.g. Adams, Lada & Shu 1987; Basri & Bertout 1993; Strom, Edwards & Skrutskie 1993), by radio observations (e.g. Beckwith & Sargent 1993; Kawabe et al. 1993; Hayashi, Ohashi & Miyama 1993; Dutrey, Guilloteau & Simon 1994; Sargent 1995; Saito et al. 1995) and by optical observations performed with the Hubble Space Telescope (O'Dell & Wen 1994). These disks are believed to be the precursors of planetary systems, and are thus called protoplanetary disks.

The theory of planet formation in protoplanetary disks has long been an active field of investigation (see review by Hayashi, Nakazawa & Nakagawa 1985; Lissauer 1993). The theory assumes a protoplanetary disk with a mass of $0.01 - 0.02 M_{\odot}$ as an initial state, and argues that planets grow via the accumulation of small bodies known as planetesimals. Although the theory successfully explains some of the physical properties of the solar system (e.g. the enhancement of the condensable material in the planets) there remain several

unresolved problems.

One of these unresolved issues concerns the mechanism of dissipation of the residual gas; the removal of the gas from the protoplanetary disk after the planet formation is needed to make the present solar system with its highly vacant interplanetary space. Photo-evaporation of the gas by the strong UV flux of a young central star was proposed as a possible mechanism(Hayashi, Nakazawa & Nakagawa 1985). However, recent calculation by Shu, Johnstone & Hollenbach (1993) showed that only the outer part of the protoplanetary disk can be dissipated through photo-evaporation.

The tidal effect of protoplanets embedded in the disk has also been suggested as a relevant mechanism for gas evacuation (Larson 1989) and has been investigated by Lin & Papaloizou (1986a, b) and Artymowicz & Lubow (1994). These calculations suggested that the tidal effect of the protoplanets is not an effective agent in eliciting the gas removal. However, these authors did not include the effect of the propagation of density waves excited by the gravity of the protoplanet, which lead them to underestimate the size of the region where the structure of the disk is changed by the protoplanet's gravity. In the calculations of Lin & Papaloizou (1986a), the effect of wave propagation was included, but in that case, attention was focused on the evolution of the disk within a dynamical time scale, and hence the long term evolution, i.e. longer than several hundred rotation periods, was not studied. It is therefore necessary to investigate how wave propagation affects the long term evolution of the disk. This is the main purpose of this thesis.

The evolution of the protoplanetary disk due to the protoplanet's gravity is also important in the formation process of giant gaseous planets. Terrestrial type planets and the cores of giant planets are formed via the accumulation of planetesimals. When the mass of a protoplanet exceeds some critical value ($\sim$ 10 Earth mass), the gas around the protoplanet begins to contract to form the gas giant (Mizuno, Nakazawa & Hayashi 1978; Mizuno 1980). On the other hand, the tidal torques due to a Jovian mass planet will tend to evacuate gas from the orbital track, which tends to open up a gap (Cameron 1979; Miki 1982; Lin

& Papaloizou 1979a,b). Consequently, gas accretion onto a protoplanet is a self-regulating process, i.e. after acquiring a critical mass for gap formation, a gap in the disk forms and quenches further growth (Sekiya, Miyama & Hayashi 1987, 1988; Lin & Papaloizou 1993).

The tidal interaction between the protoplanetary disk and the companions plays an important role, not only in planetary systems, but also in binary systems. More than half of T Tauri stars seem to have binary companions, and the observational evidence for disk evolution due to the effect of binary companions has been reported (Mathieu 1994). These subjects are also discussed in this thesis.

In summary, the major topic of this thesis concerns the evolution of a protoplanetary disk due to the companion's gravity. In particular the effect of the propagation of the density waves is studied in detail. The outline of the dissertation is as follows: We review the previous theoretical and observational work in the following sections of this chapter and discuss the nature of the unresolved problem. In chapter 2, we describe the basic equations that govern the evolution of the disk due to the wave propagation. Our numerical method for solving these equations is also described. In chapter 3, we present numerical results. The effect of the wave propagation is described in detail. In chapter 4, the applications of our results are presented. First, the spectral evolution of the protoplanetary disk is discussed. Second, we apply our results for the binary T Tauri stars and compare them with the observational results. Finally, applications for the formation process of the solar system are presented. In our work, the protoplanetary disk is assumed to be infinitesimally thin. The effect of finite thickness on the disk is discussed in chapter 5. We also discuss the self-gravity of the protoplanetary disk. Finally, we summarize our findings in chapter 6.

1.2. Tidal interaction between the protoplanet and the protoplanetary disk

The evolution of the protoplanetary disk under the protoplanet's gravity has been studied by many authors. They estimated the torque exerted on the disk by the protoplanet and investigated the evolution of the disk.

Goldreich & Tremaine (1979) studied the dynamics of the disk under the external potential (e.g. the potential of the protoplanet) using the perturbation theory and the WKB approximation. In the disk there are the special locations where the motion of the gas resonates with the external force (see e.g. Binney & Tremaine 1987). The gas whose angular velocity is commensurate with the pattern speed of the external potential always suffers the same force. This is called as the co-rotation resonance (CR). If the external force is the potential of the protoplanet with the circular orbit, the location of the CR coincides with the orbital radius of the protoplanet, r_p,

$$r_C = r_p. \tag{1.1}$$

The resonance also occurs on the gas whose frequency of the epicycle oscillation is commensurate with the frequency of the external force observed by the gas. This is called as the Lindblad resonances (LR). For the protoplanet with the circular orbit, the location of the LRs are given by [1]

$$r_L = \left(1 \pm \frac{1}{m}\right)^{2/3} r_p, \tag{1.2}$$

where m is the positive integer. For fixed m, there are two LRs; one locates outside the protoplanet's orbit (outer Lindblad resonances [OLR]) and the other locates inside it (inner Lindblad resonances [ILR]). Note that the distribution of the positions of the resonances are concentrated close to the protoplanet.

Since the effect of the external force is most effective at these resonances, Goldreich & Tremaine (1979) studied the dynamics of the gas near these resonances. They found that the density waves are excited at the LRs. If the self-gravity of the disk is negligible (this approximation is adequate for the protoplanetary disk with a mass of $\sim 0.01 M_\odot$), the waves excited at OLRs propagate outward and the waves excited at ILRs propagate inward, that is, the waves propagate away from the protoplanet. Further, they calculated the angular momentum carried by these waves and showed that the waves excited at OLR

[1] In this thesis, the upper and lower signs apply to the disk outside and inside the protoplanet, respectively.

have positive angular momentum, while the waves excited at ILR have negative angular momentum. When these waves damp through viscosity of the disk or the shock formation, the angular momentum which they have are deposited into the disk. Thus the disk material outside the protoplanet's orbit gains angular momentum and moves outward, while the disk material inside the orbit loses angular momentum and moves inward. This process of wave excitation and dissipation forms a gap around the protoplanet's orbit.

Goldreich & Tremaine (1980) calculated the angular momentum carried by the waves excited at LRs as a function of m, which is the order number of LRs (see eq.[1.2]). They found that the angular momentum is carried most effectively by the waves excited at LRs with $m \sim r_p\Omega_p/c$, where Ω_p is the angular velocity of the protoplanet and c is the sound speed in the disk (see also Artymowicz 1993a,b; Korycansky & Pollack 1993). Assuming that the waves damp immediately at LRs, they calculated the torque density exerted by the protoplanet on an annulus of unit radial width as,

$$T(r) = \pm\frac{32}{81}\{2K_0(2/3) + K_1(2/3)\}^2\frac{r\sigma(GM_p)^2}{\Omega_p^2}\frac{1}{(r-r_p)^4}, \tag{1.3}$$

where G is the gravitational constant, M_p is the mass of the protoplanet, σ is the surface density of the disk, and K_0 and K_1 are modified Bessel functions. Note that this expression is valid only for $|r - r_p| \gtrsim c/\Omega$. For $|r - r_p| \to 0$, $T(r)$ should approach zero. This formula is also derived independently by Lin & Papaloizou (1979a).

Equation (1.3) shows that the torque density rapidly decreases with the distance from the protoplanet. This is because the density of the positions of the LRs decreases with the distance(eq. [1.2]). Thus, when a gap is formed and the excitation of waves at LRs close to the protoplanet is suppressed, the torque is quite reduced as the gap width increases. On the other hand, viscous diffusion of the gas works to close the gap. Thus, the gap width is determined by the balance between the protoplanet's torque and the viscous diffusion as illustrated in Figure 1-1*a* (Lin & Papaloizou 1979a, 1986a, b; Papaloizou & Lin 1984). Since the torque is a rapidly decreasing function of the gap width, the gap width derived by this balance is rather small, i.e. the disk gas could not be dissipated completely by this

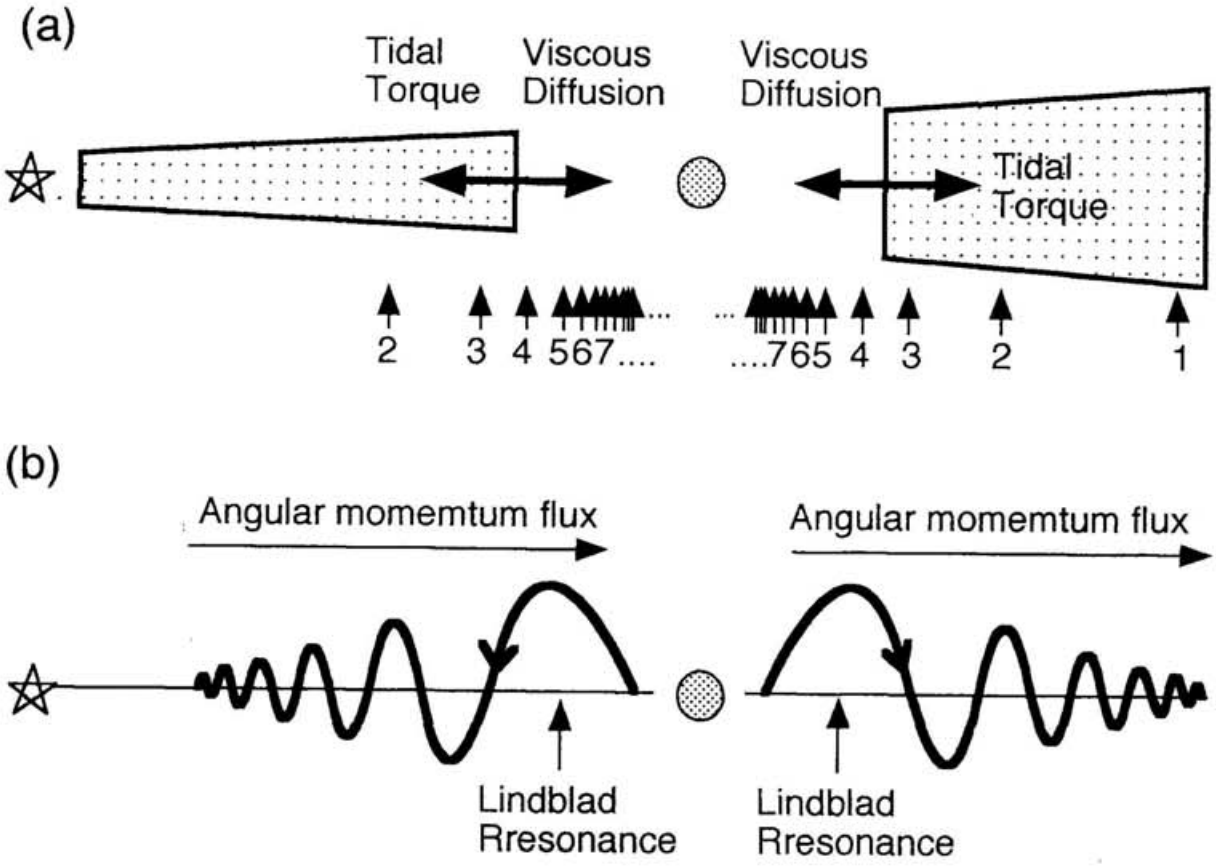

Fig. 1-1.— (a) A schematic illustration of the gap formation in the local wave dissipation model. Arrows indicate the positions of LRs with the appropriately labeled mode number, m. The position of the $m = 1$ inner LR ($r_L = 0$) is not shown in this figure. The tidal torque exerted by the protoplanet leads to the broadening of the gap. The viscous diffusion leads to the filling of the gap and therefore a reduction in the gap width. The gap size is determined by the balance between the tidal torque and the viscous diffusion. (b) A schematic illustration of wave propagation in the disk. Waves are excited at the LRs. These waves propagate away from the protoplanet's orbit, and are dissipated by the viscous stress. The angular momentum is carried by the waves, and deposited into the gas in the disk through the wave dissipation. The protoplanet's gravity indirectly affects the evolution of those regions of the disk where the waves are dissipated.

mechanism. In fact, the protoplanet can open a gap at most from the farthest ILR to the farthest OLR, i.e. from $m = 2$ ILR ($r_L = 0.63r_p$) to $m = 1$ OLR ($r_L = 1.59r_p$). [2]

Artymowicz & Lubow (1994) argued that a protoplanet which has eccentric orbit can open a wider gap. If the orbit of the protoplanet is eccentric, then there are additional LRs corresponding to the epicycle motion of the protoplanet, and some of them locate farther from the protoplanet than $r = 0.63r_p$ or $r = 1.59r_p$. However, these LRs are not effective unless the eccentricity is near unity. Thus, they argued that the wider gap than $0.63 - 1.59r_p$ is formed only if the eccentricity of the protoplanet is near unity or the viscosity of the disk is quite small. However, the eccentricity of the protoplanet's orbit is found to become nearly zero during the growth of the protoplanet via the accumulation of planetesimals (Ida 1990; Ida & Makino 1993). Hence, the effect of LRs due to the eccentricity would be very small.

In the above discussion, excited waves are assumed to damp immediately at LRs. However, if the viscosity of the disk is small enough, waves can propagate throughout the disk. Lin & Papaloizou (1986a) showed that the waves can reach the boundary between the disk and the central star if the viscosity is as small as $\alpha \equiv \nu\Omega/c^2 \sim 10^{-3}$, where ν is kinetic viscosity. If the disk is convective, α can be as large as 10^{-2} (Ruden & Lin 1986). However, the convection ceases at the late stage of the evolution of the protoplanetary disk, and small value of α are expected (Watanabe, Nakagawa & Nakazawa 1990; Ruden & Pollack 1991). The protoplanet affects the structure of the disk at the location where the waves are dissipated. Thus, if the waves propagate throughout the disk and the distribution of the angular momentum is rearranged in the whole disk, then the evolution of the disk occurs in the wider region than that derived from the above discussion (see Fig. 1-1*b*).

Thus, in order to know the evolution of the disk, we have to answer two questions. First, how far away do waves propagate and which part of the disk do these waves dissipate in? Second, how does the disk evolve under the angular momentum transfer due to the wave propagation? We will solve these problems in this thesis. The effect of the wave propagation

[2]The $m = 1$ ILR locates at $r_L = 0$ and is not effective to open a gap by the protoplanet.

on the gap formation has been suggested as a mechanism for inducing a wide gap in the Cassini division in Saturn's rings by Goldreich & Tremaine (1978).

Goldreich & Tremaine (1979) also calculated the torque exerted on the CR. Ward (1989) and Korycansky & Pollack (1993) improved their formula. The torque due to the CR is weaker than the torque due to the mth-order LRs by a factor $1/m$. Thus, the effect of the CR is negligible, because the most effective LR is with $m \sim r_p\Omega_p/c \gg 1$. Further, the disturbance at CR cannot propagate as density waves and dissipates in the narrow region around the CR, i.e. the protoplanet's orbit. Therefore, the torque exerted on the CR cannot contribute to making a wide gap.

Next, we consider the evolution of the orbit of the protoplanet as a result of the tidal interaction with the protoplanetary disk. The protoplanet exerts negative torque on the disk inside its orbit, while it exerts positive torque on the disk outside its orbit. Thus, it gains angular momentum from the disk inside its orbit and deposits angular momentum in the disk outside its orbit. The absolute values of these positive and negative torques are in general different from each other because of the asymmetry of the disk properties with regard to the orbital radius of the protoplanet. This difference causes the migration of the protoplanet. Ward (1986) argued that the asymmetry in the locations of LRs, surface density, pressure gradient and temperature profile causes the migration of the protoplanet. He calculated the time scale of the decay of the orbit and showed that the decay time for a protoplanet of an Earth mass is of order 10^5 years. This time scale is quite short in comparison with the time scale of the growth of the protoplanet (Nakagawa, Hayashi & Nakazawa 1983). Thus, protoplanets move substantial distance during their formation.

However, Lin & Papaloizou (1986b) pointed out that the gap formation suppresses the orbital migration of the protoplanet. Once a gap is formed, the torque between the protoplanet and the disk becomes small to balance with the viscous diffusion of the gas. Further, the protoplanet moves in the gap to the location where the inner torque and the outer torque balance, and it is fixed there after that. Hence, the time scale of the orbital

decay becomes about the time scale of the viscous diffusion after the gap formation.

On the other hand, Hourigan & Ward (1984) and Ward & Hourigan (1989) pointed out that rapid migration of the protoplanet suppresses the gap formation. If the protoplanet moves a distance larger than the size of the gap before the completion of the gap formation, then it escapes from the gap, and therefore the gap formation would be inhibited. They assumed that the width of the gap is comparable with the disk thickness, and estimated the condition for the gap formation against the escape of the protoplanet from the gap. However, if the wave propagation contributes to making a wider gap, their estimation should be modified. This effect will also be investigated in this thesis.

1.3. Observational evidences for the gap formation

We have not observed directly extra-solar planets up to now. Thus, we have no observational evidence for the evolution due to the protoplanet's gravity. However, an insight into the tidal interaction could be obtained from the observations of the protoplanetary disks around young binary stars. Recent surveys of young stars revealed that about half of T Tauri stars have binary companions (Simon et al. 1992, 1995; Ghez, Neugebauer & Matthews 1993; Leinert et al. 1993) and the interaction between the protoplanetary disk and binary companions is investigated by radio and infrared observations.

The truncation of the disks by the companions is suggested from the observations of the millimeter-wave continuum (Beckwith et al. 1990; Simon et al. 1992, 1995; Jensen, Mathieu & Fuller 1994, 1996; Osterloh & Beckwith 1995); the T Tauri stars with companions show less flux than the single stars. The millimeter-wave continuum is considered to be emitted from the disk with radius of 100AU and the typical separation of binaries found by infrared surveys is also about 100AU. Thus, binary companions seem to deplete the disks on the scale length of their semimajor axis. The direct images of the protoplanetary disk around GG Tau are obtained by Dutrey, Guilloteau & Simon (1994) and Roddier et al. (1996) and show the inner hole with radius of 220AU, which is several times the separation of the binary

components.

Jensen, Mathieu & Fuller (1996) measured the flux of 800 μm continuum of 25 pre-main-sequence binary stars. Only the upper limits are obtained for most of the objects. They combined their observations with the 1300 μm continuum flux in the literature and compared with the flux expected from their theoretical model. In their theoretical model, they assumed that the disk around binary stars has a gap. They used the gap size derived by assuming that the waves damp immediately at LRs according to Artymowicz & Lubow (1994) and estimated the flux emerging from such the disk. The upper limits of the observed flux for binaries with separation of several tens of AU are not inconsistent with the theoretical model. However, for close binaries with separation of several AU, the upper limits are smaller than the expected values. This discrepancy for close binaries suggests that the gas is more depleted than the prediction by their theoretical model. The wider gap than their model may explain the observed upper limits for close binaries.

Some close binaries show the presence of a gap in the protoplanetary disks by the absence of near or mid-infrared flux which would normally have emerged from that region of the disk. Since the effective temperature of a protostellar disk decreases monotonically with the distance from the central star, the spectral energy distribution (SED) of disks with a physical gap is characterized by a dip at an appropriate wavelength. This type of SED has been observed in the continuum spectrum of a classical T Tauri star GW Ori (Mathieu, Adams, & Latham 1991). This system is a spectroscopic binary with a separation of 1.1 AU and eccentricity of 0.17 (Mathieu & Jensen 1995, private communication). The dip in the SED has been interpreted as due to the presence of a gap between disk radii 0.17 and 3.3AU. The derived size of the gap is rather large, and requires low viscosity. In fact, if we assume the waves damp immediately at LRs, then we can derive the Reynolds number of the disk as $R = 10^6 - 10^8$ for the circumbinary disk and $R \gtrsim 10^{11}$ for the circumprimary disk (see Figs. 3 and 5 in Artymowicz & Lubow 1994). The luminosity of the disk around GW Ori is estimated as $34 L_\odot$. When we assume that this luminosity is emitted by the disk accretion, then a large accretion rate ($\sim 5 \times 10^{-6} M_\odot$/year) is required (Mathieu, Adams &

Latham 1991). To supply such a large accretion of mass, the viscosity of the disk is required as $R \lesssim 10^3$, if the disk mass within 100AU is less than $1M_\odot$. Therefore, the values of R required by the gap size is too large compared with the value derived by the accretion rate. This discrepancy may be resolved if the wave propagation forms a wider gap in the disk with a large viscosity.

Another example of binaries showing the SED with a dip is DF Tau (Marsh & Mahoney 1993). The projected separation of the binary is 12AU, and the SED indicates a gap from 0.1AU to 17AU. The inner radius of the circumbinary disk is consistent with the theory assuming wave damping at LRs. However, it is difficult to explain the small radius of the circumstellar disk unless the binary orbit is very eccentric or waves propagate substantial distance in the disk.

Only three close binaries have been reported to have the SED indicating the gap; GW Ori, DF Tau and 162814-2427 (Mathieu 1994). The sample is too small to discuss the gap width statistically. Further, some binaries show no evidence for the gap in their SED. For example, the binary AK Sco, with a separation of 0.2AU, shows an excess in the near-infrared without the dip(Andersen et al. 1989). The depletion of the disk by the companion does not seem to have occurred in this system. The SEDs of more close binaries should be taken in order to confirm the gap formation.

To summarize, the observational evidences for the tidal interaction between the proto-planetary disk and the companions seem to be insufficient though they are accumulating. The gap size derived from the observation are somewhat wider than the gap size inferred from the previous theory. In this thesis we discuss the effect of the wave propagation on the size of the gap in the disks around the binary stars.

Chapter 2

Formulation and numerical method

In this chapter, we present the basic equations which govern the evolution of the disk. Next, we describe our numerical procedure to solve the equations. The basic physical processes operate in the following manner. A protoplanet excites density waves in the disk at the LRs. The waves propagate away from the protoplanet and carry angular momentum. As the waves are dissipated by the viscous stress, the excess (deficit) angular momentum is deposited into the disk material exterior (interior) to the orbit of the protoplanet. This exchange of angular momentum induces the evolution of the density structure of the disk and the orbit of the protoplanet.

2.1. Basic equations

In accordance with the minimum-mass nebula model, we assume that the disk mass is negligibly small compared with the mass of the central star, M. The temperature profiles of the protoplanetary disks derived by the infrared spectra (Adams, Lada & Shu 1988) show that the sound speed, c, is much smaller than the Keplerian velocity of the disk. Hence, the effect of pressure is small in comparison with the gravity of the central star. Under these circumstances, the protoplanetary disk can be approximated as being infinitesimally thin

and rotates around the central star with a Keplerian speed $\Omega = (GM/r^3)^{1/2}$ everywhere.

We assume the presence of a turbulent shear viscosity ν and the bulk viscosity ζ. For computational convenience, we adopt the standard α prescription for the viscosity (Shakura & Sunyaev 1973). As will be discussed in §5.1.1, the protoplanetary disk at the late stage could be considered as isothermal in the vertical direction. The convection as the source of the turbulent viscosity does not occur in such a disk. There are, however, some mechanism for the source of the turbulence. For example, the differential rotation of the protoplanetary disk might cause turbulence and induce the viscosity (Papaloizou & Pringle 1984; Balbus & Hawley 1991). The energy released through the dissipation of the waves could be the source of the turbulent viscosity. In the absence of viscous damping, density waves steepen into shock waves (Larson 1990). The energy dissipation rate of these non-linear waves would provided an effective viscosity with $\alpha \sim (c/r\Omega)^3$ in the disk with a gap (Savonije, Papaloizou & Lin 1994).

During the growth of the protoplanets their eccentricity and inclination damp via the dynamical friction of the planetesimals, and are nearly zero at the stage considered in this thesis (Ida 1990). Thus, we assume the orbit of the protoplanet to be circular in the plane of the disk.

The evolution of the surface density distribution of the protoplanetary disk is caused by the viscous diffusion and the tidal effect of the protoplanet. The time scale of the evolution of the disk is much longer than the revolutionary period of the protoplanet which induces the non-axisymmetric perturbations on the disk. Then, averaging over all azimuthal phases, the equations of the angular momentum conservation and continuity of mass are

$$2\pi r\sigma \left[\frac{\partial}{\partial t} + u\frac{\partial}{\partial r}\right](r^2\Omega) = 2\pi\frac{\partial}{\partial r}\left(r^3\sigma\nu\frac{d\Omega}{dr}\right) + T, \tag{2.1}$$

$$\frac{\partial}{\partial t}\sigma + \frac{1}{r}\frac{\partial}{\partial r}(\sigma u r) = 0, \tag{2.2}$$

where σ and u are the surface density and the radial velocity component of the disk, respectively. The first term of the right-hand side of equation (2.1) is the viscous torque

(Lynden-Bell & Pringle 1974) and the second term, $T(r)$, is the torque density exerted on an annulus of unit radial width in the disk by the protoplanet. Eliminating u from equations (2.1) and (2.2), and using a Keplerian rotation law, we obtain

$$\frac{\partial \sigma}{\partial t} = \frac{3}{r}\frac{\partial}{\partial r}\left[r^{1/2}\frac{\partial}{\partial r}\left(\nu\sigma r^{1/2}\right) - \frac{1}{3\pi(GM)^{1/2}}r^{1/2}T\right]. \tag{2.3}$$

The torque density, $T(r)$, is calculated using the linear density wave theory. A protoplanet excites waves at LRs in the disk. The position of the mth-order LR is given by

$$D(r) = \kappa^2 - m^2(\Omega - \Omega_p)^2 = 0, \tag{2.4}$$

where $\kappa(r)$ is epicycle frequency, and Ω_p is angular velocity of the protoplanet. For a Keplerian disk, $\kappa = \Omega$, and the positions of the LRs are given by equation (1.2). These waves transfer the angular momentum and the torque is exerted on the disk through their dissipation. Goldreich & Tremaine(1979, 1980) derived angular momentum flux carried by the waves excited at mth-order LR as

$$F_{m0} = m\pi^2 f_c \left\{\left|\frac{\sigma}{rdD/dr}\right|\left[r\frac{d\varphi_m}{dr} + \frac{2\Omega}{\Omega - \Omega_p}\varphi_m\right]^2\right\}_{r_L}, \tag{2.5}$$

Here the mth-order Fourier component of the protoplanet's potential, $\varphi_m(r)$, are expressed by the Laplace coefficients, $b^m_{1/2}$, as

$$\varphi_m(r) = -\frac{GM_p}{2r_p}(2 - \delta_{m,0})\left(b^m_{1/2}(r') - r'\delta_{m,1}\right), \tag{2.6}$$

$$b^m_{1/2}(r') = \frac{2}{\pi}\int_0^\pi \frac{\cos m\theta d\theta}{(1 - 2r'\cos\theta + r'^2)^{1/2}}, \tag{2.7}$$

where M_p is protoplanet's mass, r_p is the radius of the protoplanet's orbit, $r' = r/r_p$, and $\delta_{m,n}$ is the Kronecker delta function. In the derivation of the original form of the angular momentum flux by Goldreich & Tremaine(1979), they approximated that $m \ll (r\Omega/c)_p$, where the subscript "p" means a quantity evaluated at the protoplanet's position. For $m \gtrsim (r\Omega/c)_p$, the correction factor f_c in equation (2.5) is needed. Goldreich & Tremaine(1980) calculated f_c numerically and Artymowicz(1993) derived an approximate formula as

$$f_c = \frac{1}{H(1 + 4\xi^2)}\left[\frac{2HK_0(2H/3) + K_1(2H/3)}{2K_0(2/3) + K_1(2/3)}\right]^2, \tag{2.8}$$

where

$$\xi = m(c/r\Omega), \tag{2.9}$$

$$H = \sqrt{1+\xi^2}, \tag{2.10}$$

and K_0 and K_1 are modified Bessel functions. For $m \ll (r\Omega/c)_p$, $f_c \approx 1$, and for $m \gtrsim (r\Omega/c)_p$, f_c decreases exponentially with m. Therefore F_{m0} has its maximum value at $m \sim (r\Omega/c)_p$, i.e. the protoplanet excites waves with $m \sim (r\Omega/c)_p$ most effectively (Fig. 2-1).

These waves propagate away from the protoplanet and dissipate either through shock formation or the action of the viscosity. If the mass ratio between the protoplanet and the central star, $q = M_p/M$, is less than 10^{-3}, the amplitude of the excited waves is small and perturbations are linear at the resonance. Because the perturbations propagate as pressure waves, and the growth of their amplitude is slow(Ward 1986), the non-linear process of the shock formation would be negligible and the waves can be considered to damp only by viscosity. In the Appendix, the propagation and the dissipation of the waves are solved using the WKB approximation, and the angular momentum flux transferred by the waves is obtained as

$$F_m(r) = \begin{cases} F_{m0} \exp\left[-\int_{r_L}^{r} \left\{ \zeta + \left(\frac{4}{3} + \frac{\kappa^2}{m^2(\Omega-\Omega_p)^2} \right) \nu \right\} \frac{m(\Omega_p - \Omega)}{c^2} k dr' \right] & (r \geq r_{OL}, \\ & \quad r \leq r_{IL}) \\ 0 & (r_{IL} < r < r_{OL}), \end{cases} \tag{2.11}$$

where r_{OL} and r_{IL} are the positions of the outer and inner Lindblad resonances, respectively. The radial wave number $k(r)$ is

$$k(r) = \left(\frac{m^2(\Omega-\Omega_p)^2 - \kappa^2}{c^2} \right)^{1/2}. \tag{2.12}$$

The dissipation of the waves causes exertion of torque on the disk. The torque density exerted on an annulus of unit radial width in the disk is

$$T_m(r) = -\frac{dF_m}{dr}. \tag{2.13}$$

The total torque density is calculated by summing over the waves excited at all resonances, as

$$\begin{aligned} T(r) &= \sum_m T_m \\ &= -\sum_m \frac{dF_m}{dr}. \end{aligned} \tag{2.14}$$

The back reaction of the excitation of waves causes the orbital evolution of the protoplanet. The change of the orbital radius is calculated by the angular momentum transfer

$$\frac{d}{dt}(M_p r_p^2 \Omega_p) = -\int_{r_{in}}^{r_{out}} T dr, \tag{2.15}$$

or

$$\frac{dr_p}{dt} = -2\frac{1}{M_p}\left(\frac{r_p}{GM}\right)^{1/2} \int_{r_{in}}^{r_{out}} T dr. \tag{2.16}$$

2.2. Numerical method

Numerical calculations are performed to solve for the surface density evolution of the disk. We introduce dimensionless variables such that $t' = (\nu_0/r_0^2)t, \sigma' = \sigma/\sigma_0, r' = r/r_0$, and $\nu' = \nu/\nu_0$, where the quantities labeled with the subscript "0" are evaluated at the initial position of the protoplanet. The time is normalized by the viscous diffusion time scale. The non-dimensional version of equations (2.3) and (2.16) are

$$\frac{\partial \sigma'}{\partial t'} = \frac{3}{r'}\frac{\partial}{\partial r'}\left[r'^{1/2}\frac{\partial}{\partial r'}(\nu'\sigma' r'^{1/2}) - r'^{1/2} T'\right], \tag{2.17}$$

$$\frac{dr_p'}{dt'} = -\frac{6\pi r_0^2 \sigma_0}{M_p} r'^{1/2} \int_{r_{in}'}^{r_{out}'} T' dr', \tag{2.18}$$

where

$$T' = \frac{1}{3\pi r_0 \Omega_0 \nu_0 \sigma_0} T. \tag{2.19}$$

Above equations are solved numerically with an explicit finite difference method.

The torque density in equation (2.14) is summed up with $m = 1 - 200$ for the outer disk and $m = 2 - 200$ for the inner disk. The contribution from $m > 200$ is negligible. The $m = 1$

ILR, which locates on $r = 0$, can be important for interactions with binary companions with the mass comparable to the central star (Ostriker, Shu & Adams 1992). For interactions with the protoplanet, however, the effect of the $m = 1$ ILR is negligible.

In the summation of equation (2.14), the terms with $m \sim (r\Omega/c)_p \gg 1$ dominate. For $m \gg 1$ the Laplace coefficients and these derivatives can be approximated by modified Bessel functions(Goldreich & Tremaine 1980), as

$$b^m_{1/2}\Big|_{r_L} \approx \frac{2}{\pi} K_0(2/3), \tag{2.20}$$

$$\left.\frac{db^m_{1/2}}{dr'}\right|_{r_L} \approx \mp\frac{2m}{\pi} K_1(2/3). \tag{2.21}$$

The position of the LRs is approximated by $r_L \approx r_p$ for $m \gg 1$ (eq. [1.2]). Thus, variables can be evaluated at r_p except for σ, which is a rapidly varying function of r. We also approximate that $rdD/dr|_{r_L} \approx \mp 3m\Omega^2(r_L)$. We use above approximation in evaluating F_{m0}, because $m \gg 1$ terms dominate the torque. Then we obtain

$$F_{m0} = \frac{4}{3} m^2 f_c \sigma(r_L) \left(\frac{GM_p}{r_p \Omega_p}\right)^2 \left[2K_0(2/3) + K_1(2/3) - \frac{\pi}{2}\delta_{m,1}\{2 \mp 1\}\right]^2. \tag{2.22}$$

Figure 2-1 shows F_{m0} as a function of m for various values of the sound speed. The waves with $m \sim (r\Omega/c)_p$ carry the maximum angular momentum. As the sound speed c becomes smaller, the larger m waves, which are excited at LRs closer to the protoplanet, becomes effective, and hence more angular momentum are carried by these waves.

2.3. Boundary condition

To solve equations (2.17) and (2.18), we need boundary conditions at the inner and outer edges of the disk. First, we consider the boundary layer between the surface of the star and the disk. The central star rotates more slowly than the inner part of the disk which rotates at a Keplerian rate. In the boundary layer, the rotation of the disk is slowed down by the friction of the central star. Thus the angular velocity, Ω, which was increasing inwards, now decreases to the rate commensurate with the central star. There must be the critical

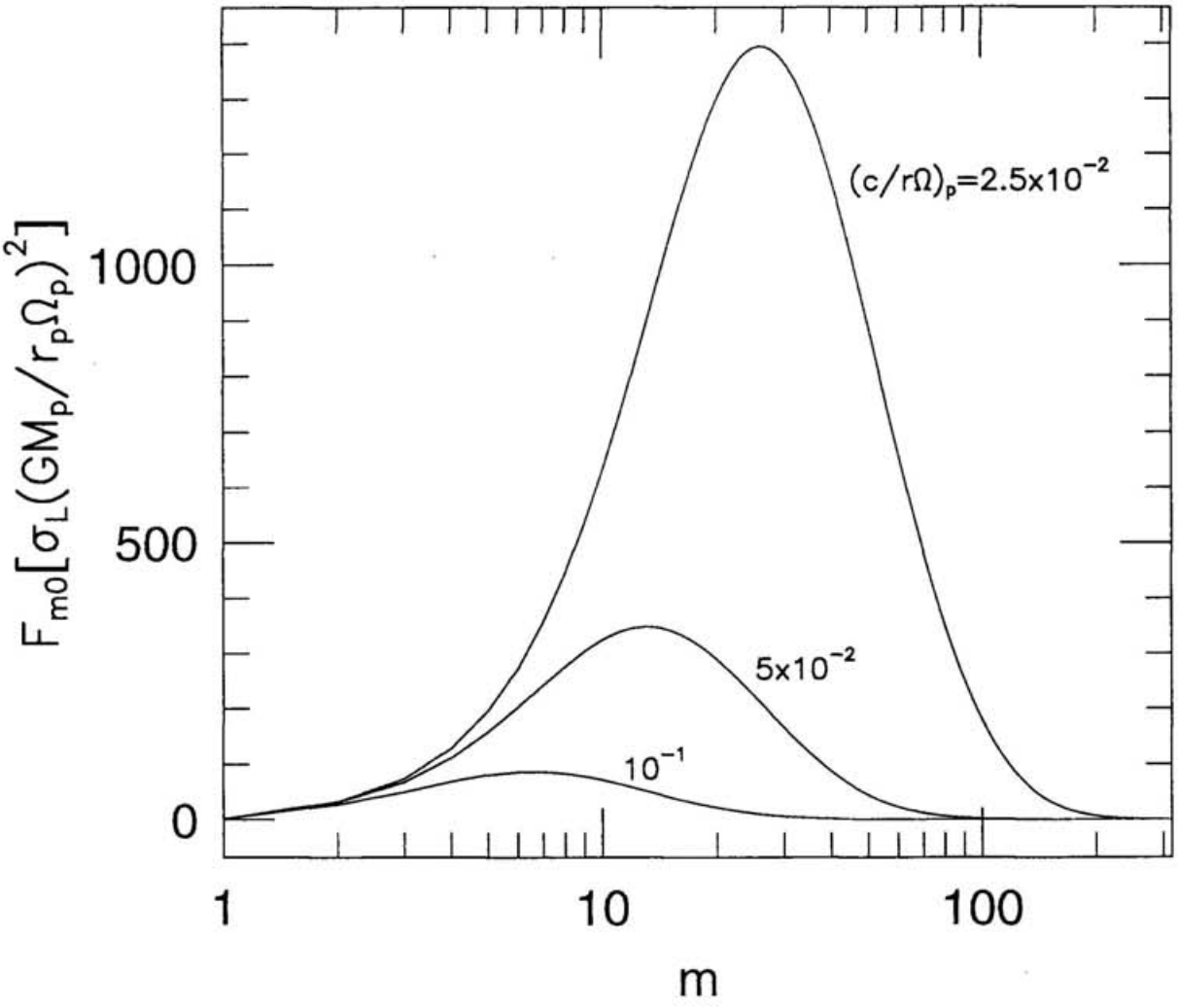

Fig. 2-1.— Angular momentum flux carried by waves excited at mth- order LRs in the disks with various sound speed.

point, r_c, where $d\Omega/dr = 0$, and the shear vanishes(Lynden-Bell & Pringle 1974). Hence, the inner boundary condition should be that there is no viscous torque at r_c. We have to solve the boundary layer to determine r_c. Instead of this, we use the simple boundary condition. We assume the Keplerian rotation law for the whole disk. The inner boundary condition is achieved by $\sigma = 0$ at the inner edge of the disk, r_{in}, rather than $d\Omega/dr = 0$ at r_c. This boundary condition assures that viscous torque vanishes at r_{in}. We checked the inner boundary condition using the analytic solution derived by Lynden-Bell & Pringle (1974). This analytic solution is derived with the boundary condition $d\Omega/dr = 0$ at $r_c = 0$. We found that the substituted inner boundary condition, $\sigma = 0$ at r_{in}, does not affect the global evolution of the disk in the numerical calculations.

We consider the stage after the formation of the protoplanetary disk has finished and the envelope from which the star and the disk was formed has dissipated. Thus, the outside of the disk is vacant, and the outer edge of the disk should be allowed to freely expand. We adopt a sufficient range in r in the numerical calculation to account for the freely expanding edge.

2.4. Disk model

The surface density profile is assumed to be a power law in r,

$$\sigma = \sigma_0 \left(\frac{r}{r_0}\right)^{-3/2}, \tag{2.23}$$

and is truncated at $r_{in} = 10^{-2} r_0$ and $r_{out} = 10 r_0$ initially. This surface density profile was derived by Hayashi(1981) for the solar nebula under the assumption that dust material accumulated into the terrestrial planets and the cores of the giant planets with minimum displacement in radial directions both inward and outward. Since dust grains in the protoplanetary disk have been accumulated into the protoplanet, the disk is transparent to the central star's visible radiation. The temperature profile of the disk is determined mainly by

this radiation, and is described by

$$T = T_0 \left(\frac{r}{r_0}\right)^{-1/2}. \tag{2.24}$$

The sound speed is given by

$$c = c_0 \left(\frac{r}{r_0}\right)^{-1/4}. \tag{2.25}$$

For simplicity we assume that the bulk viscosity, ζ, is zero and use α prescription as

$$\nu = \alpha c^2/\Omega. \tag{2.26}$$

We neglect the evolution of the temperature profile because the viscosity of the disk at the stage considered here is so small that the generation of the heat by the viscous stress is negligible.

The properties of the disk and the protoplanet are characterized by four parameters: α is the viscosity parameter, $h_0 = c_0/r_0\Omega_0$ is the scale height, $A = q^2/(3\alpha h_0^2)$ is the ratio of the strength of tidal effects to viscous effects, and $B = 3\pi\sigma_0 r_0^2/M_p$ is a measure of the mobility of the protoplanet. A and B are the same parameters which were used by Lin & Papaloizou(1986b).

In numerical calculations, the following disk properties are adopted. The mass of the central star is $M = 1M_\odot$. The disk has the minimum mass to create a planetary system like the solar system. The total mass of the disk is $0.017M_\odot$. The protoplanet is initially located at $r_0 = 5.2$AU from the central star (the present position of Jupiter). The scale height at 5.2AU is $h_0 = 0.05$. Hence, for the protoplanet with the Jupiter mass in the above disk, $A \approx 10^{-4}\alpha^{-1}$ and $B \approx 3$.

The computational space is divided into 529 cells spaced logarithmically between $r_1 = r_{in} = 10^{-2}r_0$ and $r_2 = 2r_{out} = 20r_0$. For comparison, calculations with 267 cells and 1054 cells were carried out and we found that the gap size changed by less than 6%. We also varied r_{in} from $10^{-3}r_0$ to $2 \times 10^{-2}r_0$, and the gap size changed less than 15%.

Chapter 3

Results

3.1. Estimation of gap size

The evolution of the disk is obtained by solving equations (2.17) and (2.18). Before solving the disk evolution numerically, we discuss the approximate relation between the gap size and the disk properties.

First, we derive an approximate value of the gap size appropriate for the disk whose viscosity is small enough for waves to propagate a large distance. In the region where the waves propagate, the gas of the disk interior to the protoplanet's orbit loses angular momentum, and the gas exterior to the orbit gains angular momentum, so that a gap opens in this region. It is considered that the waves can transfer angular momentum effectively in the disk where the integral of equation (2.11) is less than unity. We define the wave damping length l such that the integral of equation (2.11) becomes unity at $r_L \pm l$. An approximate value for l is obtained by

$$\left[\left|\left\{\zeta + \left(\frac{4}{3} + \frac{\kappa^2}{m^2(\Omega - \Omega_p)^2}\right)\nu\right\}\frac{m(\Omega_p - \Omega)}{c^2}kl\right|\right]_{r_L \pm l} \approx 1. \tag{3.1}$$

Near the LR, Ω is approximately

$$\Omega(r_L \pm l) \approx \Omega(r_L)\left(1 \mp \frac{3}{2}\left(\frac{l}{r_L}\right)\right). \tag{3.2}$$

Assuming that the sound speed varies slowly, equation (2.12) becomes approximately

$$k^2(r_L \pm l) \approx 3(m \pm 1)\left(\frac{\Omega^2}{c^2}\right)_{r_L}\left(\frac{l}{r_L}\right). \tag{3.3}$$

For large m, we can approximate $r_L \approx r_p$ by equation (1.2), $\Omega(r_L) \approx \Omega_p$, and $\kappa^2/m^2(\Omega(r_L \pm l) - \Omega_p)^2 \approx 0$. Then equation (3.1) becomes

$$\frac{l}{r_p} \approx \left[\frac{2c^3}{3\sqrt{3}m^{3/2}\Omega^2 r\left(\zeta + \frac{4}{3}\nu\right)}\right]_p^{2/5}. \tag{3.4}$$

We have to sum up the angular momentum flux for all m to calculate the surface density evolution of the disk, and in the next section this summation is performed numerically. The amplitude of waves has maximum value when $m \sim (r\Omega/c)_p$. We can make a rough estimate of the gap size by calculating the wave damping length of waves with $m = (r\Omega/c)_p$. Considering the gap size Δr is equal to the damping length of the wave l, the gap size becomes

$$\frac{\Delta r}{r_p} \sim \left(\frac{c}{r\Omega}\right)_p \alpha^{-2/5}, \tag{3.5}$$

where we used the α prescription for the viscosity law. If $\Delta r/r_p \gtrsim 1$, then the disk interior to the protoplanet's orbit falls onto the central star. The criterion for the removal of the inner disk becomes

$$\alpha \lesssim \left(\frac{c}{r\Omega}\right)_p^{5/2}. \tag{3.6}$$

If the viscosity of the disk is large enough for waves to damp immediately, then the effect of the wave propagation can be neglected. In this case, the protoplanet's torque works most effectively on the boundary between the disk and the gap. This torque should be balanced with the viscous torque that works to narrow the gap. The balance between tidal and viscous torque is expressed as

$$2\pi\frac{d}{dr}\left(\nu\sigma r^3\frac{d\Omega}{dr}\right) = -T(r). \tag{3.7}$$

Here we use the expression for the torque density $T(r)$ which is derived by Goldreich & Tremaine (1980) assuming the waves damp immediately at LRs and given in equation (1.3).

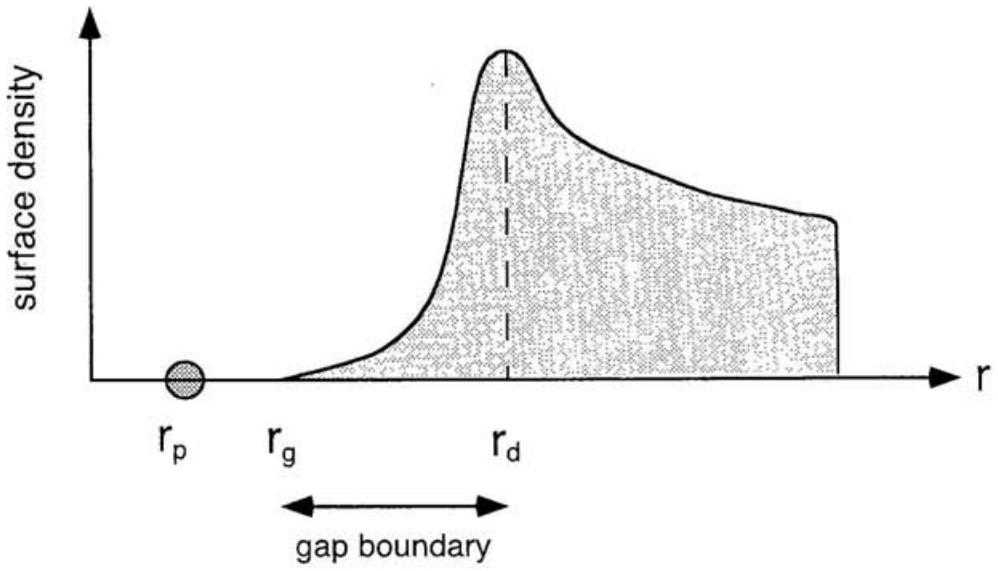

Fig. 3-1.— Illustration of the boundary between the gap and the disk. The disk and the gap outside the protoplanet's orbit is shown in this figure. The surface density inside r_d is reduced by the tidal torque of the protoplanet, and is completely reduced at r_g.

The surface density, σ, equals zero at the edge of the disk, $r_g = r_p \pm \Delta r/2$, and increases with distance from the protoplanet (see Fig. 3-1). This boundary extends between r_g and r_d, and the surface density recovers its original value at r_d. Integrating equation (3.7) between r_g and r_d, we have

$$2\pi \left[\nu\sigma r^3 \frac{d\Omega}{dr} \right]_{r_g}^{r_d} = -\int_{r_g}^{r_d} T dr. \tag{3.8}$$

In the integral of equation (3.8), $r\sigma/\Omega^2$ in equation (1.3) is evaluated approximately at r_d. Because most of the contribution to the integral comes from $r \approx r_g$, the upper boundary of the integration region is extended to infinity. Then the right hand side of equation (3.8) becomes

$$-\frac{256}{243}(GM_p)^2 \left(\frac{r\sigma}{\Omega^2}\right)_{r_d} \frac{1}{\Delta r^3}\{2K_0(2/3) + K_1(2/3)\}^2. \tag{3.9}$$

Using $\sigma = 0$ at r_g, the left-hand side of equation (3.8) becomes

$$2\pi \left(\nu\sigma r^3 \frac{d\Omega}{dr} \right)_{r_d}. \tag{3.10}$$

Assuming the Keplerian rotation law and that the gap size is small, so that $r_d \approx r_p$, the gap size is obtained as

$$\frac{\Delta r}{r_p} \sim 0.9 \left(\frac{q^2}{\alpha h_0^2} \right)^{1/3} \sim 1.3 A^{1/3}. \tag{3.11}$$

The condition for gap formation has been derived previously by Goldreich & Tremaine (1980), and also by Papaloizou & Lin(1984). The angular momentum deposited in a ring with radius from r_p to $r_p \pm \Delta r$ via the dissipation of the waves with mode m is given by (see eqs. [2.13] and [2.22])

$$\begin{aligned} \tilde{T}_m &= \pm \int_{r_p}^{r_p \pm \Delta r} T_m dr \\ &\approx \pm f_c m^2 \sigma \Omega_p^2 r^4 q^2, \end{aligned} \tag{3.12}$$

where we assumed that waves are completely dissipated within this ring. The angular momentum ΔH needed to open a gap of width Δr is

$$\Delta H \approx \sigma \Omega_p (r_p \Delta r)^2. \tag{3.13}$$

The time required to open a gap through the waves with mode m is

$$t_{open}^{(m)} \sim \frac{\Delta H}{|\tilde{T}_m|} \sim \frac{1}{f_c m^2 q^2 \Omega_p} \left(\frac{\Delta r}{r_p}\right)^2, \tag{3.14}$$

On the other hand, the time to fill up a gap by the viscous diffusion is

$$t_{close} \sim \frac{\Delta r^2}{\nu}. \tag{3.15}$$

The condition for gap formation through the waves with mode m is $t_{close} \gtrsim t_{open}^{(m)}$ or

$$q \gtrsim \frac{1}{f_c m} \left(\frac{c}{r\Omega}\right)_p \alpha^{1/2}. \tag{3.16}$$

For small m such that $f_c \approx 1$, i.e. $m \lesssim (r\Omega/c)_p$, this condition is rewritten using A defined in §2.4 as

$$A \gtrsim \frac{1}{m^2}. \tag{3.17}$$

The total torque due to all m waves is given by

$$\tilde{T} = \sum_{m=1}^{\infty} \tilde{T}_m \approx \sigma \Omega_p^2 r^4 q^2 \int_0^{\infty} m^2 f_c(m) dm, \tag{3.18}$$

where we approximate summation by integrals. This integral is approximated by $(r\Omega/c)_p^3$ (Goldreich & Tremaine 1980; Ward 1986). Hence,

$$\tilde{T} \approx \sigma \Omega^2 r^4 \left(\frac{r\Omega}{c}\right)_p^3 q^2. \tag{3.19}$$

The time to open a gap by all m waves is

$$t_{open} \sim \frac{1}{q^2} \left(\frac{c}{r\Omega}\right)_p^3 \left(\frac{\Delta r}{r_p}\right)^2 \frac{1}{\Omega_p}. \tag{3.20}$$

The condition for gap formation becomes

$$q \gtrsim \left(\frac{c}{r\Omega}\right)_p^{5/2} \alpha^{1/2}. \tag{3.21}$$

In the following sections, the approximate formula for the gap size (3.5) and (3.11) are compared with the numerical results. The condition for the gap formation through the waves with mode m (3.17) and through all m waves (3.21) will be used to understand the numerical results.

3.2. Protoplanet's torque

The torque density, $T(r)$, is calculated numerically from equations (2.11), (2.14) and (2.22), and is shown in Figures 3-2 – 3-6. In this section, the surface density profile is assumed to be constant with radius for simplicity, whereas elsewhere in this thesis the surface density is treated as a function of radius and time. The scale height is $h_0 = 0.05$. Figure 3-2 shows the torque density exerted through the $m = 2$ waves. Near the LRs (0.63 for $m = 2$ ILR and 1.31 for $m = 2$ OLR), because wave length of excited waves is large as seen from equations (2.4) and (2.12), the waves can propagate suffering little damping. After they have propagates some distance from the LR, the wave length becomes short enough to suffer viscous damping, and deposit their angular momentum into the disk. Therefore, the torque density profiles have their peak at somewhat distant place from LR. The position where the absolute value of the torque density has maximum grows farther away from the protoplanet's position as the viscosity parameter α decreases. If α is less than 10^{-3}, the $m = 2$ waves reach the boundary between the central star and the disk. The m dependence of torque density is shown in Figure 3-3. In these calculations, α is set at 10^{-2} for each value of m. The position of the LR grows nearer to the protoplanet's position as m increases. The length of the wave propagation becomes shorter as m increases. The protoplanet exerts the largest torque through the waves with $m \sim (r\Omega/c)_p \sim 20$. The summation of the torque exerted through the waves with all m are shown in Figure 3-4. The region where the protoplanet exerts the torque effectively becomes wider as α decreases. If α is less than 10^{-4}, then the protoplanet exerts the torque effectively on the disk material near the central star, because the waves with $m \sim (r\Omega/c)_p \sim 20$ can reach the central star in such a disk with low viscosity.

The torque density is calculated for additional values of scale height, $h_0 = 2.5 \times 10^{-2}$ and 10^{-1}, and shown in Figure 3-5, where each torque density is normalized as the total torque exerted on the disk inside and outside the orbit of the protoplanet are unity. Note that the total torque is inversely proportional to the cube of the scale height (eq. [3.19]), because the waves with higher m contribute to the total torque as scale height (sound speed)

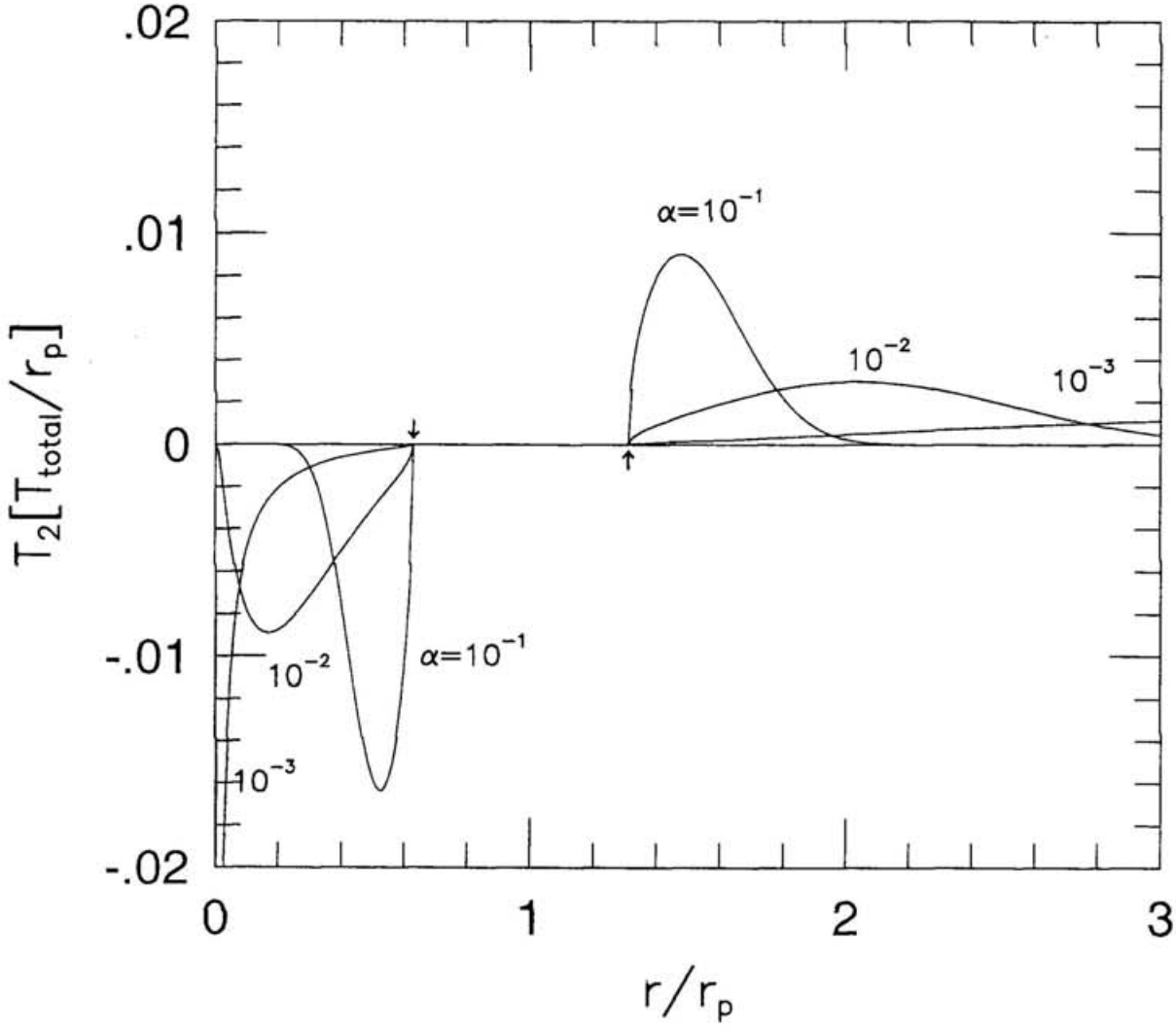

Fig. 3-2.— Torque density exerted on the disk through the $m = 2$ waves, normalized by the total torque exerted by the protoplanet, T_{total}, and divided by the orbital radius of the protoplanet, r_p. Each line is labeled by the appropriate value of α. The scale height is $h_0 = 0.05$. Arrows show the positions of the $m = 2$ LRs.

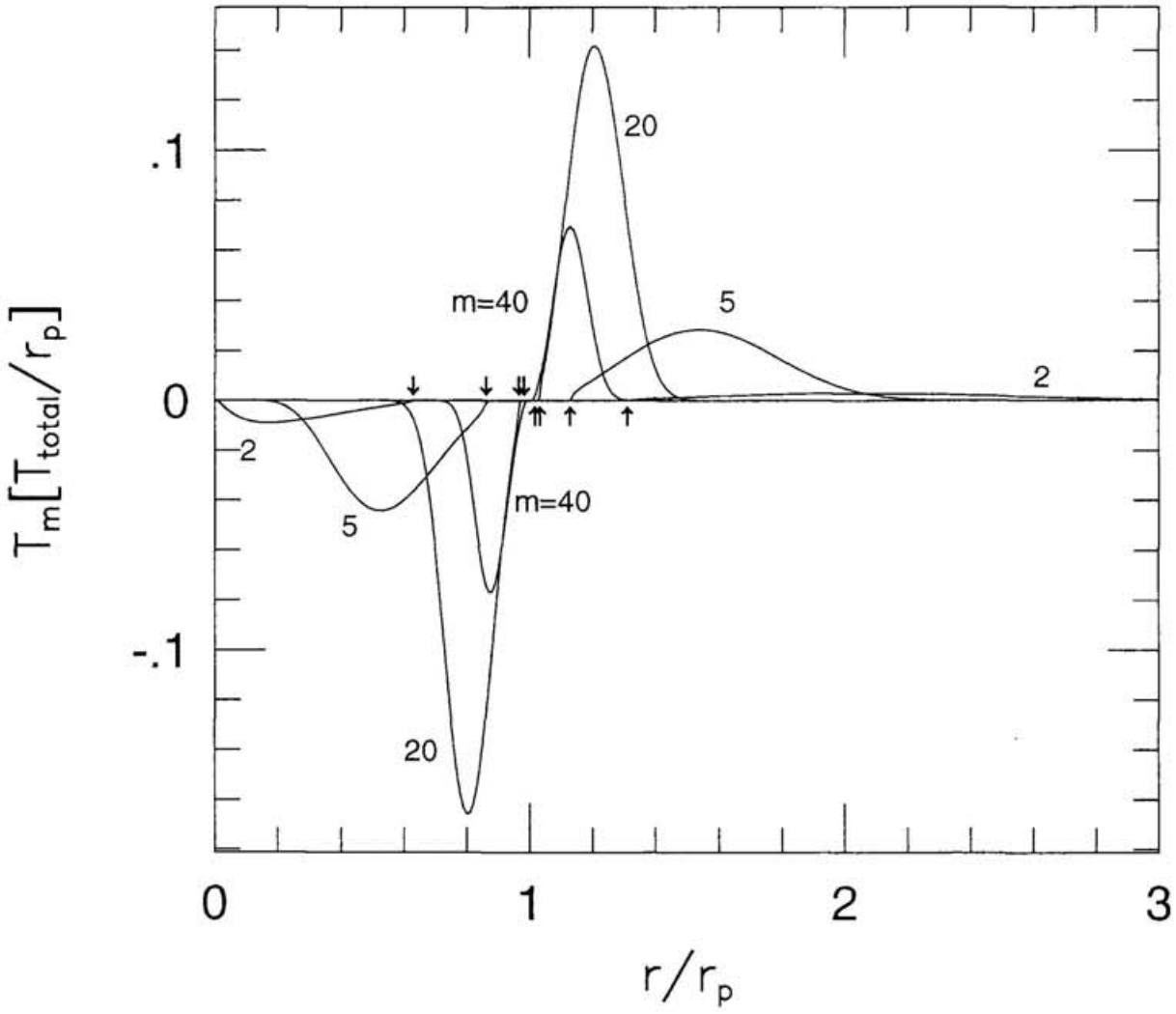

Fig. 3-3.— Torque density through the waves with various modes. The viscosity parameter is $\alpha = 10^{-2}$. Each line is labeled by the appropriate value of m. The scale height is $h_0 = 0.05$. Arrows show the positions of the $m = 2, 5, 20$, and 40 LRs.

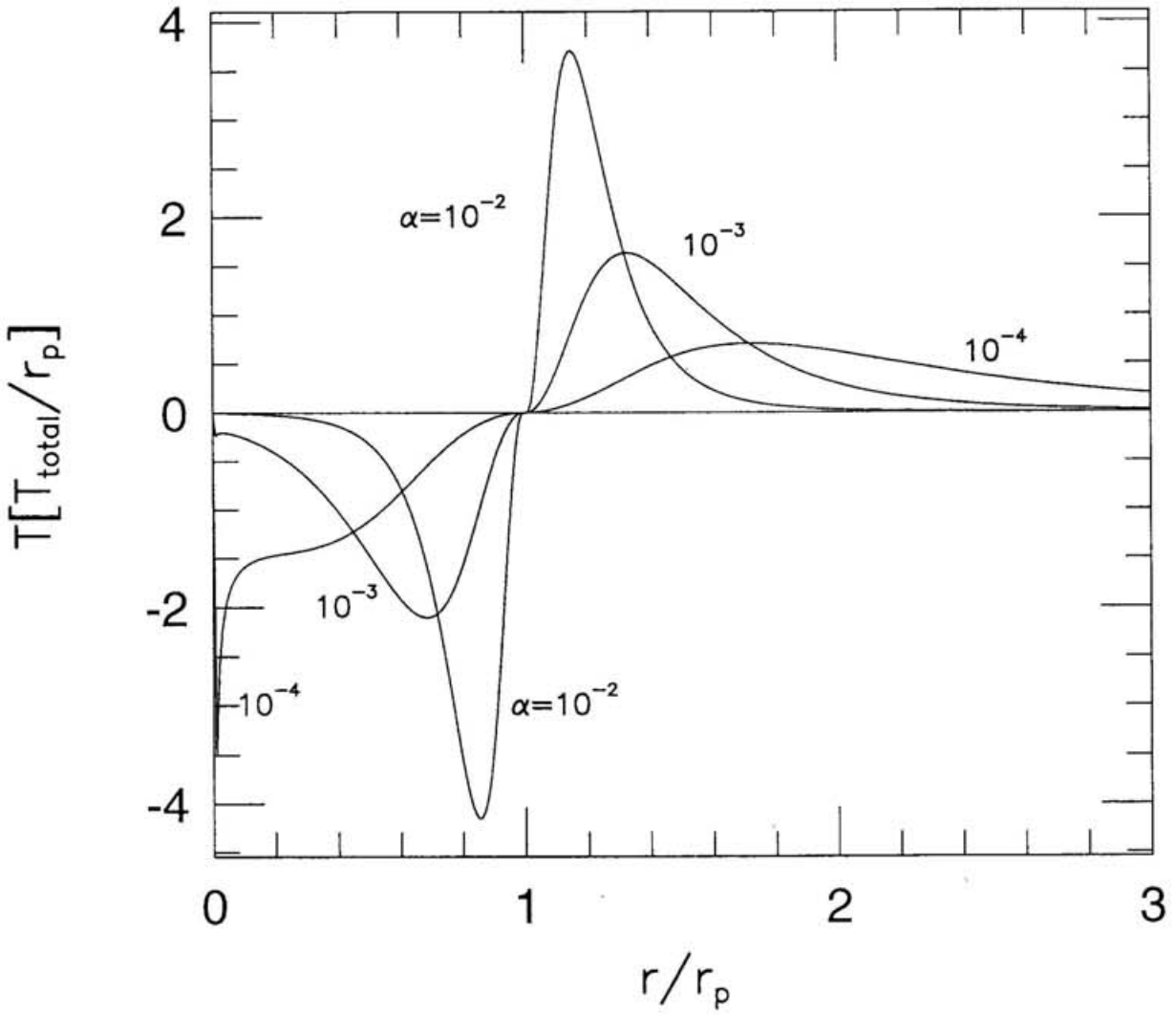

Fig. 3-4.— Summation of the torque density through the waves with all modes. Each line is labeled by the appropriate value of α.

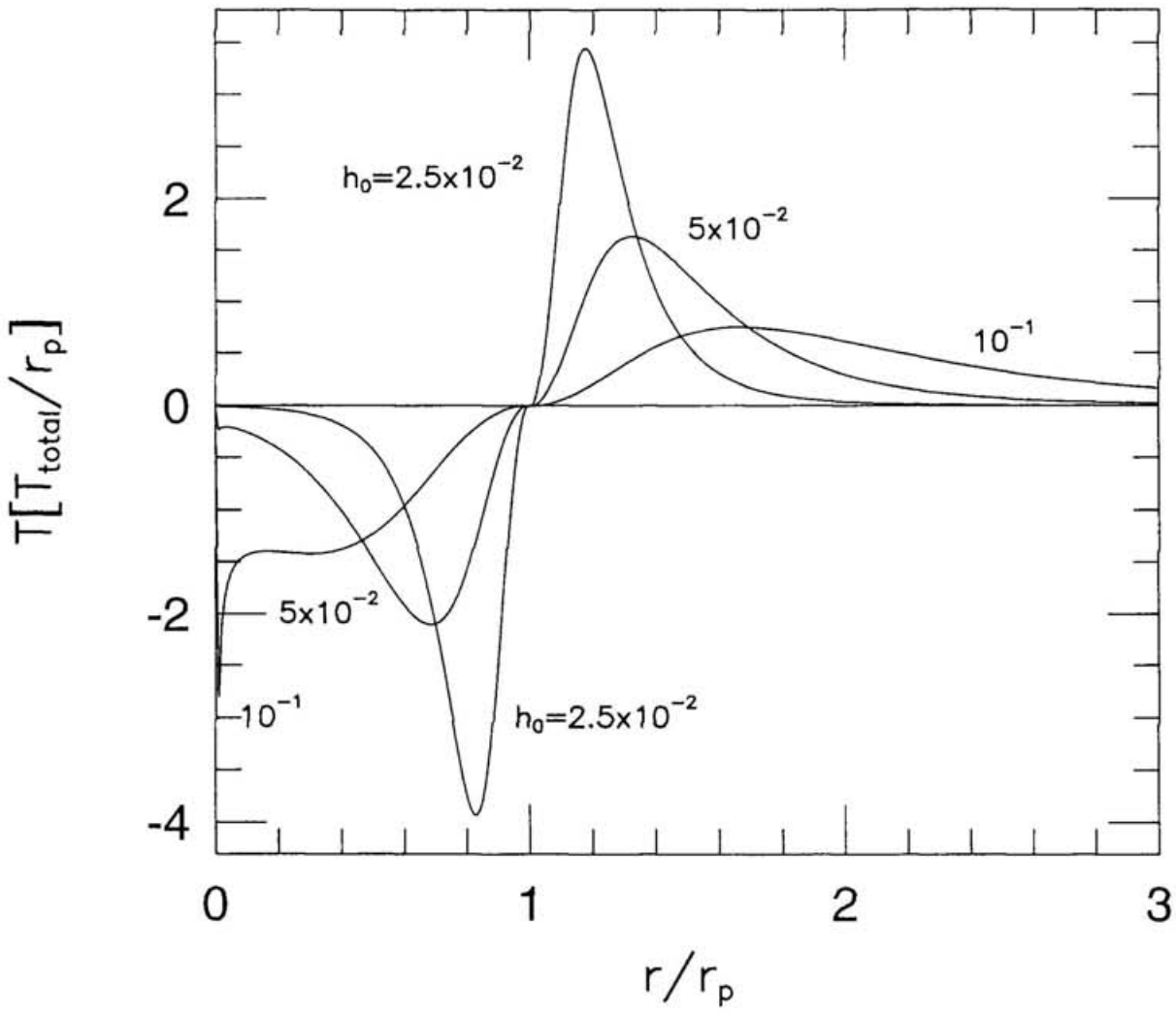

Fig. 3-5.— Torque density exerted on the disk through the waves with all modes. Each line is labeled by the appropriate value of h_0. The viscosity parameter is $\alpha = 10^{-3}$.

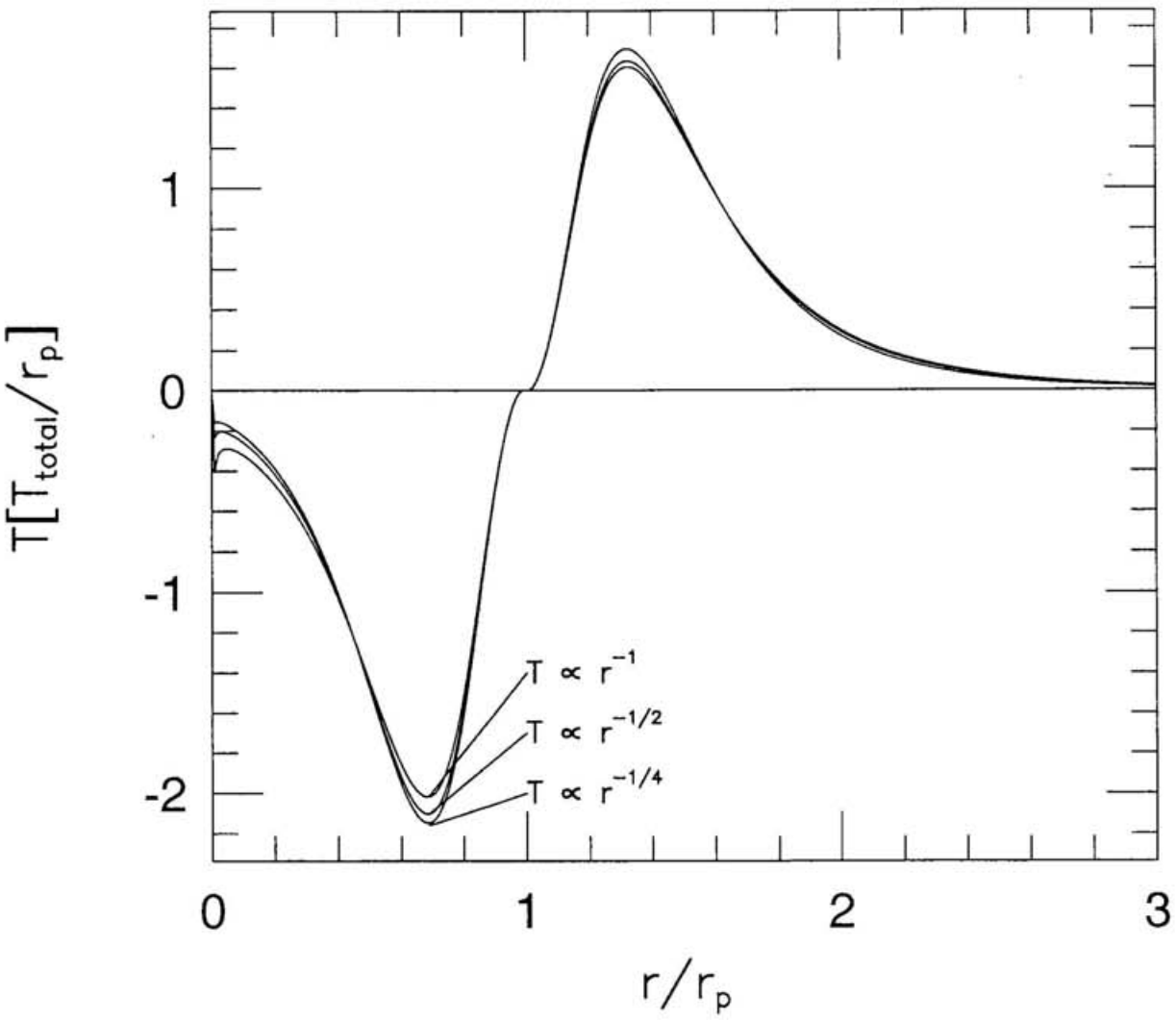

Fig. 3-6.— Torque density exerted on the disk through the waves with all modes. Each lines show the torque density for various temperature profiles. The scale height is $h_0 = 0.05$. The viscosity parameter is $\alpha = 10^{-3}$.

becomes smaller. Thus, normalization factors for each lines in Figure 3-5 are quite different from each other. As the scale height (sound speed) increases, the wave length at same radius becomes larger (eq. [2.12]), and viscous damping of waves is reduced. Therefore, the waves can propagate wider regions.

In Figure 3-6, calculations for the models with different temperature distributions are shown. There is only a small differences in torque density when the power law index for the temperature profile is varied by a factor 2. This is because sound speed is proportional to the square root of the temperature, and then varies slowly with r near the protoplanet. In the following sections, the calculations only for the models with $T \propto r^{-1/2}$ are presented.

3.3. Gap size

In this section the parameter of protoplanet's mobility, B, is set to be zero and the effects of the orbital migration of the protoplanet are neglected, because we are interested in how the wave propagation affects the process of the gap formation. The effects of the orbital migration on the gap formation are discussed in the next section. The parameters, $A = 10^{-1}$ and $h_0 = 0.05$, are adopted as a standard model. These parameters correspond to the protoplanet with the Jupiter mass in the disk with the minimum mass when $\alpha = 10^{-3}$.

Equation (2.17) is integrated numerically up to a non-dimensional time $t' = 10^{-1}$. In the standard model, the process of the gap formation finishes by $t' = 10^{-1}$. The evolution of the disk after that time is dominated by the viscous diffusion process and the rate of the change of the gap size is slow (see Fig. 3-8). We are interested in evolution with a time scale shorter than the time scale of the viscous diffusion and hence we terminate time integration at $t' = 10^{-1}$.

Figure 3-7 shows the evolution of the surface density of the protoplanetary disk without the protoplanet. In this case the disk evolves only through the viscous diffusion process. It can be seen that the disk experiences little evolution in $t' = 10^{-1}$. Figure 3-8 show the gap

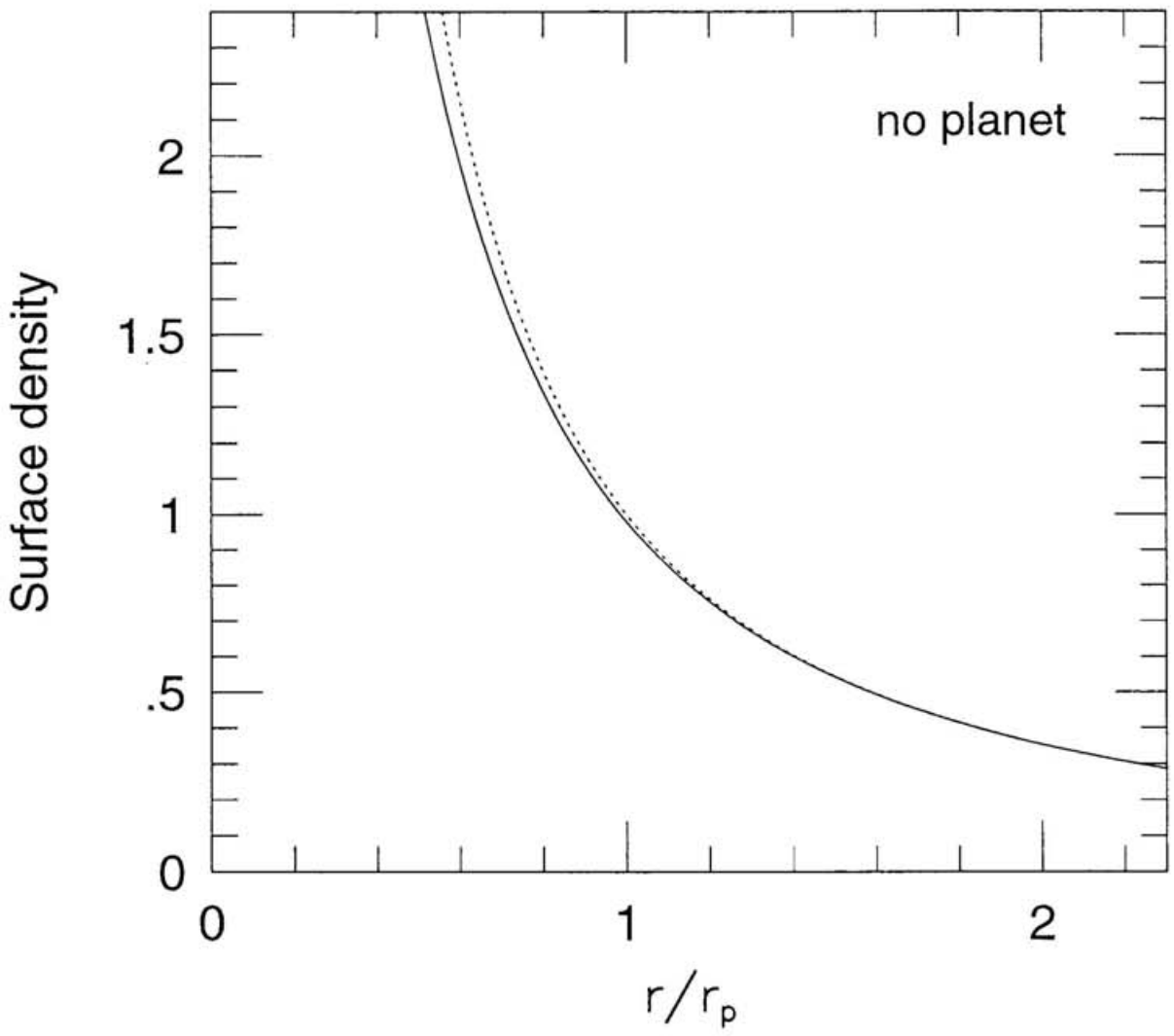

Fig. 3-7.— Surface density evolution of the disk without the protoplanet. The dots and solid curve correspond to non-dimensional time, $t' = 10^{-3}, 10^{-1}$, respectively.

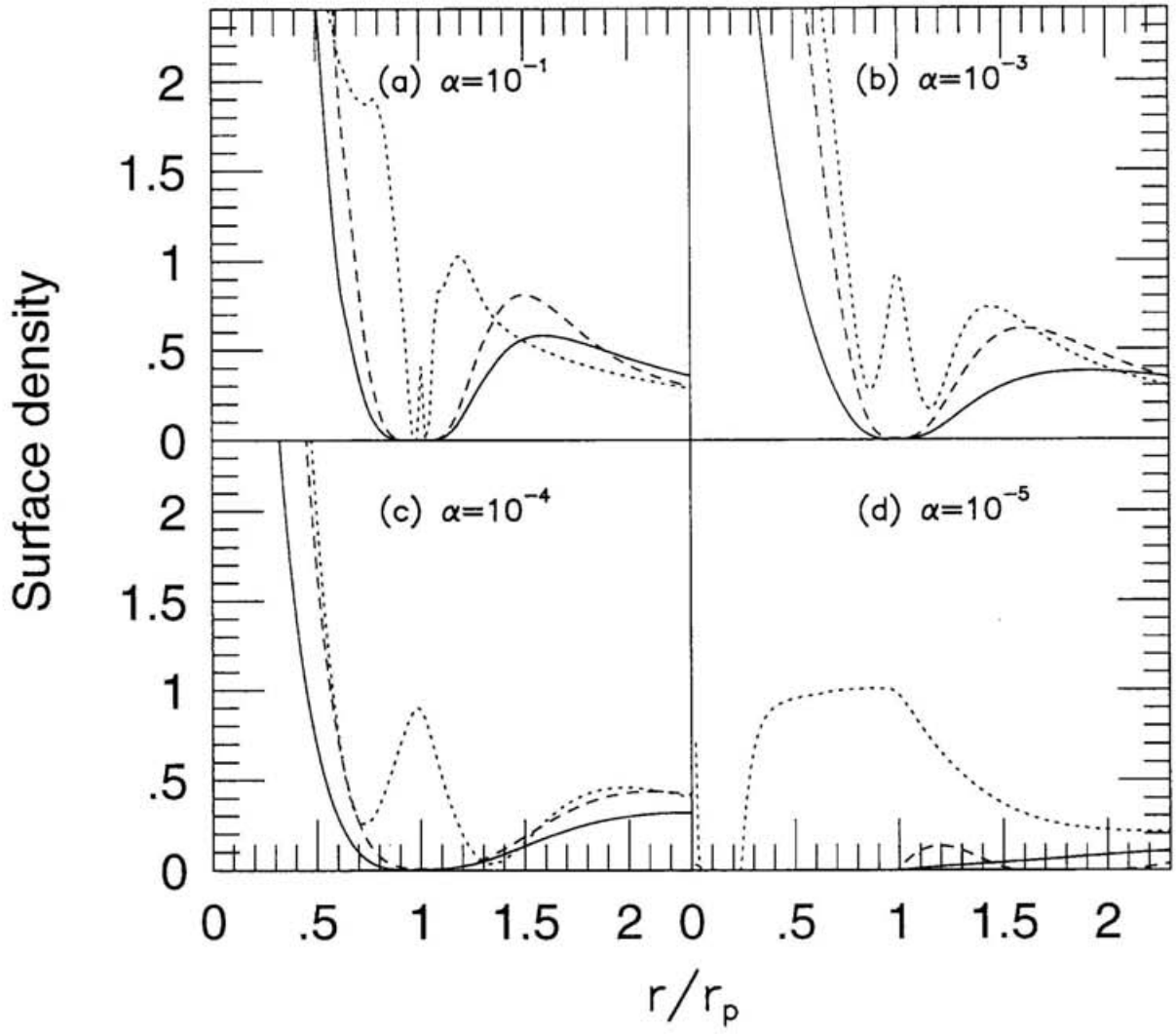

Fig. 3-8.— Surface density evolution of the disk. We set $A = 10^{-1}, B = 0$ and $h_0 = 0.05$. The viscosity parameter is $\alpha =$ (a) 10^{-1} (b) 10^{-3}, (c) 10^{-4}, (d) 10^{-5}. The dots, dashes, and solid curve correspond to $t' =$ (a) $4\times10^{-5}, 10^{-2}, 10^{-1}$, (b) $10^{-4}, 10^{-2}, 10^{-1}$, (c) $5\times10^{-4}, 10^{-2}, 10^{-1}$, (d) $3\times10^{-3}, 10^{-2}, 10^{-1}$, respectively.

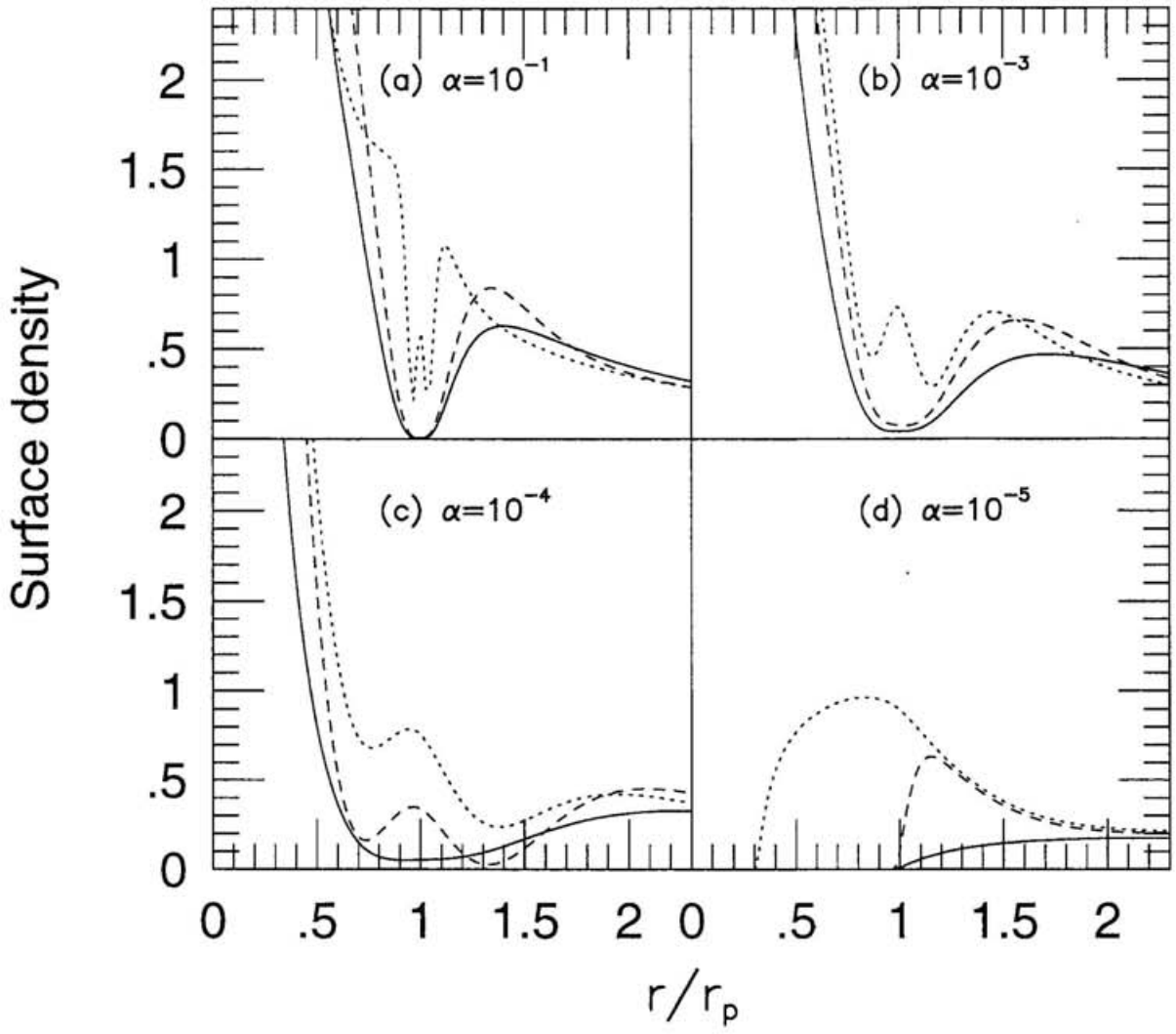

Fig. 3-9.— Surface density evolution of the disk for $A = 10^{-2}$. The viscosity parameter is α = (a) 10^{-1} (b) 10^{-3}, (c) 10^{-4}, (d) 10^{-5}. The dots, dashes, and solid curve correspond to t' = (a) $10^{-4}, 10^{-2}, 10^{-1}$, (b) $10^{-3}, 10^{-2}, 10^{-1}$, (c) $4\times10^{-3}, 10^{-2}, 10^{-1}$, (d) $8\times10^{-3}, 10^{-2}, 10^{-1}$, respectively.

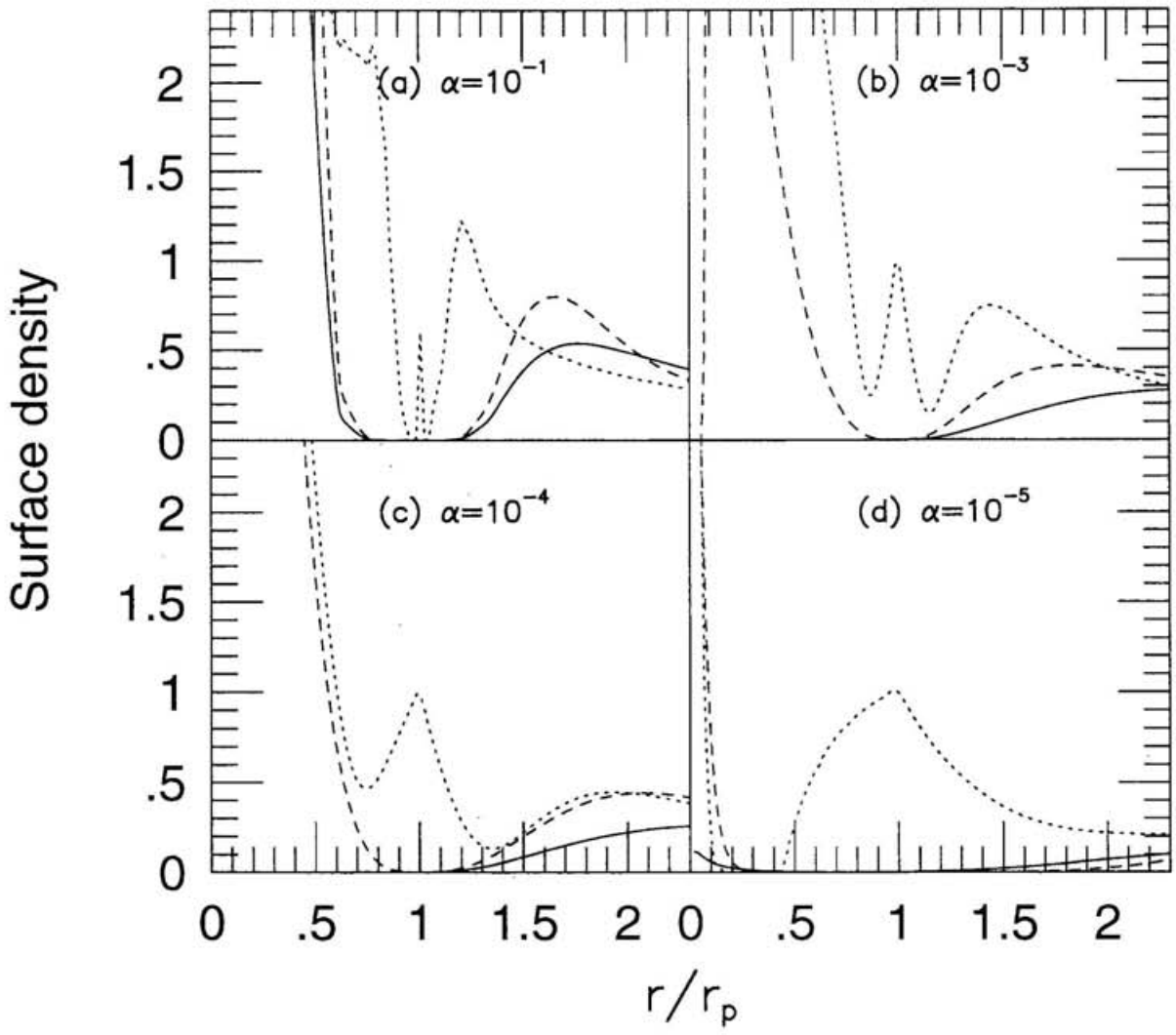

Fig. 3-10.— Surface density evolution of the disk for $A = 1$. The viscosity parameter is α = (a) 10^{-1} (b) 10^{-3}, (c) 10^{-4}, (d) 10^{-5}. The dots, dashes, and solid curve correspond to t' = (a) $10^{-5}, 10^{-2}, 10^{-1}$, (b) $10^{-5}, 10^{-2}, 10^{-1}$, (c) $4 \times 10^{-5}, 10^{-2}, 10^{-1}$, (d) $10^{-4}, 10^{-2}, 10^{-1}$, respectively.

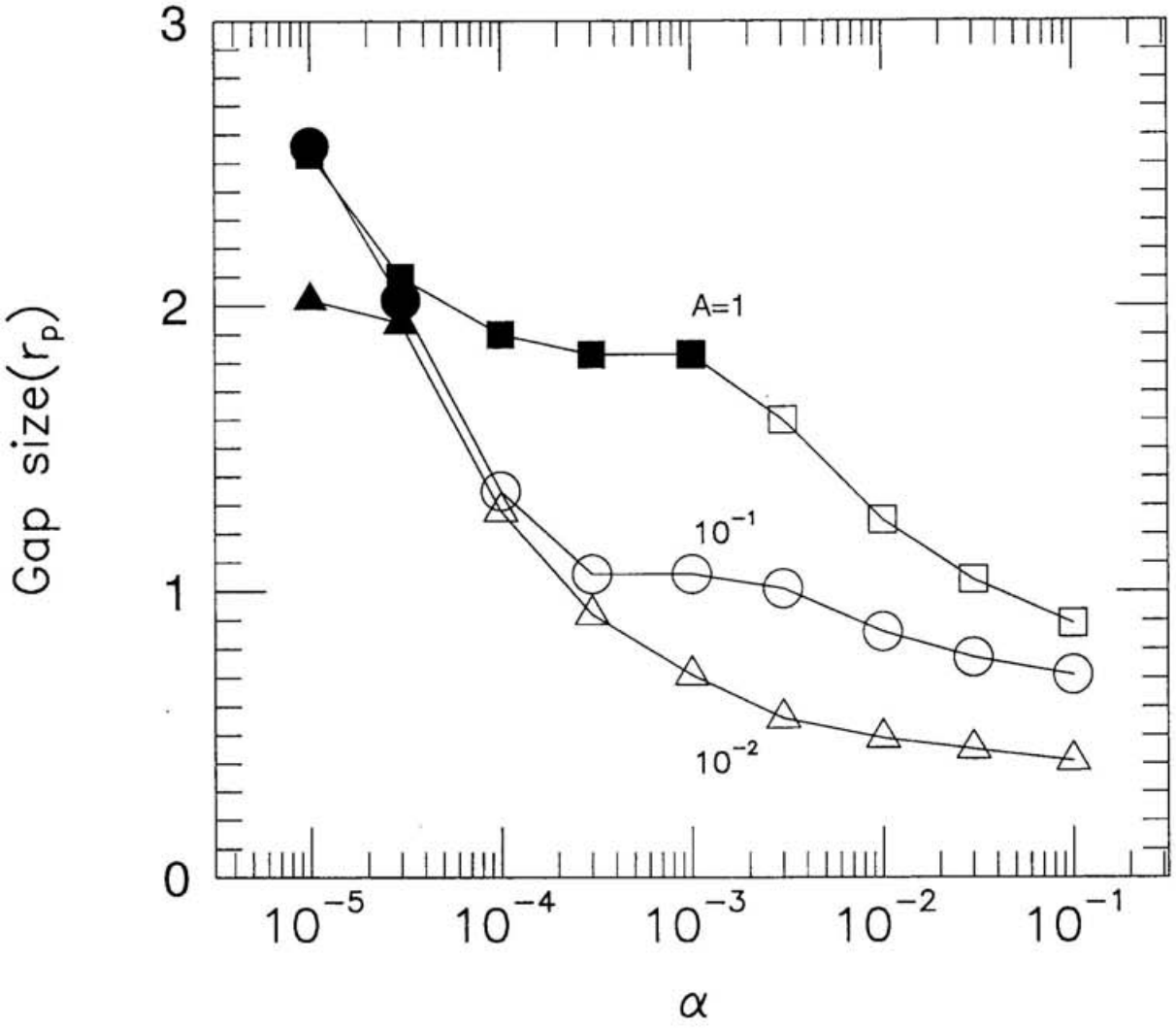

Fig. 3-11.— Relation between the gap size and the viscosity parameter α. The gap size is defined as the width of the region where the surface density of the disk is reduced to less than half the value for the disk without a protoplanet. The gap sizes are evaluated at $t' = 10^{-1}$. The values of B and h_0 are 0 and 0.05. The squares, circles and triangles correspond to $A = 1$, $A = 10^{-1}$, and 10^{-2}, respectively. The filled symbols indicate that the inner disk has fallen onto the central star. If the inner disk is removed, the radius of the inner edge of the outer disk is plotted.

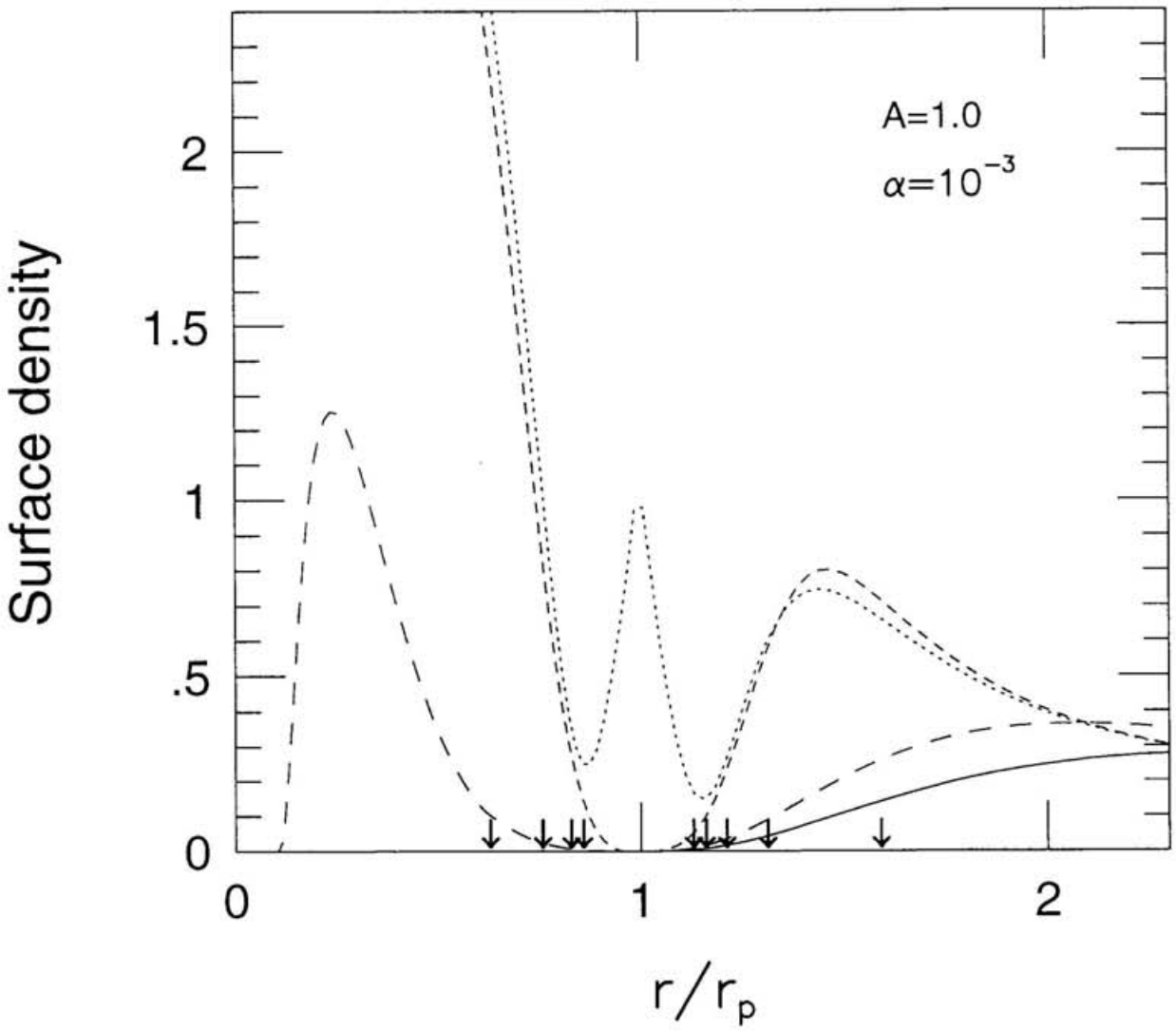

Fig. 3-12.— Surface density evolution of the disk for $A = 1, B = 0, h_0 = 0.05$, and $\alpha = 10^{-3}$. The dots, short dashes, long dashes, and solid curve correspond to $t' = 10^{-5}, 10^{-3}, 2 \times 10^{-2}, 10^{-1}$, respectively. Arrows show the positions of inner LRs($m = 2 - 5$) and outer LRs($m = 1 - 5$).

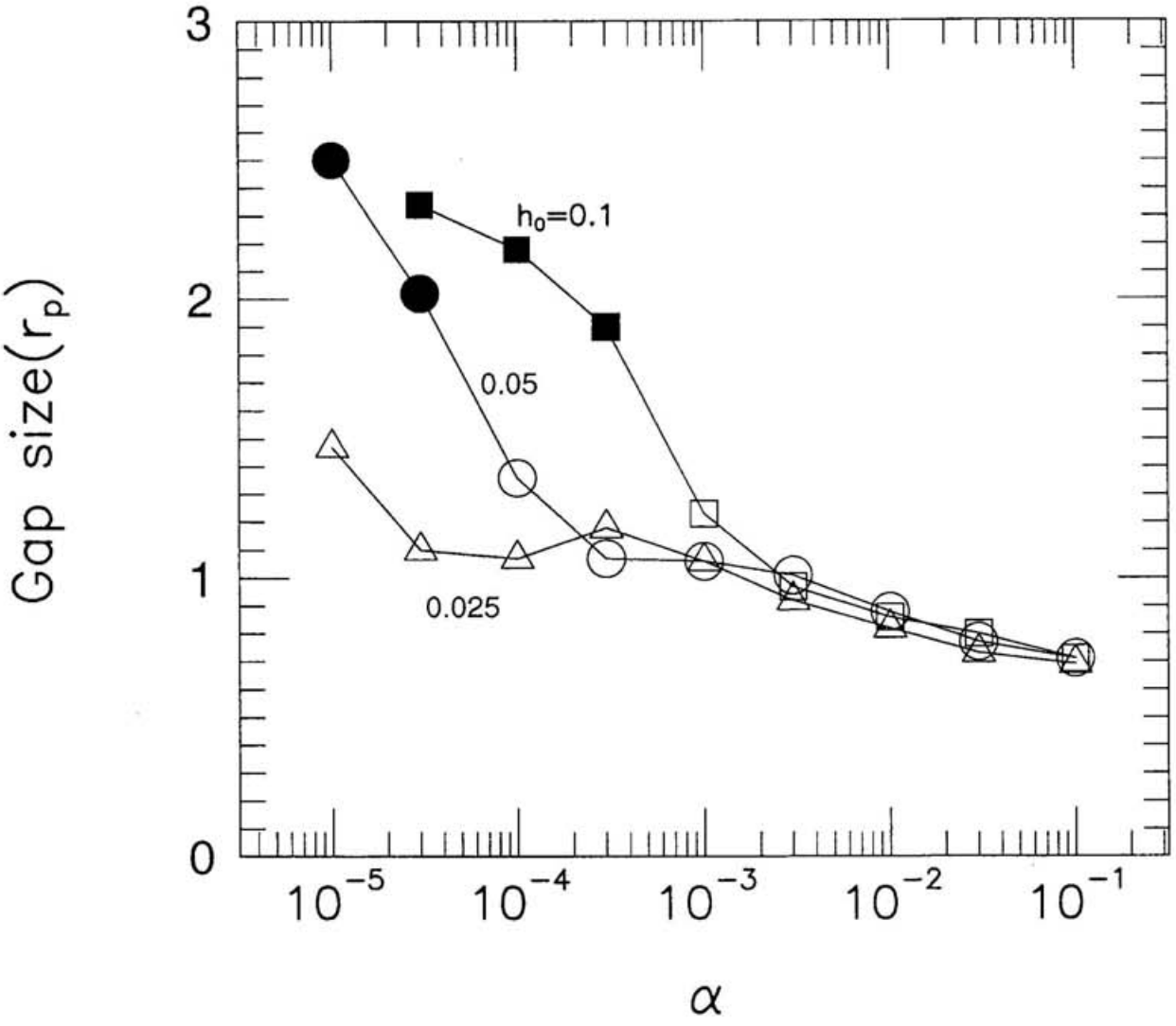

Fig. 3-13.— Relation between the gap size and the viscosity parameter α. The values of A and B are 10^{-1} and 0. The squares, circles and triangles correspond to $h_0 = 0.1, 0.05$ and 0.025, respectively.

formation by the protoplanet in the standard model. The viscosity parameter, α, is 10^{-1}, 10^{-3}, 10^{-4}, and 10^{-5} in Figures 3-8 $(a), (b), (c)$ and (d), respectively. The protoplanet is put at $r' = 1$ at $t' = 0$. Because of the wave propagation protoplanet exerts maximum torque on the disk distant from it (see Fig. 3-4). The gap formation occurs at the distant place from the protoplanet at first, and the surface density profiles have two dips. The dips grows toward the protoplanet, and the gap formation finishes by $t' = 10^{-2}$. Once gap formation is completed, the development of the gap size is slow after that. The size of the gap becomes wider as α becomes smaller. For $\alpha = 10^{-5}$, the waves can reach the inner edge of the disk, and dissipate there. The disk material falls onto the central star from the innermost part of the disk. Finally the disk inside the protoplanet's orbit is removed.

The evolution of the surface density for $A = 10^{-2}$ is shown in Figure 3-9. The evolution is quite similar to the case of $A = 10^{-1}$. Figure 3-10 shows the evolution of the surface density for $A = 1$. It is seen that the removal of the inner disk occurs even if the viscosity is as large as $\alpha = 10^{-3}$.

The gap sizes at $t' = 10^{-1}$ are plotted as a function of the viscosity parameter α in Figure 3-11 for $A = 1, 10^{-1}$ and 10^{-2}. The gap size is defined as the width of the region where the surface density of the disk is reduced to less than half the value for the disk without a protoplanet. The filled marks in Figure 3-11 show the removal of the inner disk. If the inner disk is removed, then the radius of the inner edge of the outer disk is plotted. It can be seen from Figure 3-11 that the gap size increases with increasing A. The gap size decreases with increasing α. For $A = 10^{-2}$, the decrease in the gap size with α stops for $\alpha \gtrsim 10^{-2}$, and for $A = 10^{-1}$ it stops for $\alpha \gtrsim 10^{-3}$. However, for $A = 1$ the gap size decreases with α even if viscosity is as large as $\alpha \sim 10^{-1}$. For $A = 10^{-1}$ and 10^{-2}, the disk material inside the protoplanet's orbit is removed if α is less than 3×10^{-5}. For $A = 1$, the disk material inside the orbit is removed if α is less than 10^{-3}.

For $A = 10^{-1}$ and 10^{-2}, the α dependence of the gap size is explained as follows. The region in which torque is exerted effectively on the disk material becomes narrower as α

increases (Fig. 3-4). Hence, the gap size decreases with α. The α dependence of the gap size is compared with the approximate formula (3.5). Our approximation for the radial wave number (eq. [3.3]) tends to be an underestimate as the waves propagate from the LR. The wave dissipation is also underestimated. Hence, the gap size increases more slowly with decreasing α than equation (3.5). The numerical results are described by the formula

$$\frac{\Delta r}{r_p} = 1.3 \left(\frac{c}{r\Omega}\right)_p \alpha^{-1/4}. \tag{3.22}$$

For highly viscous disks ($\alpha \gtrsim 10^{-2}$ for $A = 10^{-2}$, and $\alpha \gtrsim 10^{-3}$ for $A = 10^{-1}$), waves damp immediately near the LRs. In this case the effect of the wave propagation can be neglected, and the gap size is approximated by equation (3.11). This approximation formula agrees with the numerical result.

For $A = 1$, protoplanet's mass is sufficiently large to open a gap through the lowest m waves (i.e. $m = 1$ for outer disk, and $m = 2$ for inner disk). Of course, the waves with $m \sim (r\Omega/c)_p \sim 20$ are most effective in opening a gap. However, if $A \gtrsim 1$, even the lowest m waves can be effective as seen from equation (3.17). The $m \sim (r\Omega/c)_p$ waves open a relatively narrow gap quickly. Most of the LRs fall into the gap, and the wave excitation is suppressed. Only LRs with small m survive, because their positions are far from the protoplanet. After that, small m waves broaden the gap. Because the $m = 1$ or 2 waves can propagate even if the viscosity of the disk is as large as $\alpha = 10^{-1}$(Fig. 3-2), the effect of the wave propagation cannot be neglected. The gap size increases with decreasing α even if α is as large as 10^{-1}. If $\alpha \lesssim 10^{-3}$, $m = 2$ waves can arrive at the inner radius of the disk(Fig. 3-2) and the disk material interior to the protoplanet's orbit falls onto the central star. Figure 3-12 shows the evolution of the disk for $A = 1$ and $\alpha = 10^{-3}$. High m waves open the narrow gap quickly. This gap formation suppresses the wave excitation at most of the LRs. Only small m LRs can contribute to the evolution of the disk after the formation of a narrow gap. However, protoplanet's mass is large, therefore, the inner disk is removed even by the $m = 2$ waves.

The gap sizes are calculated for additional values of the sound speed, c_0. In Figure 3-13 the gap sizes are shown for $h_0 = (c/r\Omega)_0 = 0.025, 0.05$ and 0.1. In each case $A = 10^{-1}$ and

$B = 0$. The gap size increases with h_0. This is due to the fact that the length of wave propagation increases with sound speed (eq. [3.4]). For $\alpha \gtrsim 10^{-3}$, the waves excited at LR damp immediately. In this case the gap size is determined by the balance of the tidal and viscous torques (eq. [3.11]). The same value, 10^{-1}, is adopted for A in each calculations. Thus the same gap size is obtained for different h_0 for $\alpha \gtrsim 10^{-3}$.

3.4. Effects of orbital migration

In this section the effect of the protoplanet's orbital migration on the gap formation is discussed. The protoplanet gains the angular momentum via the tidal interaction with the disk inside its orbit, while it loses the angular momentum via the tidal interaction with the disk outside its orbit. The difference between the gains and losses of the angular momentum causes the migration of the protoplanet (Ward 1986; Lin & Papaloizou 1986b). If the protoplanet migrates to a larger distance than the size of the gap before the completion of the gap formation, then it escapes from the gap, and the gap formation is inhibited (Hourigan & Ward 1984; Ward & Hourigan 1989). If protoplanet cannot escape from the gap, then a gap opens. Once a gap is opened, the interaction between the protoplanet and the protoplanetary disk is reduced until the tidal torque balances with the viscous torque. The protoplanet's orbital migration is suppressed and proceeds on a viscous diffusion time scale after the gap formation(Lin & Papaloizou 1986b).

In order to calculate protoplanet's orbital migration we must know the density and temperature structure of the disk near the protoplanet exactly. However, we have little information about the structure of the disk at present. Thus, it is difficult to calculate the orbital migration exactly. Therefore, we have simplified the problem and considered only the effects of the surface density profile on the changes in the orbit. Note that other ignored effects due to the pressure or temperature profile may be on the same order as the effects due to the surface density profile(Ward 1986), and hence, our calculation may contain order-unity uncertainties. Therefore, this discussion of orbital migration must be considered as

qualitative.

In Figure 3-14, the evolution of the orbital radius of the protoplanet is plotted. We adopt $A = 10^{-1}, \alpha = 10^{-3}$ and $h_0 = 0.05$, and vary the protoplanet's mobility, B, from 3 to 70. For the protoplanet with the Jupiter mass in a minimum-mass disk (Hayashi 1981), the value of B is about 3. The evolution of the surface density and the position of the protoplanet for $B = 50$ are shown in Figure 3-15. Because the surface density decreases with the radius, the protoplanet interacts more strongly with the inner disk than the outer disk. Thus, the protoplanet gains angular momentum from the inner disk and migrates outward. Concurrently, the protoplanet changes the surface density profile. At $t' = 2 \times 10^{-3}$, the surface density near the protoplanet increases with radius. Therefore, the protoplanet deposits its angular momentum into the outer disk and turns inward. By $t' = 3 \times 10^{-3}$, the protoplanet forms a gap around it. The orbital migration of protoplanet is suppressed after the gap formation occurs. If B is smaller than 50, the gap formation suppresses the orbital migration. The gap size is not affected by the orbital migration. On the other hand, for $B \gtrsim 60$, the protoplanet moves rapidly such that it escapes from the gap. Thus, in this case, protoplanet moves large distance, and the gap formation is inhibited.

The condition for the inhibitation of gap formation is derived as follows. The differential between the inner and outer torque is derived by Ward(1986) as

$$\Delta T = -Cq^2 \left(\frac{\sigma r^6 \Omega^4}{c^2} \right)_p , \tag{3.23}$$

where C is a numerical factor of order of unity. This differential torque causes the change of protoplanet's angular momentum, written as

$$\frac{d}{dt}(M_p r_p^2 \Omega_p) = \Delta T. \tag{3.24}$$

The rate of the orbital drift is

$$\frac{dr_p}{dt} = \frac{2\Delta T}{M_p \Omega_p r_p}. \tag{3.25}$$

The time required for the protoplanet to escape from the gap of the size Δr is

$$t_{escape} = \Delta r \left| \frac{dr_p}{dt} \right|^{-1} = \frac{M}{2Cq} \left(\frac{c^2}{\sigma r^5 \Omega^3} \right)_p \Delta r. \tag{3.26}$$

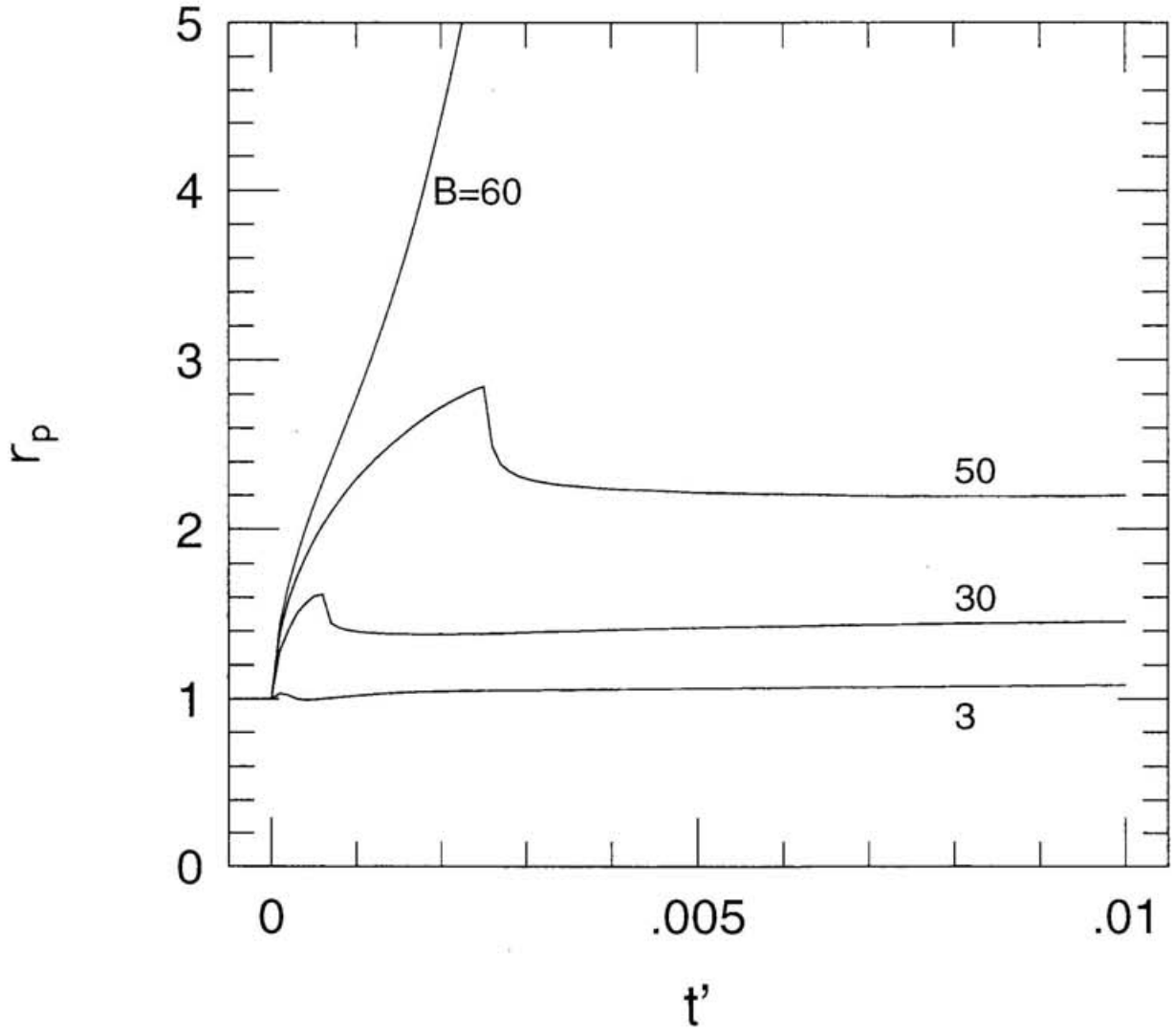

Fig. 3-14.— Evolution of the orbital radius of the protoplanet. The values of A, h_0 and α are $10^{-1}, 0.05$ and 10^{-3}, respectively. Each line is labeled by the protoplanet's mobility, B. At $t' = 0$, the protoplanet is located at $r_p = 1$.

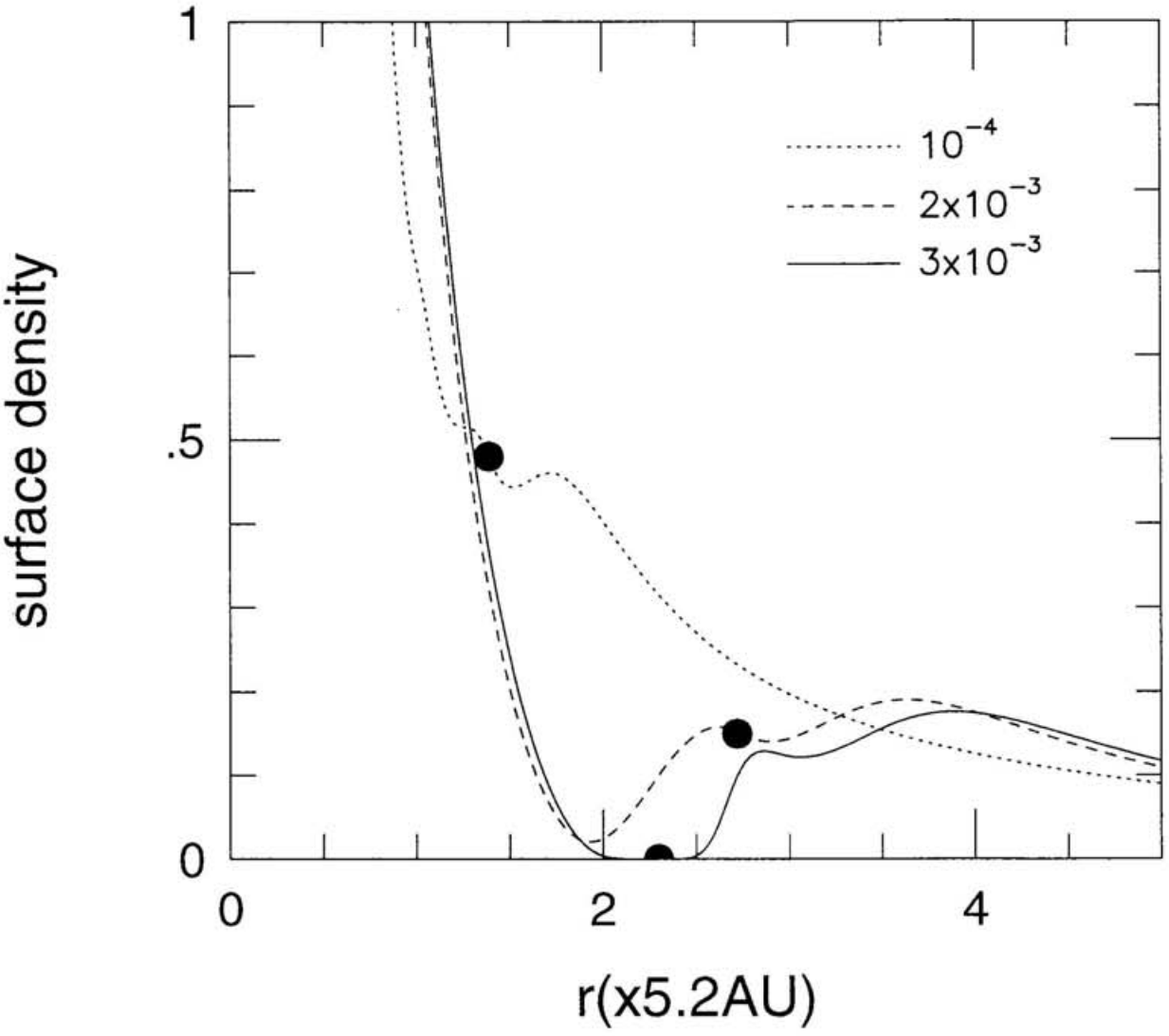

Fig. 3-15.— Surface density evolution of the disk for $B = 50$. The values of A, h_0 and α are $10^{-1}, 0.05$ and 10^{-3}, respectively. The dots, dashes, and solid curve correspond to $t' = 10^{-4}, 2 \times 10^{-3}, 3 \times 10^{-3}$, respectively. The locations of the protoplanet are shown by the filled circles.

From equations (3.20), (3.22) and (3.26) the condition for the gap formation against the escape of the protoplanet, $t_{open} \lesssim t_{escape}$ becomes

$$q \gtrsim 2.6C \left(\frac{c}{r\Omega}\right)_p^2 \frac{(\sigma r^2)_p}{M} \alpha^{-1/4}. \tag{3.27}$$

The gap formation occurs only if both conditions (3.27) and (3.21) are satisfied.

The α dependence in equation (3.27) implies that for large α's, the gap is narrow and the surface density in the vicinity of the protoplanet's orbit can quickly self adjust in order to maintain a torque balance. This limiting case is equivalent to the impulse approximation adopted by Lin & Papaloizou (1986b) which is based on the assumption that the density waves are dissipated just at the location where they are excited and launched. In this case, when the condition (3.21) is satisfied, gap formation is unlikely to be inhibited by the protoplanet's orbital migration. In the limit of small α, however, the protoplanet's tidal effect spreads over the entire disk such that the disk response becomes more inert. This is equivalent to the situation considered by Ward & Hourigan (1989). In this case, the evolution of disk surface density is inadequate to halt the orbital migration of the protoplanet.

3.5. Calculation for various models

We present the results of the calculation for various models of the protoplanetary disks and discuss the condition for gap formation and the size of the gap formed by a protoplanet with the Jupiter mass in this section.

Table 1 lists the parameters for the protoplanetary disks used in our calculations. Model A is the standard model introduced in §2.4. Variation from the standard model is examined by models B-G; surface density profile is changed in models B and C, sound speed is changed in models D and E, the disk mass is changed in model F, and the initial location of the protoplanet is changed in model G.

Model A — The condition for the gap formation is shown in Figure 3-16. We consider gap formation in the numerical calculation to have occurred if the surface density at the

Table 1. Model parameters.

Model	σ	r_{in}(AU)	r_{out}(AU)	$M_D(M_\odot)$	T	h_0	r_0(AU)	$M(M_\odot)$
A	$\propto r^{-3/2}$	5.2×10^{-2}	52	1.7×10^{-2}	$\propto r^{-1/2}$	5×10^{-2}	5.2	1
B	$\propto r^{-2}$	5.2×10^{-2}	52	8.2×10^{-3}	$\propto r^{-1/2}$	5×10^{-2}	5.2	1
C	*const.*	5.2×10^{-2}	52	1.4×10^{-3}	$\propto r^{-1/2}$	5×10^{-2}	5.2	1
D	$\propto r^{-3/2}$	5.2×10^{-2}	52	1.7×10^{-2}	$\propto r^{-1/2}$	2.5×10^{-2}	5.2	1
E	$\propto r^{-3/2}$	5.2×10^{-2}	52	1.7×10^{-2}	$\propto r^{-1/2}$	10^{-1}	5.2	1
F	$\propto r^{-3/2}$	5.2×10^{-2}	52	1.7×10^{-1}	$\propto r^{-1/2}$	5×10^{-2}	5.2	1
G	$\propto r^{-3/2}$	5.2×10^{-2}	52	1.7×10^{-2}	$\propto r^{-1/2}$	5×10^{-2}	9.6	1

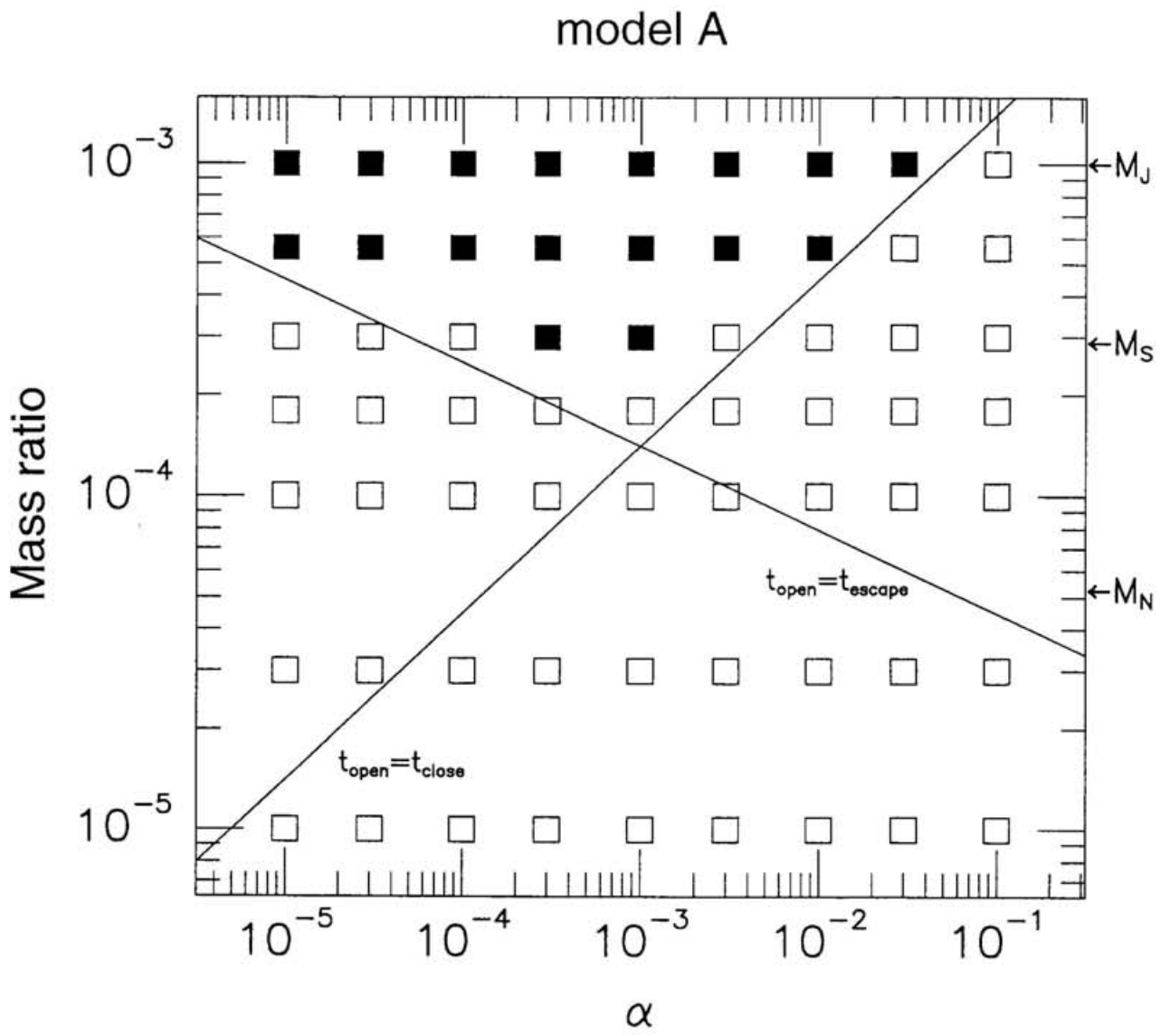

Fig. 3-16.— Condition for gap formation in model A. The filled squares represent the gap formation in the numerical calculation. The open squares represent the absence of a gap in the numerical calculation. Two solid lines indicate the critical conditions for the gap formation, $t_{open} < t_{close}$ and $t_{open} < t_{escape}$. The masses of Jupiter, Saturn, and Neptune are indicated on right axis.

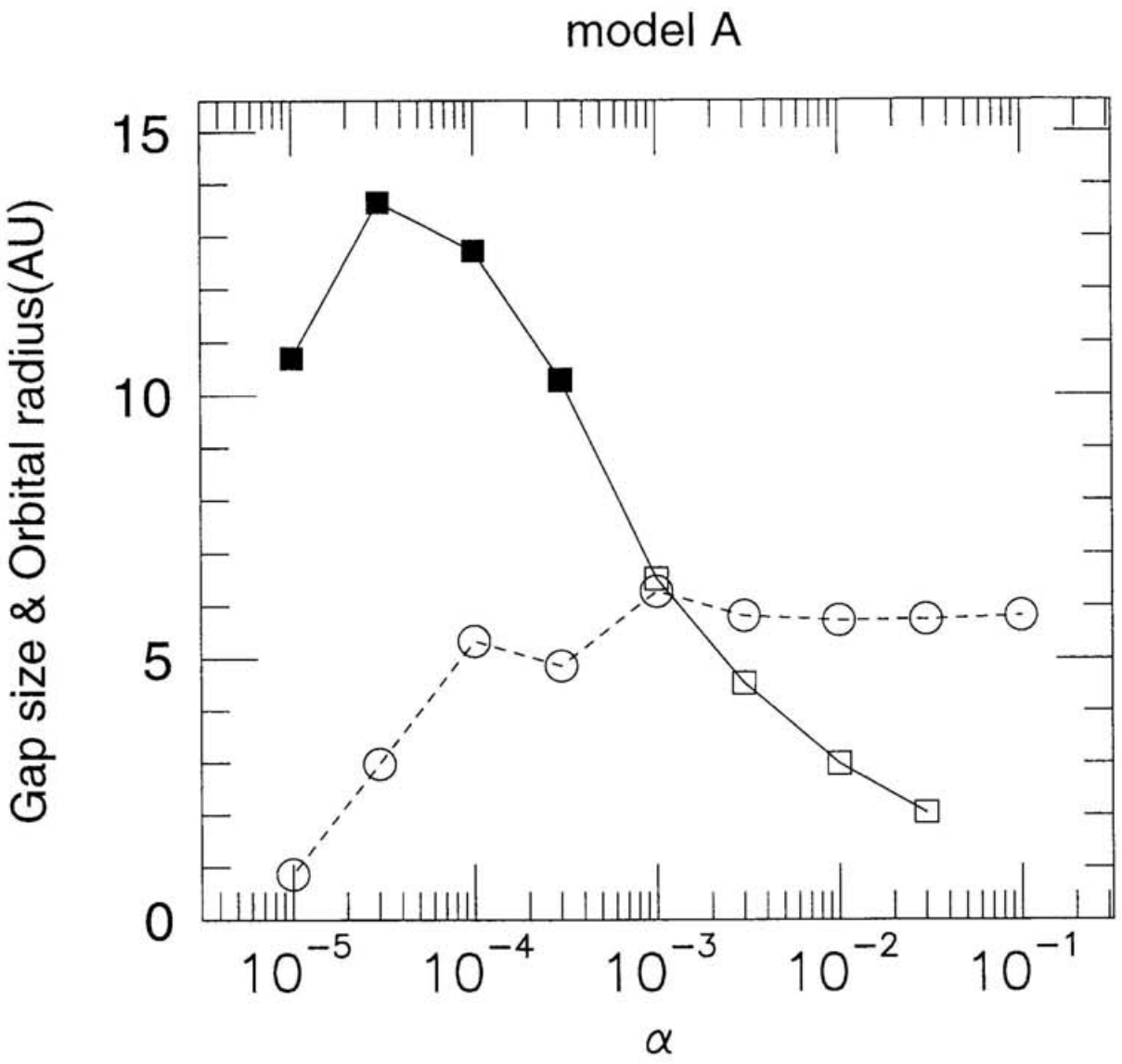

Fig. 3-17.— Gap size opened by a Jupiter mass protoplanet and location of the protoplanet in model A. The squares show gap size at $t' = 10^{-1}$. The filled symbols indicate that the inner disk has fallen onto Sun. If the inner disk is removed, the radius of the inner edge of the outer disk is plotted. The circles show the location of the protoplanet at $t' = 10^{-1}$.

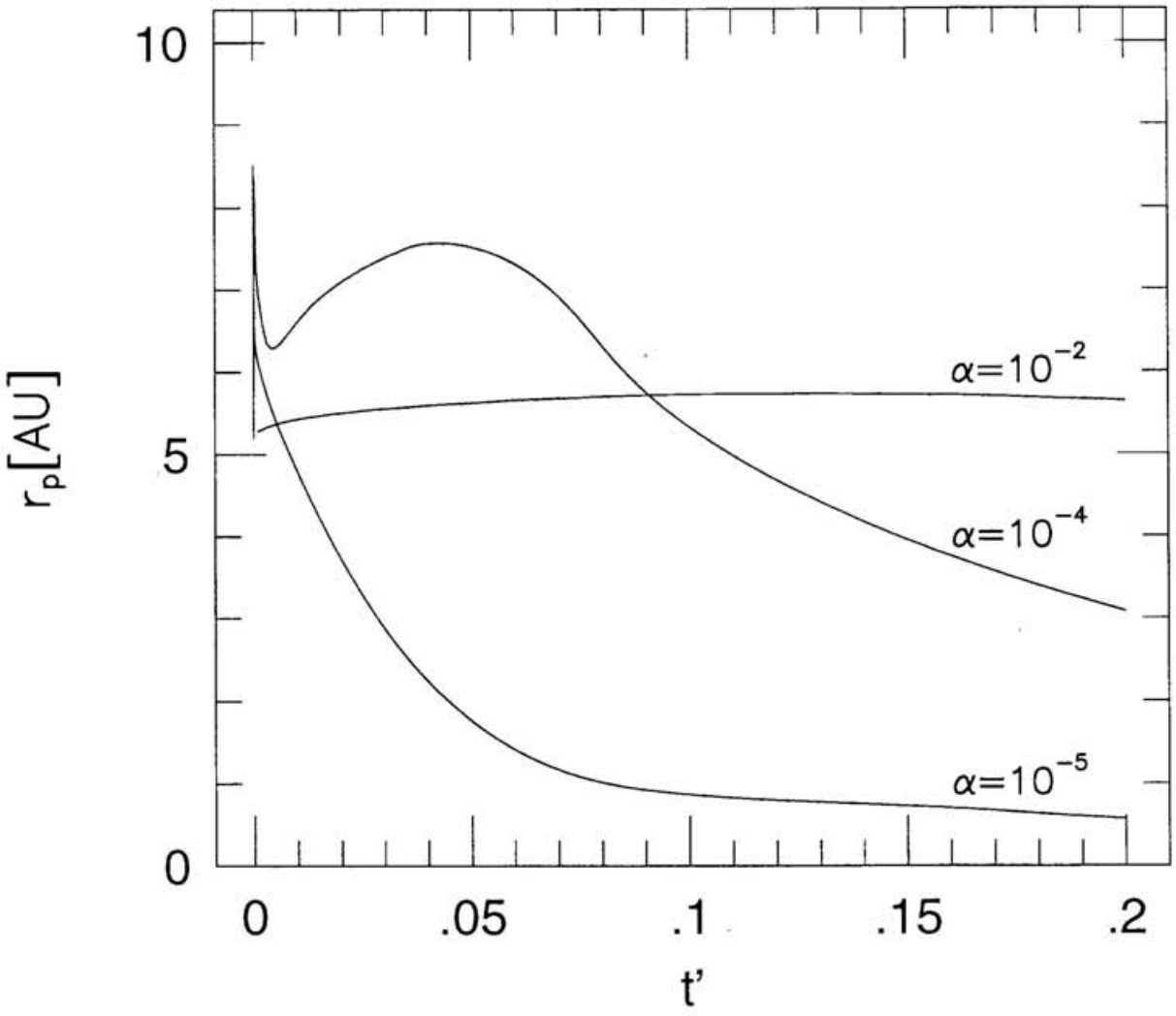

Fig. 3-18.— Orbital evolution of the protoplanet with Jupiter mass in model A.

protoplanet's position is reduced to less than the one tenth of the value for the disk without the protoplanet. The filled squares represent that a gap opens in the numerical calculation. The open squares indicate the absence of a gap. Two solid lines show the boundary of the conditions for the gap formation, $t_{open} \lesssim t_{close}$ and $t_{open} \lesssim t_{escape}$, with a numerical correction factor applied in order to fit the numerical result. With these correction factors, $t_{open} \lesssim t_{close}$ (inequality [3.21]), becomes

$$q \gtrsim 8.0 \left(\frac{c}{r\Omega}\right)_p^{5/2} \alpha^{1/2}, \tag{3.28}$$

and $t_{open} \lesssim t_{escape}$ (inequality [3.27] with opposite inequality sign) becomes

$$q \gtrsim 8.4C \left(\frac{c}{r\Omega}\right)_p^{2} \frac{(\sigma r^2)_p}{M} \alpha^{-1/4}. \tag{3.29}$$

The numerical results in Figure 3-16 indicate that a gap opens when both conditions are satisfied. For the adopted model parameters, the mass of the protoplanet must be larger than $3 \times 10^{-4} M$ in order to form a gap. This value is about the Saturn mass.

Figure 3-17 shows the gap size formed by a protoplanet with the Jupiter mass ($q = 10^{-3}$) at $t' = 10^{-1}$. It also shows the location of the protoplanet at $t' = 10^{-1}$.

For the protoplanet with the Jupiter mass, $A = q^2/(3\alpha h_0^2) \approx 10^{-4}\alpha^{-1}$ is much less than unity if $\alpha \gtrsim 10^{-3}$. The condition for gap formation through the waves with mode $m = 1$ or 2 (eq. [3.17]) is not satisfied if $A \ll 1$. Thus, for $\alpha \gtrsim 10^{-3}$, we argue the gap size according to the discussion for $A = 10^{-1}$ or 10^{-2} cases described in §3.3. In this case the gap size is obtained as the larger one of the values derived from equations (3.11) and (3.22). For the protoplanet with the Jupiter mass in the disk model A with $\alpha \gtrsim 10^{-3}$, the gap size derived from equation (3.11), which is derived under the assumption of immediately damping of the waves, exceeds the value derived as the damping length of the waves from equation (3.22). Hence, the gap size is mainly determined by the balance between the tidal torque and viscous diffusion. The gap size increases as α decreases, because the effect of viscous diffusion becomes weak. For $\alpha \gtrsim 10^{-1}$, A is smaller than 10^{-3}. Under such the large viscosity, even the waves with $m \sim (r\Omega/c)_p \sim 20$ cannot open a gap against the viscous diffusion, as seen from equation (3.17). Thus, the gap formation is inhibited. The

protoplanet moves in viscous time scale after the gap formation. In model A, the surface density profile, $\sigma \propto r^{-3/2}$ is adopted. In this case, the protoplanet happens to move little distance. However, the protoplanet can move large distance in the disk with the another surface density profile (see model B or C).

For $\alpha \lesssim 3 \times 10^{-4}$, A is as large as or larger than unity. In this case, $m = 2$ waves can be effective to open a gap, as discussed $A = 1$ case in §3.3. The protoplanet removes the disk inside it through the $m = 2$ waves, because $m = 2$ waves can propagate throughout the inner disk if $\alpha \lesssim 10^{-3}$ (see Fig. 3-2). The time scale of the removal of the inner disk is about 10^5 years. If the viscosity is enough small, such that $m \sim (r\Omega/c)_p$ waves can propagate throughout inner disk ($\alpha \lesssim 10^{-5}$), the removal of the inner disk occurs through $m \sim (r\Omega/c)_p$ waves, and the time scale of the removal is quite short ($\sim 10^3$ years).

After the removal of the inner disk, the protoplanet interacts with only the outer disk. The protoplanet deposits its angular momentum into the outer disk and migrates inward. Thus, the distance between the protoplanet and the outer disk increases, and the tidal interaction is reduced. Hence, a protoplanet cannot dissipate the outer disk. It can only push the disk material away to a distance of about 15AU. For $\alpha = 10^{-5}$, the inner radius of the outer disk is smaller than the case of $\alpha = 3 \times 10^{-5}$. For $\alpha = 10^{-5}$, the waves in the outer disk can propagate substantial distance from the protoplanet, and the gap size which protoplanet should form is quite wide. In this case, the gap formation should take a long time, and when inner disk is removed, gap formation in the outer disk have not finished(see Fig. 3-8d). Hence, the protoplanet migrates inward largely after the removal of the inner disk, and the inner radius of the outer disk remains small.

Figure 3-18 shows the orbital evolution of the protoplanet with Jupiter mass. Note that r_p is plotted as a function of non-dimensional time t'; for $\alpha = 10^{-2}, 10^{-4}$ and 10^{-5}, $t' = 10^{-1}$ corresponds respectively to $10^4, 10^6$ and 10^7 years in real time. For $\alpha = 10^{-2}$, the gap formation completes by $t' = 10^{-3}$. It suppresses the rapid migration of the protoplanet. For $\alpha = 10^{-4}$, it takes longer time than $\alpha = 10^{-2}$ to open a gap, because the gap is wider. Thus,

the protoplanet migrates outward rapidly during the gap formation. After the gap formation ($t' = 3 \times 10^{-4}$), the migration of the protoplanet becomes mild. As $m = 2$ waves remove the inner disk, the interaction between the protoplanet and the inner disk becomes weaker, and the protoplanet turns to inward. The removal of the inner disk finishes at $t' = 9 \times 10^{-2}$. For $\alpha = 10^{-5}$, the protoplanet moves outward and reach about 9.5AU quickly. However the inner disk is removed through $m \sim (r\Omega/c)_p$ waves by $t' = 10^{-5}$. The protoplanet migrates inward after that.

Model B — The profile of the initial surface density of model B is $\sigma \propto r^{-2}$. The surface density at the initial location of the protoplanet, $\sigma(r_0)$, is set as the same value with model A because the same amount of the material of the protoplanetary disk around the protoplanet is needed to form the protoplanet with the same mass as model A. This surface density profile yields the disk mass, $M_D = 8.2 \times 10^{-3} M$.

Figure 3-19 shows the condition for gap formation, and Figure 3-20 shows the gap size and the location of the protoplanet at $t' = 10^{-1}$. The protoplanet gains much more angular momentum from the disk inside its orbit than the loss of the angular momentum by the disk outside its orbit because of rapid decrease of the surface density with radius. Thus, the protoplanet migrates outward, where surface density is smaller (Fig. 3-20). This migration reduces the torque exerted on the disk. Consequently, it takes much longer time for the protoplanet to remove the inner disk than model A. The protoplanet removes the inner disk through $m = 2$ waves in $10^6 - 10^7$ years (in non-dimensional time, $t' \approx 3 \times 10^{-1}$) for $3 \times 10^{-5} \lesssim \alpha \lesssim 3 \times 10^{-4}$. In Figure 3-20 the removal of the inner disk for $3 \times 10^{-5} \lesssim \alpha \lesssim 3 \times 10^{-4}$ is not shown, because the disk removal has not completed at $t' = 10^{-1}$, when this figure is plotted. For $\alpha = 10^{-5}$ the inner disk is removed through $m \sim (r\Omega/c)_p$ waves by $t' = 5 \times 10^{-2}$. The protoplanet migrates inward after that.

Model C — The surface density of model C is initially constant, which is the value at the initial position of the protoplanet, $\sigma(r_0)$, in model A. The mass of the disk is $M_D = 1.4 \times 10^{-1} M$. In our calculation, the protoplanet does not move if there is no gradient in

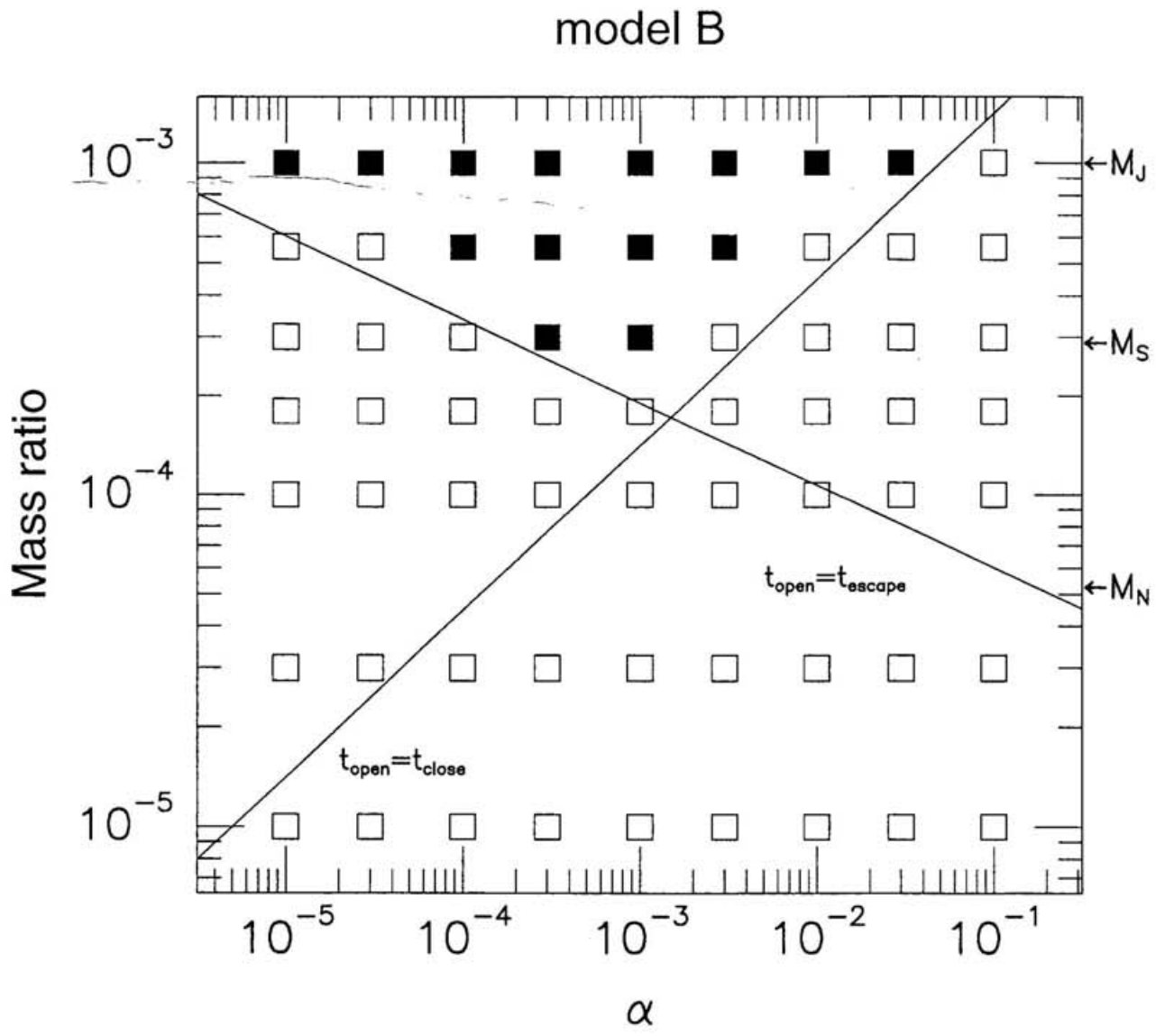

Fig. 3-19.— Condition for gap formation in model B.

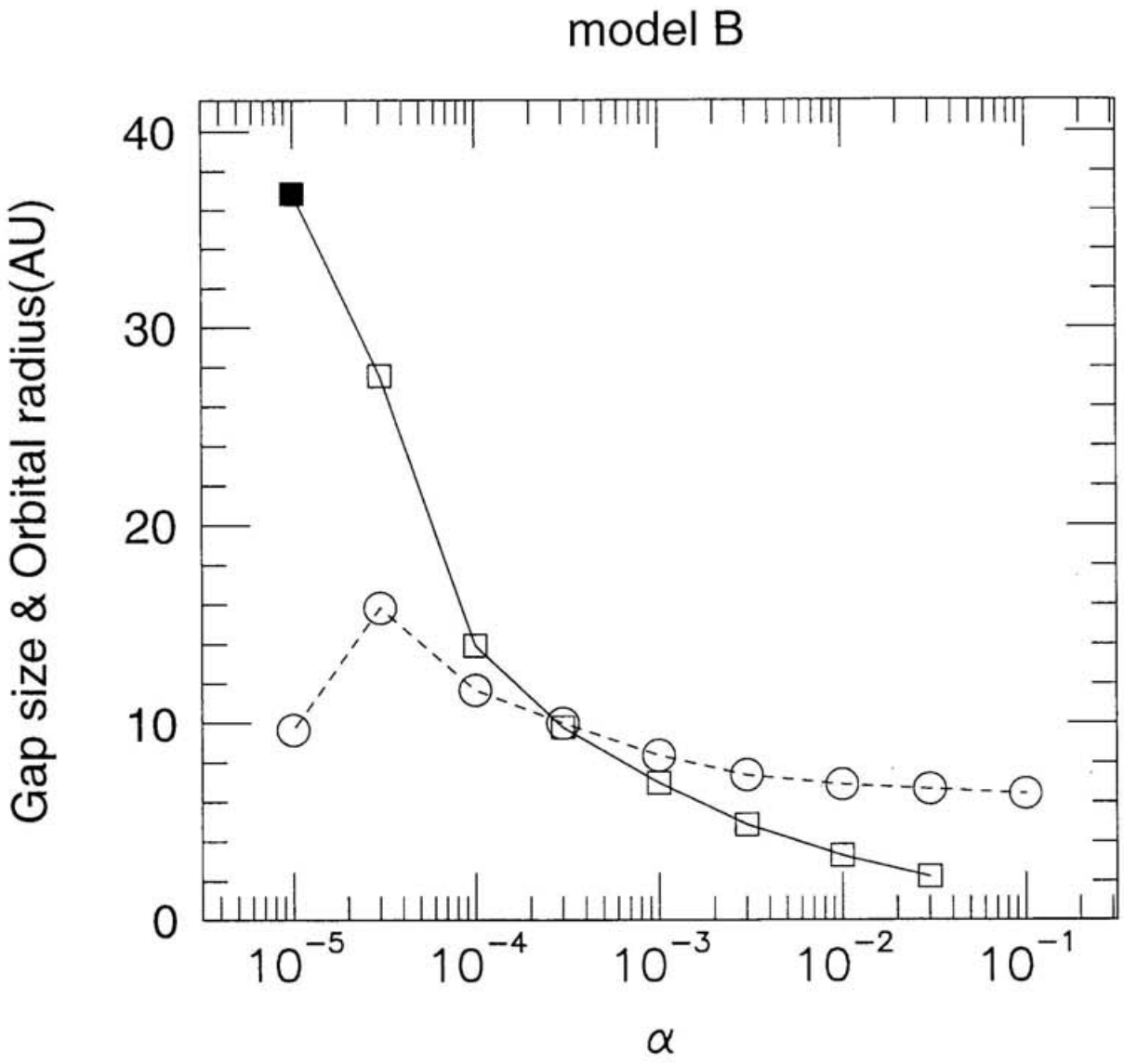

Fig. 3-20.— Gap size opened by a Jupiter mass protoplanet and location of the protoplanet at $t' = 10^{-1}$ in model B.

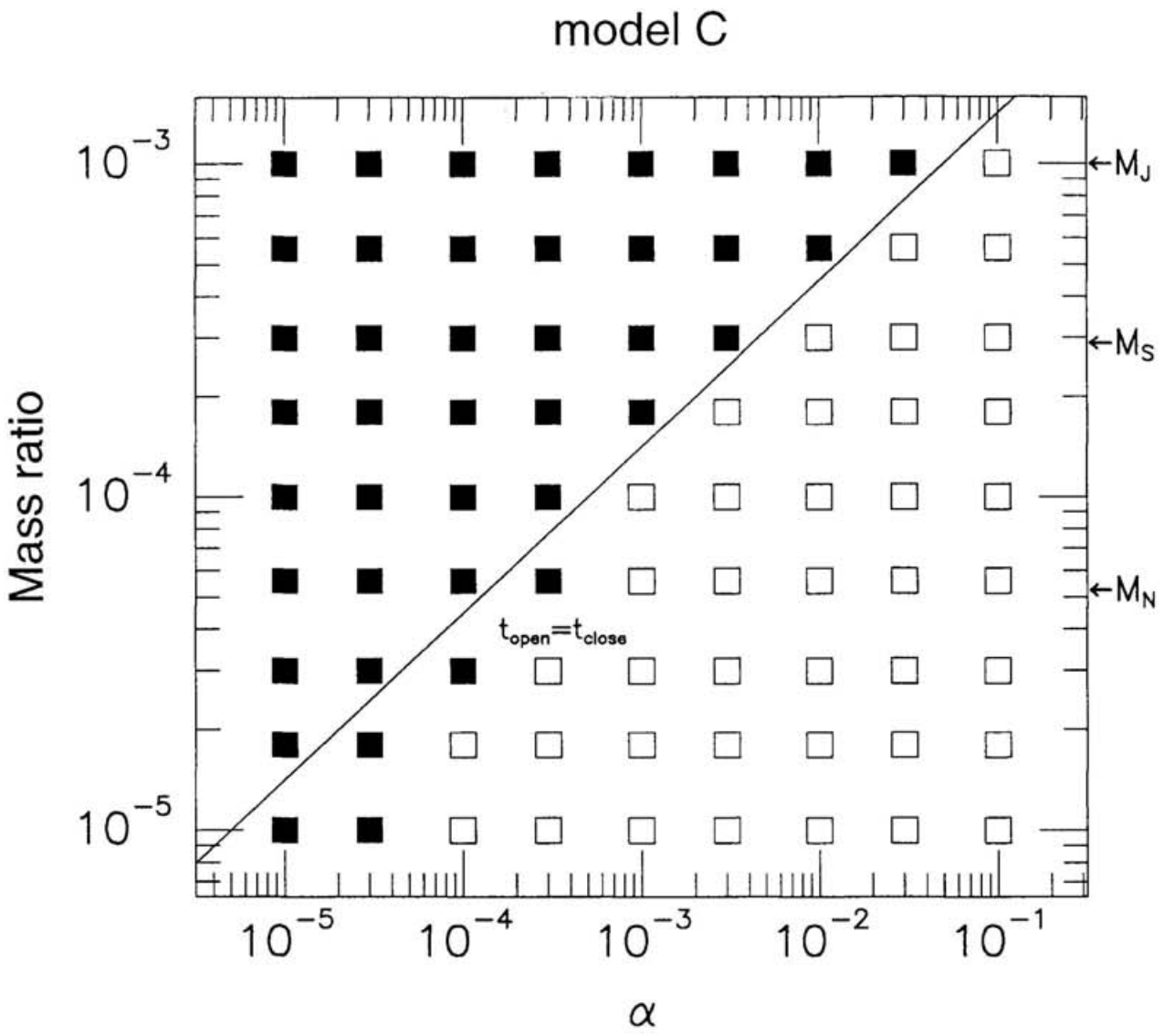

Fig. 3-21.— Condition for gap formation in model C.

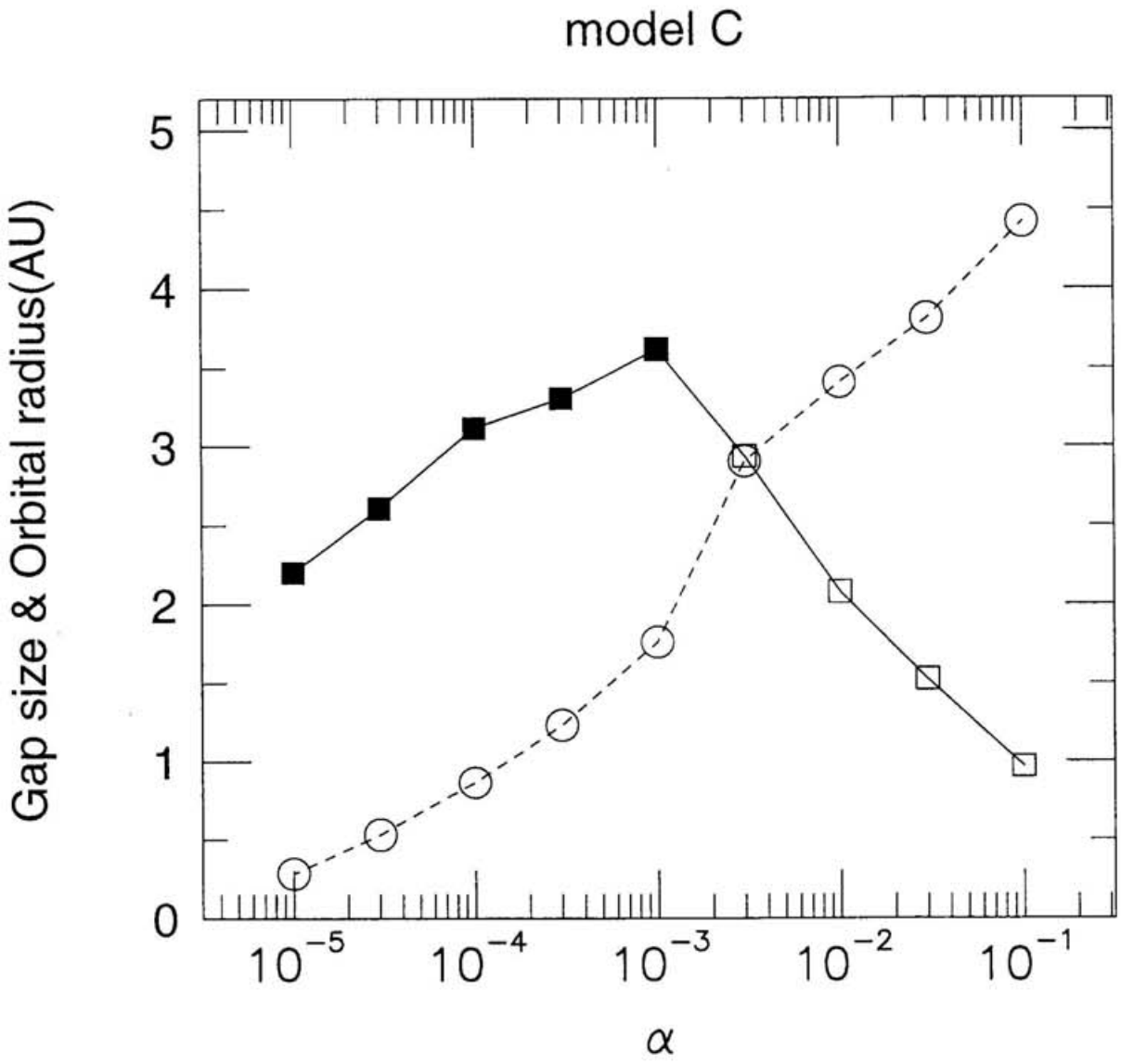

Fig. 3-22.— Gap size opened by a Jupiter mass protoplanet and location of the protoplanet at $t' = 10^{-1}$ in model C.

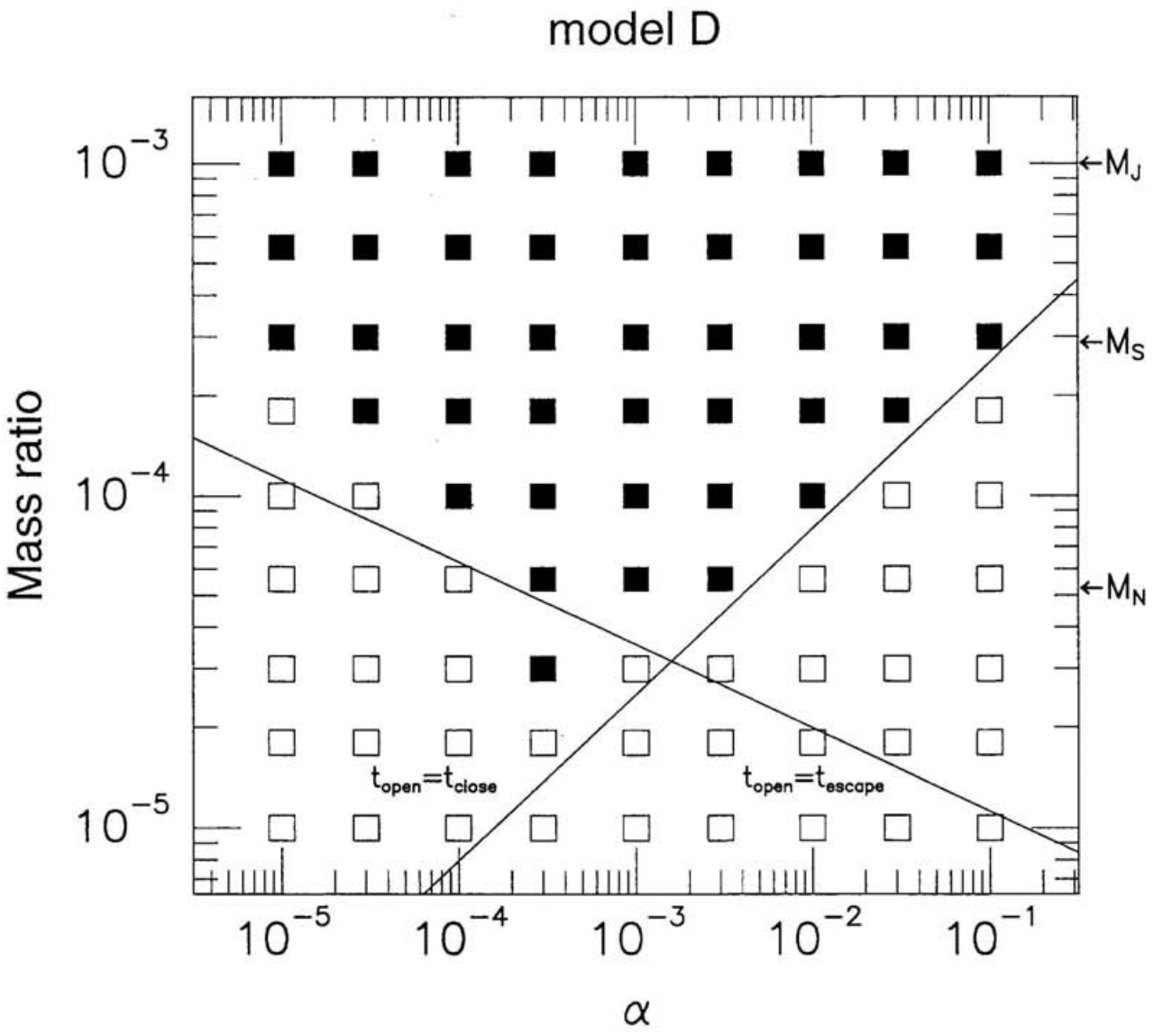

Fig. 3-23.— Condition for gap formation in model D.

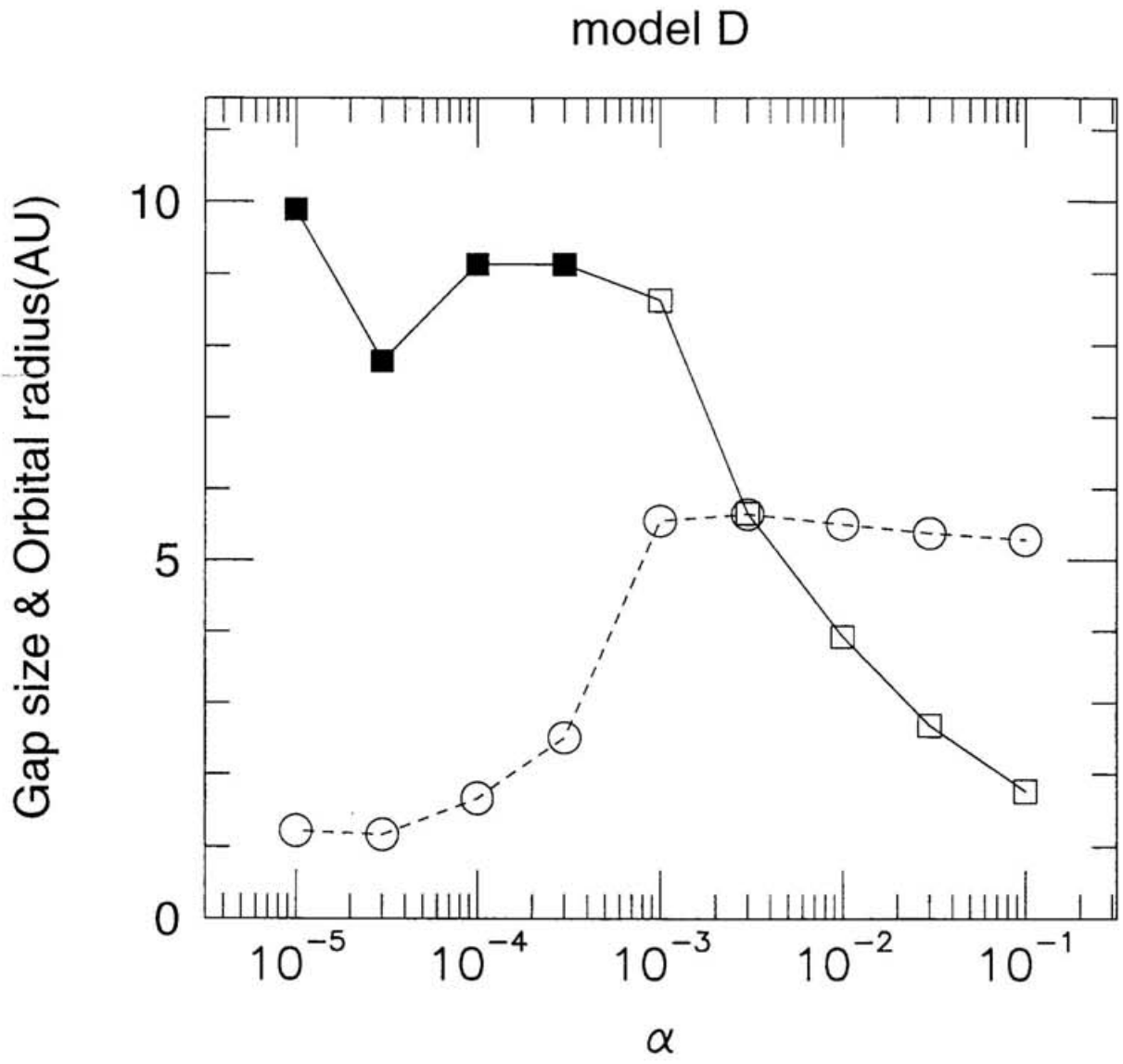

Fig. 3-24.— Gap size opened by a Jupiter mass protoplanet and location of the protoplanet at $t' = 10^{-1}$ in model D.

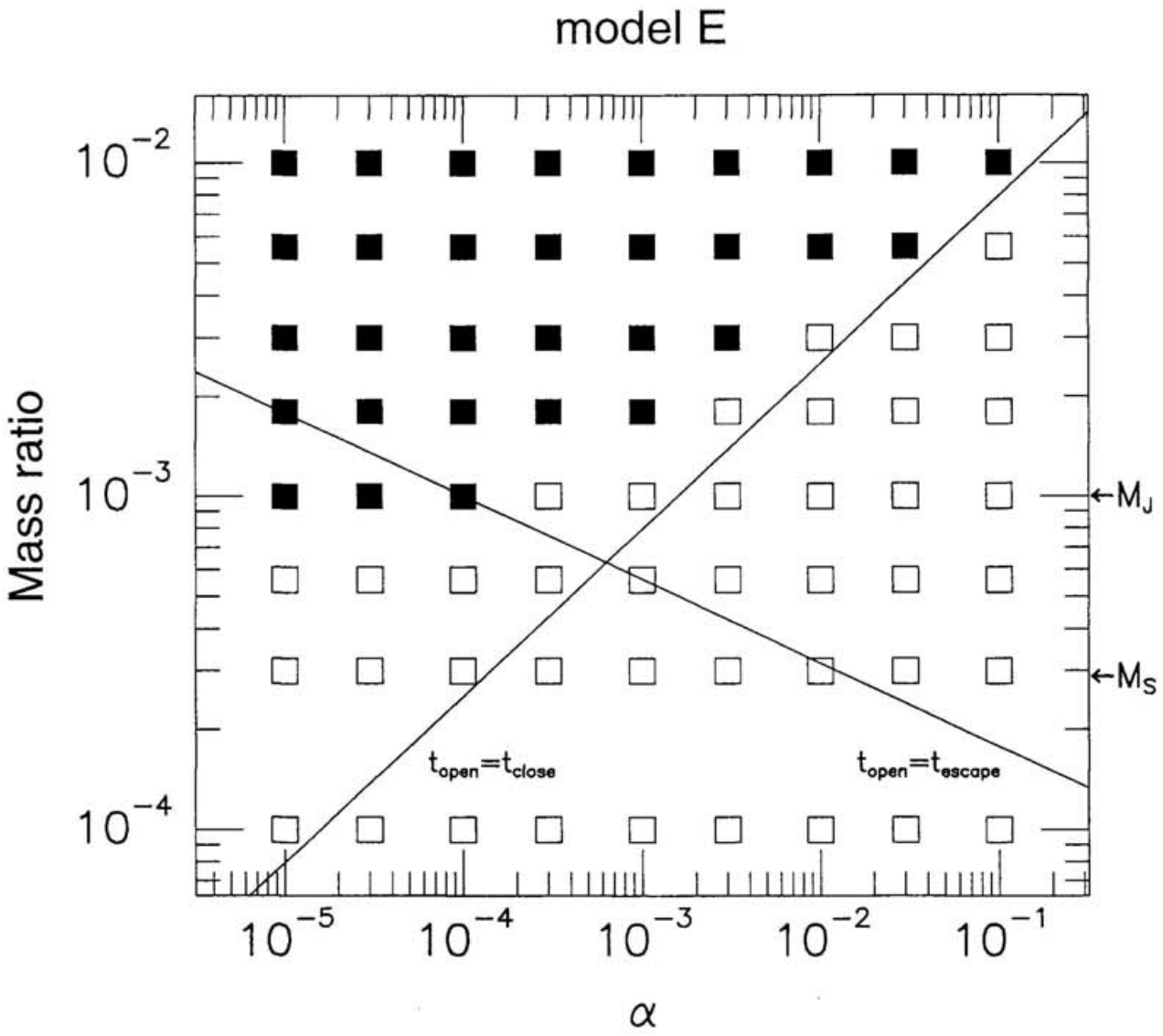

Fig. 3-25.— Condition for gap formation in model E.

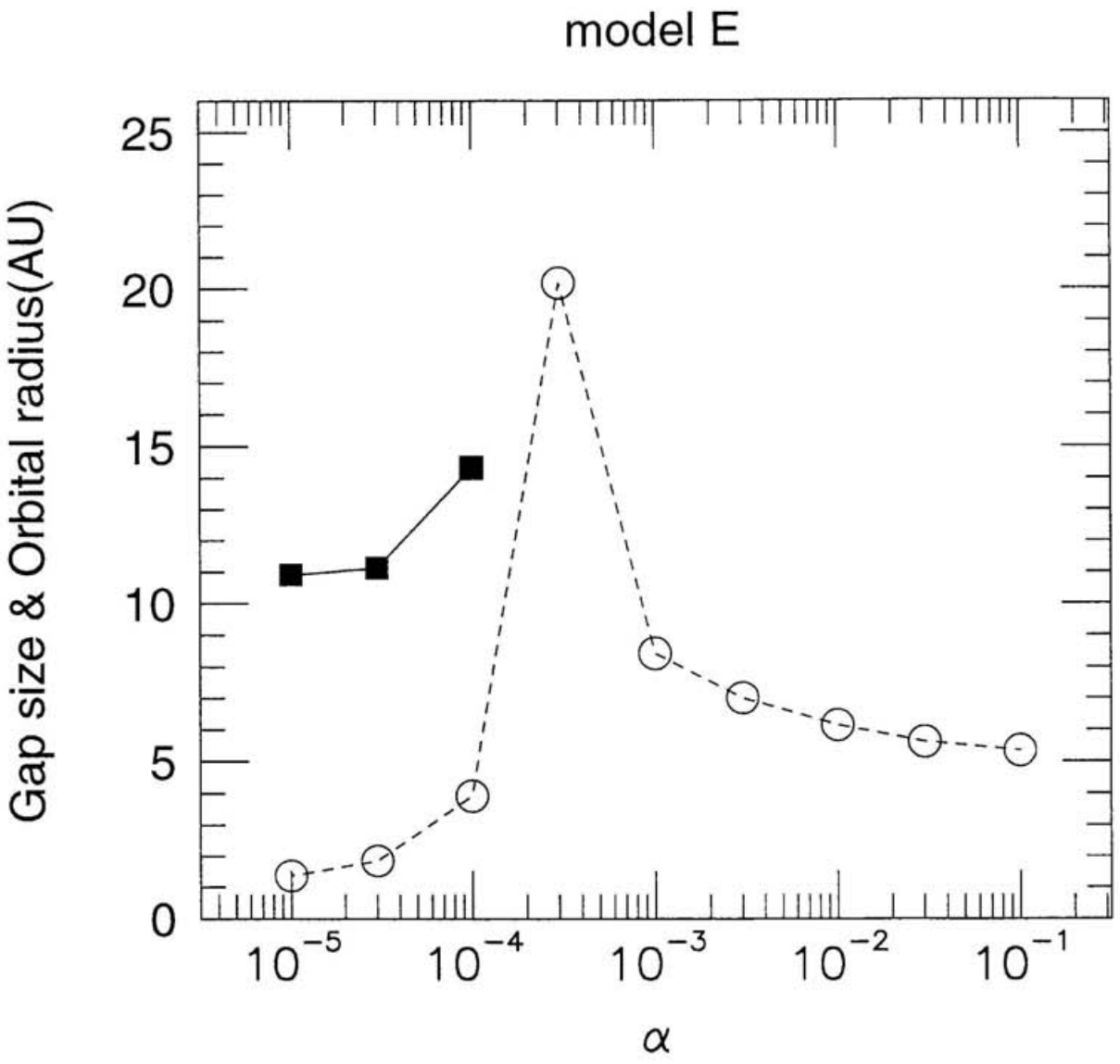

Fig. 3-26.— Gap size opened by a Jupiter mass protoplanet and location of the protoplanet at $t' = 10^{-1}$ in model E.

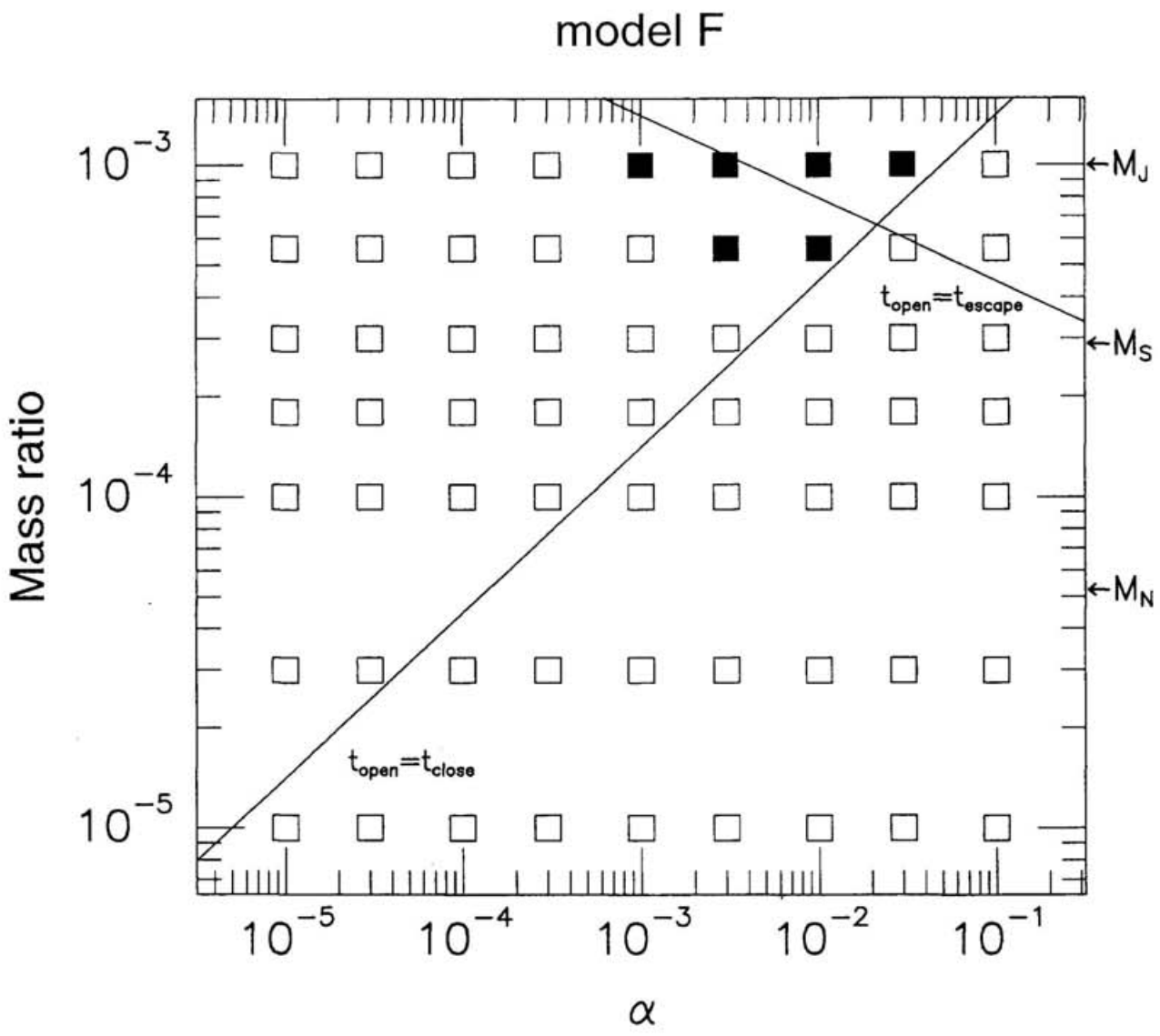

Fig. 3-27.— Condition for gap formation in model F.

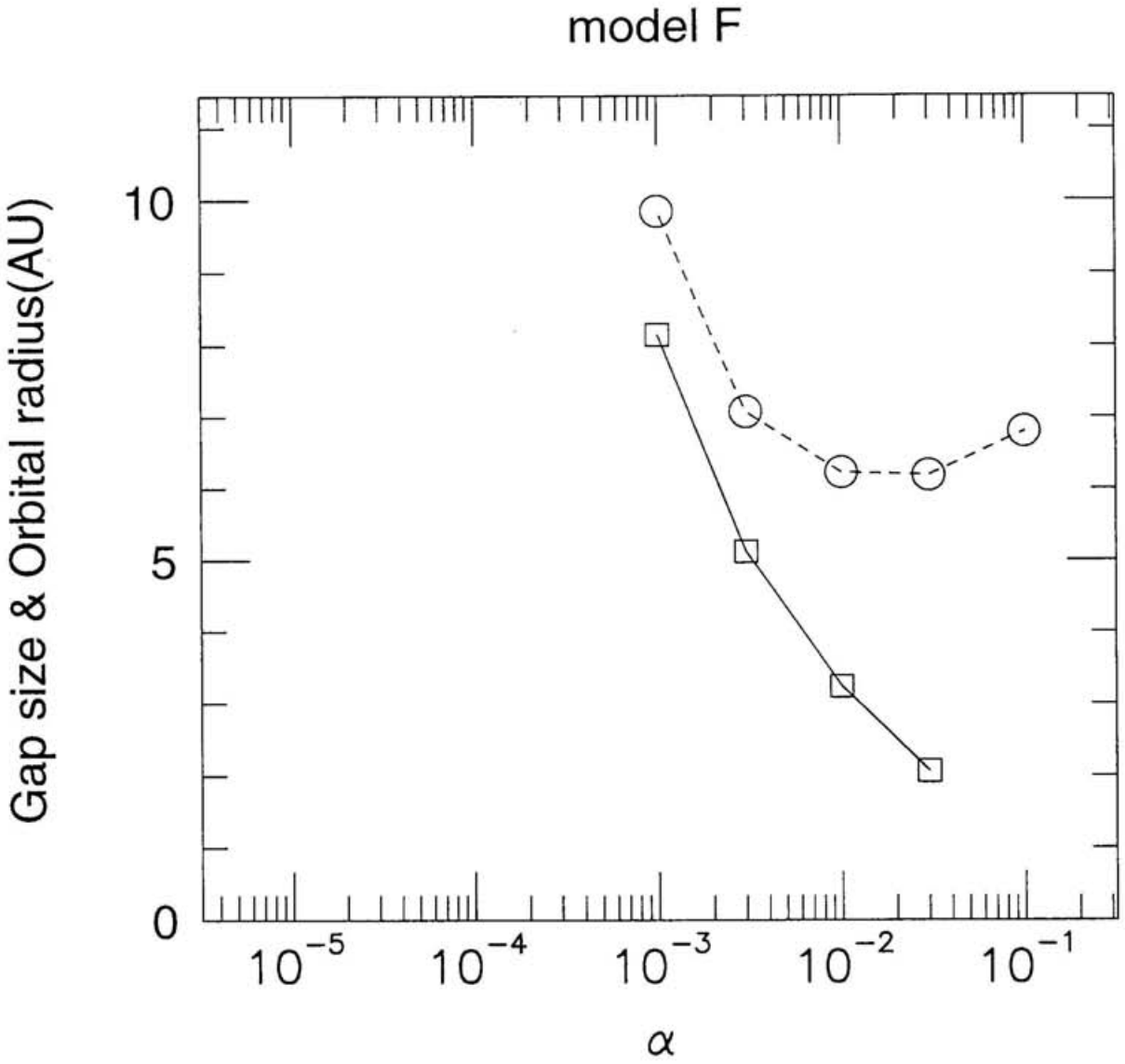

Fig. 3-28.— Gap size opened by a Jupiter mass protoplanet and location of the protoplanet at $t' = 10^{-1}$ in model F.

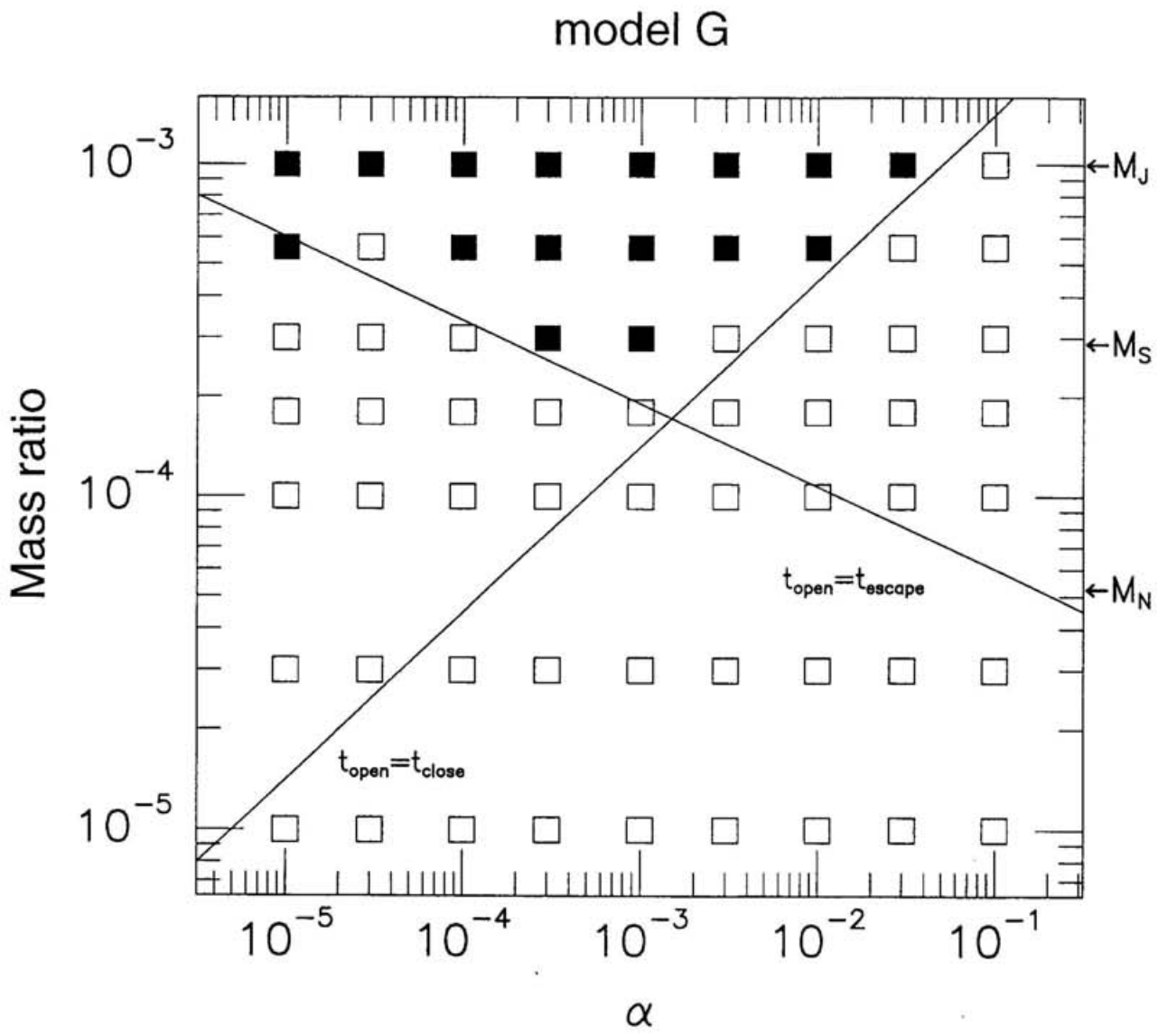

Fig. 3-29.— Condition for gap formation in model G.

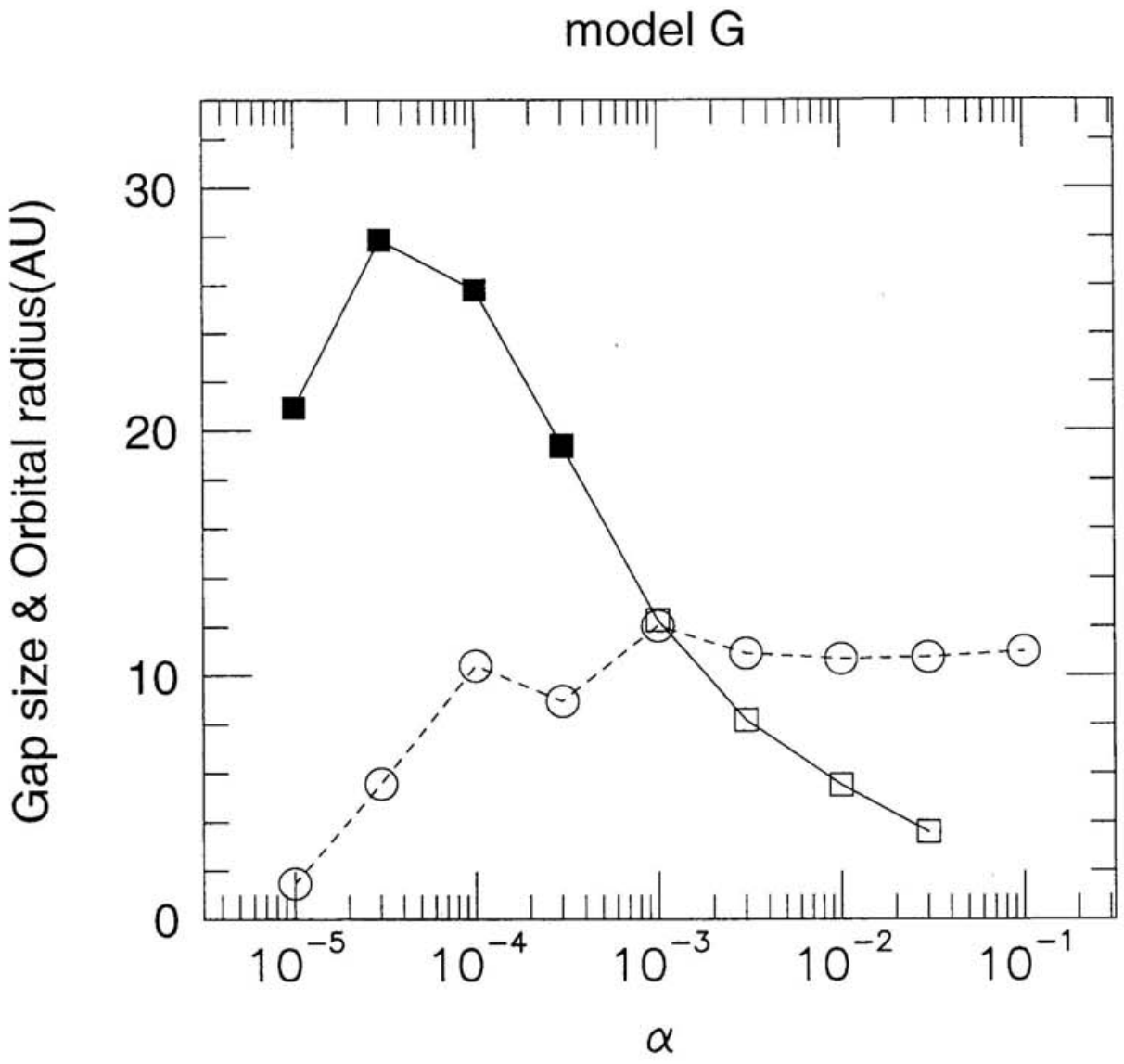

Fig. 3-30.— Gap size opened by a Jupiter mass protoplanet and location of the protoplanet at $t' = 10^{-1}$ in model G.

density profile (see discussion in §3.4). Thus, the protoplanet does not migrate at first. After the surface density profile was changed by the protoplanet's torque and the density gradient was produced, the protoplanet begins to move. Because the protoplanet moves toward where the surface density is reduced, it would be trapped in the gap. Thus, the inhibitation of gap formation due to the rapid migration of the protoplanet does not occur (Fig. 3-21). Because there is little material in the innermost part of the disk with the constant surface density, the protoplanet opens an inner hole quickly if the waves reach the innermost part of the disk. Even the protoplanet with a mass as small as $q = 10^{-5}$ can open a inner hole ($\sim$ 3AU) if $\alpha \lesssim 3 \times 10^{-5}$, in spite of the condition $t_{open} < t_{close}$ is not satisfied. The protoplanet's torque changes the surface density to be increasing with radius. This evolution of the surface density causes the inward migration of the protoplanet (Fig. 3-22). In particular, when an inner hole is formed, the protoplanet migrates inward quickly to be trapped in the inner hole. Hence, the protoplanet can make only a small inner hole with radius of $\sim$ 3AU, and its orbital radius is quite reduced.

Model D — The scale height (i.e. sound speed) at the initial position of the protoplanet is half of model A ($h_0 = (c/r\Omega)_p = 2.5 \times 10^{-2}$). The LRs up to $m \sim (r\Omega/c)_p$ are effective in exerting torque. Thus, the protoplanet exerts more torque as sound speed decreases. The protoplanet larger than about Neptune mass ($q \gtrsim 3 \times 10^{-5}$) can open a gap in model D (Fig. 3-23). The gap size and the location of the protoplanet is shown in Figure 3-24.

Model E — The scale height (i.e. sound speed) at the initial position of the protoplanet is twice of model A ($h_0 = (c/r\Omega)_p = 10^{-1}$). The condition of gap formation is shown in Figure 3-25. With the large value of the sound speed, in this model the LRs only up to $m \sim (r\Omega/c)_p \sim 10$ are effective in exerting torque. Hence, even the protoplanet with a Jupiter mass cannot open a gap against viscous diffusion if $\alpha \gtrsim 3 \times 10^4$. For the cases of $q = 10^{-3}$ and $\alpha \approx 10^{-5}$, a gap is formed, although these cases locate in the region of the inhibitation of gap formation due to the migration of the protoplanet in Figure 3-25. This is because the gap size is overestimated in the process of deriving the condition $t_{open} < t_{escape}$ for these cases. For $\alpha \lesssim 10^{-4}$, the gap size, Δr, derived from equation (3.22) with such

a large sound speed is larger than r_p. Because the distance between the inner edge of the gap and the protoplanet cannot exceed r_p, equation (3.22) overestimates the size of the gap formed inside the protoplanet's orbit. Using $\Delta r = r_p$ as the size of the gap, the condition, $t_{open} < t_{escape}$ with the correction factor same as equation (3.29) becomes

$$q \lesssim 6.5C\frac{(\sigma r^2)_p}{M}\left(\frac{c}{r\Omega}\right)_p \sim 8 \times 10^{-4}, \tag{3.30}$$

which explains the numerical results. The gap size and the location of the protoplanet is shown in Figure 3-26.

Model F — The mass of the protoplanetary disk ($M_D = 1.7 \times 10^{-1} M$) is 10 times larger than model A. As the disk mass increases, the disk becomes more inert, and the tidal torque works to move protoplanet rather than to change disk structure. For $\alpha \lesssim 10^{-3}$, the protoplanet with a Jupiter mass moves outward rapidly and cannot open a gap (Fig. 3-27). Therefore, the removal of the inner disk due to the protoplanet does not occur (Fig. 3-28).

Model G — The initial position of the protoplanet is 9.6AU (present position of Saturn). The scale height at the initial position of the protoplanet is $h_0 = 5 \times 10^{-2}$, same as model A. The result is quite similar to that obtained in model A, except that the values of the gap size and the position of the protoplanet become about twice of that in model A (Figs. 3-29 and 3-30). Hence, we conclude that the initial position of the protoplanet does not affect neither the condition for the gap formation nor the gap size within the scaling factor. However, if the scale height of the disk varies with the radius, the protoplanets with the different initial positions cause the different results via the variation of the scale height at the position of the protoplanets, as discussed in models D and E.

To summarize, the essential conclusions to be drawn from above results are:

1. The condition for the gap formation are written by $t_{open} < t_{close}$ and $t_{open} < t_{escape}$.

2. The protoplanet with the Jupiter mass removes the disk inside its orbit for $\alpha \lesssim 3 \times 10^{-4}$ unless it migrates outward rapidly. This removal of the inner disk can occur even through $m = 2$ waves.

3. After the removal of the inner disk, the protoplanet migrates inward in viscous time scale.

Chapter 4

Application

4.1. Spectral evolution of the protoplanetary disks

Recent observations of binary pre-main-sequence stars show that binary companions affect the structure of protoplanetary disks (Dutrey, Guilloteau & Simon 1994; Mathieu 1994; Roddier et al. 1996). In particular for close binary systems, infrared spectral energy distribution (SED) shows the presence of a gap in protoplanetary disks by the absence of radiation flux which would normally have emerged from that region of the disk (Mathieu, Adams & Latham 1991; Marsh & Mahoney 1992; Mathieu 1994). Marsh & Mahoney(1992, 1993) reported the similar changes in the SEDs of the protoplanetary disks around pre-main-sequence stars, whose binary companions are not detected. They argued the presence of the unseen companions, i.e. planets.

Another mechanisms are also proposed to explain the SED with a dip. Boss & Yorke (1993) showed that the temperature distribution which shows a dip in the SED can be produced during the formation process of the protoplanetary disks. Miyake & Nakagawa (1995) pointed out that some objects show mass accretion rates higher in innermost parts than in outer parts of the disks. These different mass accretion rates in the inner and outer parts of the disks could produce inner holes in the disks, which cause the deficit in near-infrared fluxes. They also argued that the rapid growth of the dust particle in the inner part

of the disks can cause a dip in the SED.

In this section, we investigate the evolution of the SED due to the presence of the protoplanet with the Jupiter mass. To make models for the SED of pre-main-sequence stars with planets, we adopt the following simplifying assumptions.

1. We assume that the central star has the typical values for T Tauri stars (Beckwith et al. 1990): the effective temperature and the luminosity are respectively $T_* = 4000$K and $L_* = 1L_\odot$. With these parameters, we obtain the stellar radius $R_* = (L_*/L_\odot)^{1/2}(T_*/T_\odot)^{-2}R_\odot$ $= 2.09R_\odot \simeq 9.70 \times 10^{-3}$AU.

2. We assume that the protoplanetary disk extends from R_* to $R_d = 100$AU. The temperature distribution is assumed to be a power law in radial distance,

$$T = T_0 \left(\frac{r}{1\mathrm{AU}}\right)^{-p}, \tag{4.1}$$

and isothermal vertically. Here we take $T_0 = 280$K and $p = 1/2$ (Hayashi 1981). This choice of T_0 and p produces the flat spectrum in the SED. If the temperature distribution of the real disks has p greater than $1/2$, then the SED shows less flux in longer wavelengths than our model (Kenyon & Hartmann 1987; Miyake & Nakagawa 1995), but essence of our conclusion does not change.

We use the surface density distribution of the standard model(model A) calculated in the previous chapter. Our calculation of the evolution of the surface density was performed only between 5.2×10^{-2}AU $-$ 52AU. To obtain the surface density profile between R_* and 5.2×10^{-2}AU, it is extrapolated linearly from innermost two meshes of our numerical calculation. For the disks between 50AU and 100AU, we simply use the surface density profile of the power law form according to Hayashi(1981)

$$\sigma = 1700 \left(\frac{r}{1\mathrm{AU}}\right)^{-3/2} \mathrm{g/cm^2}, \tag{4.2}$$

because the protoplanet at several AU does not affects the spectrum emerged from that region.

3. We use the simple opacity law as

$$\kappa_\nu = \begin{cases} 10^{-25.5}\nu^2 & \text{for } \log\nu < 13.05 \\ 10^{0.6} & \text{for } 13.05 \leq \log\nu \leq 13.75 \\ 10^{-23.6}\nu^{1.76} & \text{for } 13.75 \leq \log\nu \end{cases} . \tag{4.3}$$

This approximates the opacity law used in Adams & Shu (1986) and Adams, Lada & Shu (1988), except for the H_2O ice and silicate resonance features. The growth of the dust particles in the protoplanetary disks reduces the power law index of the opacity law in the long wavelength side (Beckwith & Sargent 1991; Miyake & Nakagawa 1993). Although this change of the opacity affects the millimeter wave emission, we neglect this change, because the gap formation due to the protoplanet affects only the near and mid-infrared emission. We also neglected the effect of the evaporation of dust particles near the stellar surface, because we are interested in the evolution of the disk of several AU scale, most of where the dust particles are coagulated. The effect of scattering is also neglected.

Adopting above assumptions, the radiative flux of the entire disk received by an observer at distance D (do not confuse D defined in §2.1) and polar angle θ can be computed from

$$4\pi D^2 F_\nu^D = 4\cos\theta \int_{R_*}^{R_D} \pi B_\nu[T(r)]\{1-\exp(-\tau_\nu)\}2\pi r dr, \tag{4.4}$$

where B_ν is the Planck function and the slant optical depth τ_ν is given by

$$\tau_\nu = \frac{\kappa_\nu \sigma(r)}{\cos\theta}. \tag{4.5}$$

In a similar fashion, the radiant flux received from the star is given through

$$4\pi D^2 F_\nu^* = 4\pi^2 R_*^2 B_\nu(T_*) g_D(\theta). \tag{4.6}$$

Here, $g_D(\theta)$ is the function which takes into account the shadowing of the star by the disk (Adams, Lada & Shu 1988). On the other hand, the shadowing of the disk by the star is neglected. In the following calculations, θ is assumed to be 60° ($\theta = 0°$ is face on).

Figure 4-1 shows the evolution of the surface density for $\alpha = 3 \times 10^{-4}$. The mass of the protoplanet is assumed as the Jupiter mass ($M_p/M = 10^{-3}$). First, a gap is formed around

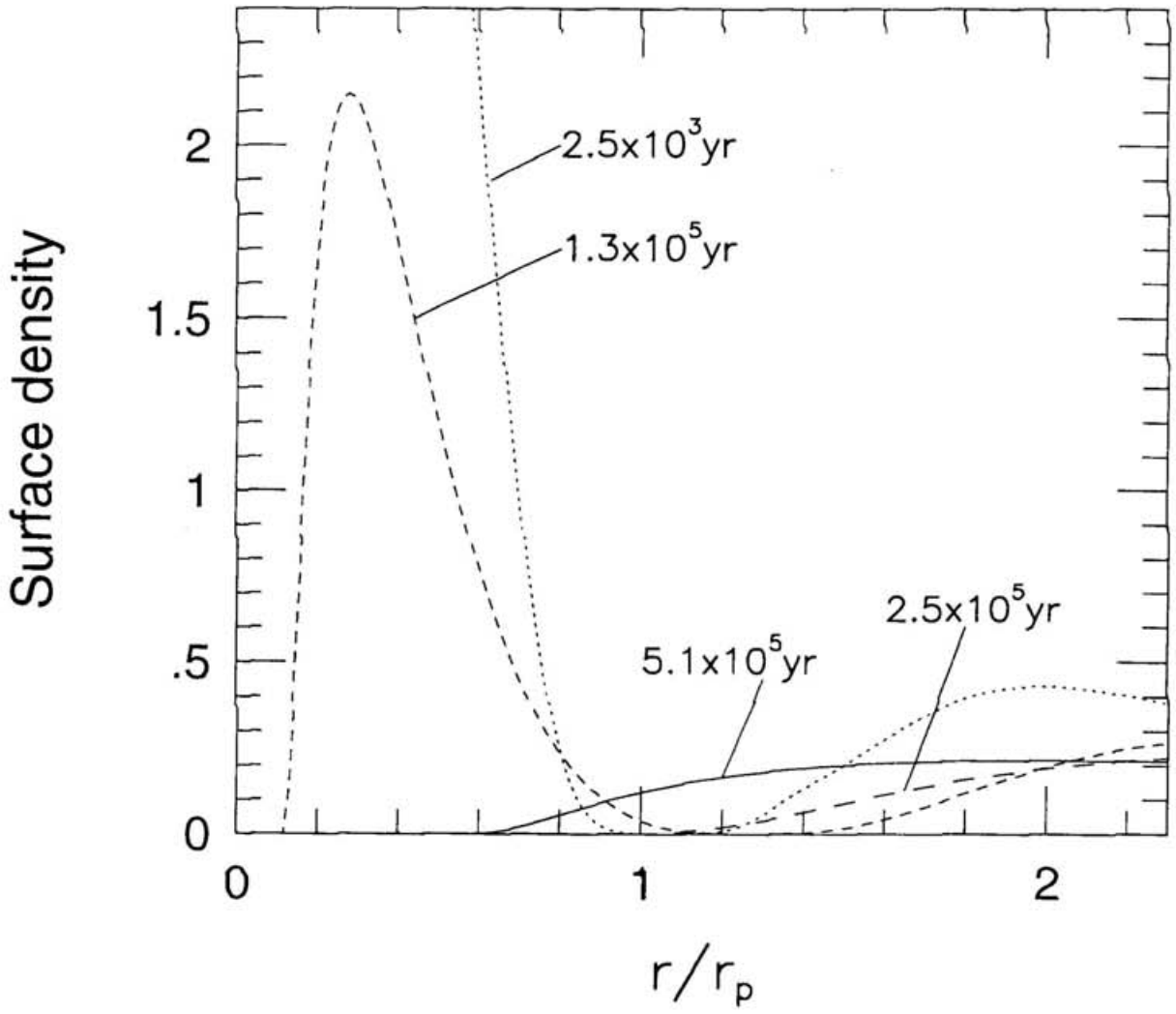

Fig. 4-1.— Evolution of the surface density distribution for model A. Protoplanet's mass is $10^{-3}M$.

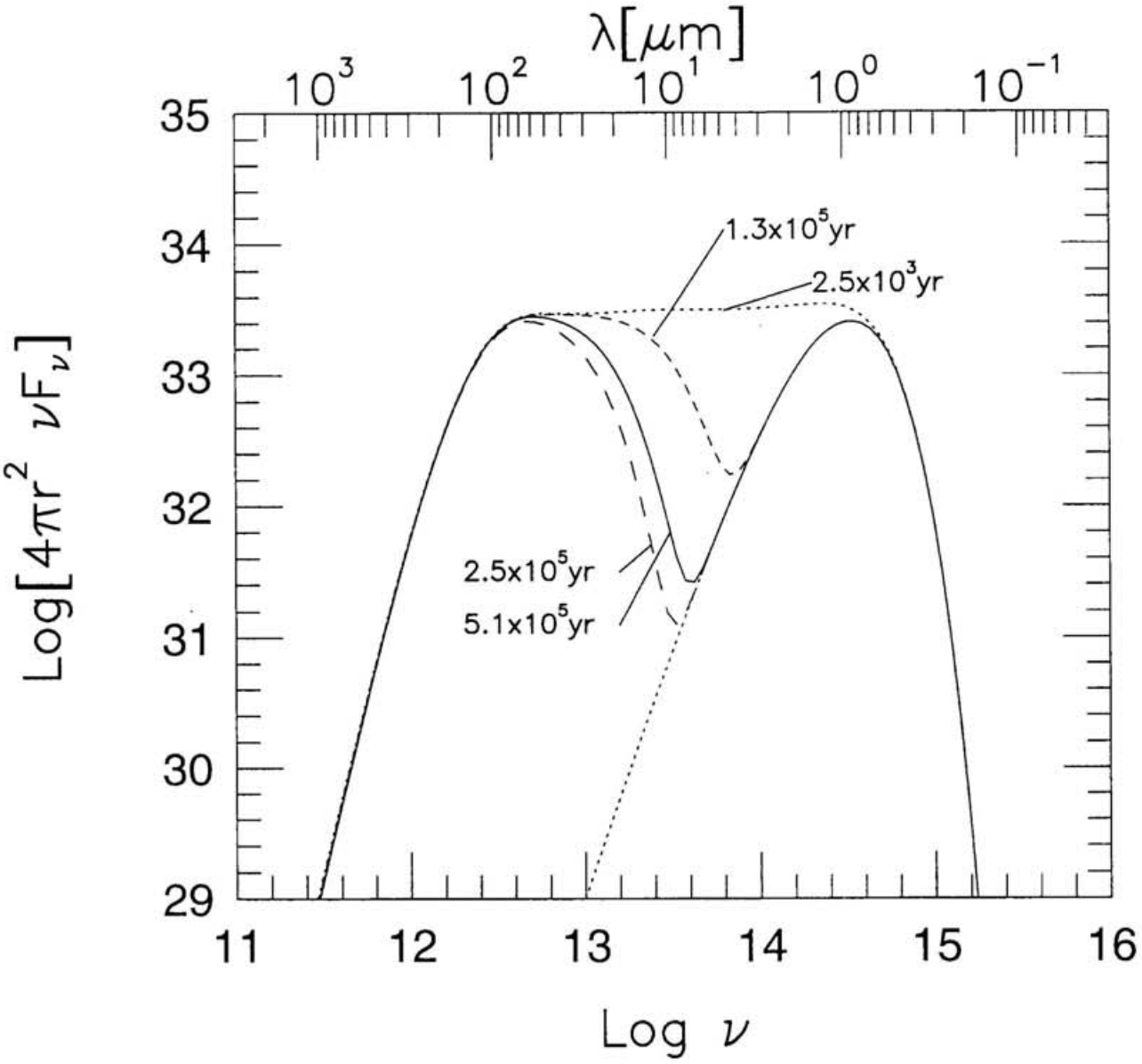

Fig. 4-2.— Evolution of the spectral energy distribution of the disk for model A. Protoplanet's mass is $10^{-3}M$. Dotted line correspond to the contribution from the star.

the protoplanet's orbit (2.5×10^3yr after the formation of the planet). Next, the disk inside protoplanet's orbit falls onto the central star from inside (1.3×10^5yr). By 2.5×10^5yr the inner region of the disk is removed. Finally, the protoplanet migrates inward due to the tidal torque from the outer disk, and the inner edge of the outer disk also moves inward due to the viscous diffusion of the gas (5.1×10^5yr).

The corresponding evolution of the SED is shown in Figure 4-2. At 2.5×10^3 years, although the protoplanet has formed a gap, the SED does not show any sign of the gap formation. This is because the slope of the surface density profile at the edge of the gap is rather gentle, and a small amount of the gas (and dust) is still remained near the protoplanet. The protoplanet has to excite density waves at the LRs which locate near it to maintain a wide gap against the viscous diffusion of the gas. Therefore, a small amount of the gas near the protoplanet is needed for the protoplanet to excite density waves even after a wide gap has formed. The amount of the dust remained in the gap is enough large to be opaque at near and mid-infrared, such that the SED is not affected by the gap formation. However, when the inner region of the disk is removed, the SED begins to show a dip in the near-infrared. The dip becomes deeper as the removal of the inner disk proceeds. It is seen that the SED changes in a time scale of 10^5 yr. At 5.1×10^5yr, the dip in the SED becomes shallower than that at 2.5×10^5yr, because inner edge of the outer disk moves inward after the removal of the inner disk.

To summarize our result, the protoplanet makes a dip at near and mid-infrared in the SED, if the viscosity of the disk is enough small such that the protoplanet removes the disk inside its orbit.

Next, we discuss the gap size derived from the infrared observations of the SED of some T Tauri stars without any binary companions. Table 1 lists the gap sizes derived by Marsh & Mahoney (1992, 1993). In Table 1, r_1 and r_2 are inner and outer radius of the edge of the gap, respectively. Note that the derived gap sizes show the large ratio between the inner and outer radius of the gap. It suggests that the inner region of the disk is almost removed.

Table 1. Observed gap size.

Star	r_1(AU)	r_2(AU)	r_2/r_1	Ref.
GM Aur	0.02	0.7	35	1
HK Tau	0.06	0.9	15	2
GK Tau	0.065	2.4	37	2
RY Tau	0.20	3.0	15	1

References. — (1) Marsh & Mahoney 1992 (2) Marsh & Mahoney 1993

This large gap size can be explained if the viscosity of the disk is small ($\alpha \lesssim 10^{-3}$).

4.2. Application for binary T Tauri stars

As discussed in §1.3, many of pre-main-sequence stars have been found to have binary companions. Some of these objects show the deficit of the radiative flux in the infrared or the millimeter-wave, suggesting the presence of a gap in the protoplanetary disk. However, the gap sizes estimated from observations are rather wider than the prediction by the previous theoretical models. We apply our wave propagating model to interpret the observed gap sizes.

In the previous sections, the influence of the protoplanet is considered and the linear approximation is used to calculate wave propagation. However, the binary companion has enough mass to disturb the disk non-linearly and induce shocks. Paczyński(1977) showed that the binary companion induces shock in the disk near its orbit and opens a relatively narrow gap quickly. After this gap formation, the companion's tidal disturbance may continue to induce non-linear spiral density waves. However, the amplitude of the waves is rapidly decreasing function of the distance between the edge of the gap and the companion's orbit (Savonije, Papaloizou & Lin 1994). Thus, the gap formation quite reduces the amplitude of the waves. We consider the stage after the gap formation reduced the wave amplitude such that these waves can be treated by the linear approximation. These waves can propagate over a substantial region of the disk, and broaden the gap.

4.2.1. GW Ori

GW Ori is a classical T Tauri star of 2.5 $M_\odot$ with a binary companion which was discovered by spectroscopic observations. From radial velocity measurements, Mathieu et al.(1991) derived the separation between the primary and the secondary, $a \approx 1.1$ AU, and the secondary mass, $M_s \approx 0.6 M_\odot$. The eccentricity of the orbit is small($e = 0.17 \pm 0.06$,

Mathieu & Jensen, 1995 private communication). The SED of GW Ori has a dip in the continuum near 10μm which is interpreted as due to the presence of the gap from 0.17AU to 3.3AU. Since the eccentricity of the binary orbit is small and the extent of the gap is wide, the theoretical model assuming that the waves damp immediately at LRs requires the extremely small viscosity (Artymowicz & Lubow 1994).

Mathieu, Adams & Latham (1991) argued the minimum size of the gap. The orbit of the gas which resided initially between $0.37a$ and $1.75a$ intersects other orbit by the strong disturbance of the companion, and hence cannot be stable. Thus, the companion opens a gap quickly from $0.37a$ to $1.75a$ via strong shock dissipation. Here, we consider the evolution of the gap subsequent to its formation. The inner radius of the circumbinary disk, $1.75a$, is near the position of the $m = 1$ LR($1.59a$). The companion can excite $m = 1$ waves near the disk edge. The gap becomes wider through the propagation and non-local dissipation of these $m = 1$ waves. The gap width is increased by the damping length of $m = 1$ waves. The damping length, l, is calculated by (see eq. [2.11])

$$\int_{r_1}^{r_1+l} \left\{ \zeta + \left(\frac{4}{3} + \frac{\kappa^2}{m^2(\Omega - \Omega_p)^2} \right) \nu \right\} \frac{m(\Omega_p - \Omega)}{c^2} k dr' \approx 1, \tag{4.7}$$

where r_1 is the initial radius of disk edge, $1.75a$. The temperature profile of the disk is estimated as

$$T = 535 \left(\frac{r}{1.1\mathrm{AU}} \right)^{-1/2} \mathrm{K}, \tag{4.8}$$

by fitting the theoretical model to the profile of the SED of the disk (Mathieu, Adams & Latham 1991; Mathieu et al. 1995). Using the α prescription for the viscosity law, the condition that the radius of the inner edge of the circumbinary disk is 3.3AU yields $\alpha \approx 7 \times 10^{-3}$. The circumprimary disk truncates to $0.37a$ through the shock formation initially and has no strong LR located within it. The companion may excite the $m = 2$ waves at the outer edge of the disk even though the relevant LR is excluded (Savonije, Papaloizou & Lin 1994). These waves also broaden the gap. The outer edge of the circumprimary disk is calculated from equation (4.7). Substituting $\alpha = 7 \times 10^{-3}$ into equation (4.7), we find that the edge radius is reduced to $r_i \approx 0.20$AU, which is in good agreement with the observation.

We compare $\alpha \approx 7 \times 10^{-3}$ derived above with the value derived from the luminosity of the disk. The luminosity of the disk around GW Ori is estimated as $34L_{\odot}$. When we assume that this luminosity is emitted by the disk accretion, then the accretion rate is $5 \times 10^{-6}M_{\odot}$/year(Mathieu, Adams & Latham 1991). If the disk mass within 100AU is less than $1M_{\odot}$, this accretion rate infer that the Reynolds number $R \lesssim 10^3$, i.e. $\alpha \gtrsim 10^{-1}$. Thus there still remains a discrepancy between the value derived from the gap size and from the disk luminosity by a factor 10. The estimation of the gap size from the infrared spectrum and the derivation of α from the gap size are crude. It needs more precise estimation of α to resolve the above discrepancy.

4.2.2. GG Tau

With near infrared speckle interferometry, Leinert et al.(1991) found GG Tau to be a binary with an angular separation of 0.255" on the plane of the sky. Images of the gas and dust disk around GG Tau were obtained using the interferometer of millimeter-wave(Kawabe et al. 1993; Dutrey, Guilloteau & Simon 1994) and recently by infrared (Roddier et al. 1996). The dust images show that the disk has an inner cavity of radius 220AU. The orbit of the binary is estimated from the infrared observations. There still remains uncertainty in the orbit because of the uncertainty of the total mass of the binary. Roddier (1996) showed that If the total mass of the binary is less than $1.6M_{\odot}$, then the semi-major axis of the binary orbit is larger than 73AU and the eccentricity is larger than 0.58. The total mass less than $1.6M_{\odot}$ is inferred from the gas motion of the circumbinary disk (Kawabe et al. 1993; Dutrey, Guilloteau & Simon 1994). If the total mass is less than $1.4M_{\odot}$, then the semi-major axis is larger than 117AU and the eccentricity is larger than 0.72. We simply assume that the components of the binary system have equal mass, because the mass ratio does not affect our analysis largely. The temperature profile of the disk is estimated as

$$T = 30 \left(\frac{r}{73\mathrm{AU}} \right)^{-1/2} \mathrm{K}, \tag{4.9}$$

by fitting the theoretical model to the profile of the $^{12}CO(J = 1 - 0)$ line emitted from the disk (Kitamura et al. 1993). Initially, the binary would truncate the circumbinary disk to the radius $r \approx 1.68a$ through strong shock dissipation (see Table 1 of Artymowicz & Lubow 1994). To explain the gap size, the waves excited at $m = 1$ LR ($r_L = 1.59a$) must damp before reaching at 220AU. Using the above temperature profile, we conclude that $\alpha \gtrsim 2 \times 10^{-2}$. If total mass is less than $1.4M_{\odot}$, a large value of the viscosity, $\alpha \gtrsim 4 \times 10^{-1}$ is required.

4.3. Application for proto-Jupiter

In this section, the interaction between a proto-giant-planet and the solar nebula is discussed. For the purpose of illustration, we adopt the minimum-mass nebula model (Hayashi 1981), which adequately accounts for the mass in the cores of giant planets today.

According to this model, planetesimals grow through coagulation which eventually leads to the formation of solid cores of giant planets (Nakagawa, Hayashi & Nakazawa 1983). At radii commensurate with the position of Jupiter, the core mass reaches 10 earth masses in 10^7 years. With such a large mass, the protoplanetary core rapidly acquires an atmosphere via gas accretion (Mizuno 1980). The gas accretion timescale for a protoplanet with a mass comparable to that of Jupiter is of order 10^3 yr (Bodenheimer & Pollack 1986; Sekiya et al. 1987). Concurrently, the protoplanet exerts a tidal torque on the disk. When the protoplanet grows to Saturn or Jupiter mass, it opens a gap (Fig. 3-16). This gap formation occurs through $m \sim (r\Omega/c)_p$ waves. The timescale for gap formation is a decreasing function of protoplanet's mass and viscosity. When the timescale for the gap opening becomes comparable with the accretion timescale, a gap is formed and the gas accretion phase is terminated (Lin & Papaloizou 1980). Our numerical calculations showed that the protoplanet with a Saturn mass opens a gap in $10^3 - 10^4$ years, and that the protoplanet with a Jupiter mass opens a gap in $10^2 - 10^3$ years. Therefore, when the protoplanet grows to the Jupiter mass, the gap formation predominates over the gas accretion onto the protoplanet, and the

accumulation of the gas stops.

After the gap formation through $m \sim (r\Omega/c)_p$ waves, the lowest m waves broaden the gap size. For $\alpha \lesssim 3 \times 10^{-4}$, the $m = 2$ waves can propagate to the inner edge of the disk, and deposit negative angular momentum there. The results described in §3.5 show that if $\alpha \lesssim 3 \times 10^{-4}$, the entire disk interior to the orbit of a proto-Jupiter would be depleted onto the Sun. Such a low value for α is possible if convection is stabilized by the surface irradiation (Watanabe, Nakagawa, & Nakazawa 1990), provided it occurs after the proto-Jupiter has already acquired most of its present mass. The time scale for the removal of the inner disk is about 10^5 years.

After the removal of the inner disk, a proto-Jupiter interacts with only the outer disk, and migrates inward. The distance between proto-Jupiter and the outer disk increases, and the tidal interaction is reduced. Hence, a proto-Jupiter cannot dissipate the outer disk. However, the depletion of the outer regions of the solar nebula is inferred from the present masses of the atmospheres of Saturn, Uranus, and Neptune, which are considerably smaller than that of Jupiter. If all the gaseous planets in the solar system were formed under the assumed conditions, only Jupiter and Saturn would have terminated their growth through gap formation. The smaller masses of Uranus and Neptune imply that either they did not acquire sufficient mass to undergo dynamical accretion or that there was little residual gas in the solar nebula left for them to accrete. Further, unless the outer disk is removed by some mechanism, the inward migration of the proto-Jupiter continues on viscous diffusion time scale. Shu, Johnstone & Hollenbach (1993) suggested photo-evaporation by strong UV flux from the Sun as a possible mechanism of removal of the outer part of the disk.

Chapter 5

Discussion

5.1. Waves in the disk with finite thickness

In the previous chapters, the protoplanetary disk is assumed as infinitesimally thin and the vertical structure of the disk is neglected. In such a disk a protoplanet with no inclination excites only two-dimensional waves, i.e. the waves without velocity component in the vertical direction. However, the radius of the protoplanet (10^{10}cm for the proto-Jupiter and 10^{9}cm for the proto-Earth) is much smaller than the thickness of the protoplanetary disk ($\gtrsim 10^{11}$cm at 1AU in the model of the minimum-mass disk). Therefore, the protoplanet may induce waves with the non-zero vertical component of the velocity, i.e. three-dimensional waves. In this section, the effect of the finite thickness of the disk on the gap size is discussed.

5.1.1. Unperturbed disk

A protoplanetary disk may have the temperature gradient in the vertical direction immediately after the formation from the molecular cloud core (Lin & Papaloizou 1980). At the late stage of the evolution, however, the protoplanetary disk becomes isothermal in the vertical direction. Ruden & Pollack(1991) solved for the long term evolution of the density and temperature structures within protoplanetary disks. They assumed that initially the

disk is optically thick, and the temperature gradient in the vertical direction is large, and that the whole disk is convectively unstable. However, they found that the disk outside 1AU becomes optically thin in 10^7 years, and the convective instability disappears. Hence, isothermal structure in the vertical direction is expected at late times. Watanabe et al.(1990) solved the vertical structure of the protoplanetary disk at 1AU. They found that the radiation of the central star heats the surface of the disk, and stabilize the disk against the convection. The disk inside 1AU evolves toward an isothermal structure on a time scale of 10^3 years. Finally, in the stage considered in this thesis, a substantial fraction of dust grains may have already accumulated into the protoplanetary cores. Thus, the disk is expected to be optically thin and isothermal.

We assume that the protoplanetary disk rotates around the central star with Keplerian velocity and that the orbit of the protoplanet is circular with no inclination.

For the region of the disk where the distance from the protoplanet is much larger than the disk thickness, the disk can be treated as infinitesimally thin. Thus if the protoplanet has no inclination, it cannot induce the waves with the non-zero vertical component of the velocity at that region, where the gravity of the protoplanet points nearly horizontal direction. Therefore, it is sufficient that we investigate the dynamics of the disk only near the protoplanet to study the three-dimensional waves. We set up Cartesian axes (x, y, z) with origin at the location of the protoplanet. The z-axis is perpendicular to the equatorial plane of the disk. The x and y-axes rotate around the z-axis with angular velocity Ω_p such that the x-axis points outward from the central star. We consider only the region near the protoplanet such that $|x|, |y|$ and $|z|$ are much smaller than the orbital radius of the protoplanet, r_p.

Because the dimension of the region considered here is small in comparison with the length scale of the variation of the density, temperature and scale height, they can be considered as constant in the horizontal direction. Since the disk is assumed as isothermal in

the vertical direction, the density profile in the vertical direction is given by

$$\rho_0(z) = \rho_{00} \exp\left(-\frac{z^2}{2h^2}\right), \tag{5.1}$$

where ρ_{00} is the density at the equatorial plane and $h = c/\Omega_p$ is the scale height of the disk at the location of the protoplanet. The unperturbed flow of the disk is approximated as

$$\boldsymbol{v}_0 = (u_0, v_0, w_0) = (0, 2Ax, 0), \tag{5.2}$$

where A is Oort's parameter defined as

$$A = \frac{r_p}{2}\left.\frac{d\Omega}{dr}\right|_{r_p}. \tag{5.3}$$

This unperturbed state is the three-dimensional version of the shearing sheet model (Goldreich & Lynden-Bell 1965).

5.1.2. Perturbation equations

We assume that the perturbations are isothermal. This is due to a technical reason (Chiueh & Tseng 1994). The perturbation equations are in general the partial differential equations and complicated to be solved. However, this assumption makes the perturbation to be separable in the radial and vertical directions and simplifies the mathematics considerably. Thus, we adopt this assumption as the first step to attack the problems of the three-dimensional waves. The equation of motion and the equation of continuity describing perturbations are

$$\frac{\partial u_1}{\partial t} + 2Ax\frac{\partial u_1}{\partial y} - 2\Omega_p v_1 = -\frac{1}{\rho_0}\frac{\partial p_1}{\partial x} - \frac{\partial \varphi_1}{\partial x}, \tag{5.4}$$

$$\frac{\partial v_1}{\partial t} + 2Ax\frac{\partial v_1}{\partial y} - 2Bu_1 = -\frac{1}{\rho_0}\frac{\partial p_1}{\partial y} - \frac{\partial \varphi_1}{\partial y}, \tag{5.5}$$

$$\frac{\partial w_1}{\partial t} + 2Ax\frac{\partial w_1}{\partial y} = -\frac{1}{\rho_0}\frac{\partial p_1}{\partial z} - \frac{z}{\rho_0 h^2}p_1 - \frac{\partial \varphi_1}{\partial z}, \tag{5.6}$$

$$\frac{1}{c^2}\frac{\partial p_1}{\partial t} + \frac{2Ax}{c^2}\frac{\partial p_1}{\partial y} + \rho_0\left(\frac{\partial u_1}{\partial x} + \frac{\partial v_1}{\partial y} + \frac{\partial w_1}{\partial z}\right) - \frac{\rho_0 z}{h^2}w_1 = 0, \tag{5.7}$$

where φ_1 is the potential of the protoplanet

$$\varphi_1 = -\frac{GM_p}{(x^2+y^2+z^2)^{1/2}}, \tag{5.8}$$

p_1 is the pressure perturbation, B is Oort's parameter defined as

$$B = \frac{1}{2r}\frac{d}{dr}(r^2\Omega)\bigg|_{r_p}, \tag{5.9}$$

and the subscript "1" means the perturbed quantity.

Without loss of generality, we write each perturbation variable X in the form

$$X(x,y,z,t) = X(x,z)\exp i(k_y y - \omega t). \tag{5.10}$$

Because the potential of the protoplanet is stationary in this coordinate, ω becomes zero for the forced oscillations. Eliminating the velocity components from equations (5.4)-(5.7) and introducing the non-dimensional coordinate variables as

$$\xi = \frac{2Ak_y}{\Omega_p}x, \tag{5.11}$$

$$\zeta = \frac{z}{h}, \tag{5.12}$$

we have a partial differential equation for $p_1(\xi,\zeta)$ as

$$\begin{aligned}\left\{\frac{\partial^2}{\partial\xi^2}+\frac{2\tilde{\omega}\Omega_p}{D}\frac{\partial}{\partial\xi}+\frac{2\Omega_p^3}{DA}-\frac{\Omega_p^2}{4A^2}-\frac{\Omega_p^2 D}{4A^2k_y^2c^2}\right\}p_1 - \frac{\Omega_p^4 D}{4A^2\tilde{\omega}^2k_y^2c^2}\left\{\frac{\partial^2}{\partial\zeta^2}+\zeta\frac{\partial}{\partial\zeta}+1\right\}p_1 \\ = -\rho_0\left\{\frac{\partial^2}{\partial\xi^2}+\frac{2\tilde{\omega}\Omega_p}{D}\frac{\partial}{\partial\xi}+\frac{2\Omega_p^3}{DA}-\frac{\Omega_p^2}{4A^2}\right\}\varphi_1 + \frac{\Omega_p^4 D\rho_0}{4A^2\tilde{\omega}^2k_y^2c^2}\left\{\frac{\partial^2}{\partial\zeta^2}-\zeta\frac{\partial}{\partial\zeta}\right\}\varphi_1,\end{aligned} \tag{5.13}$$

where

$$\tilde{\omega} = \Omega_p\xi \tag{5.14}$$

and

$$D = 4B\Omega_p - \tilde{\omega}^2. \tag{5.15}$$

In this coordinate, the positions of the LRs become $\xi = \pm 1$. For farther progress, we expand p_1 in the separable form

$$p_1(\xi,\zeta) = \sum_n P_n(\xi)Z_n(\zeta), \tag{5.16}$$

and the right hand side of the equation (5.13) in the form

$$RHS = \sum_n \Psi_n(\xi) Z_n(\zeta). \tag{5.17}$$

Substituting above expressions, equation (5.13) is rewritten in the two ordinary differential equations,

$$\left\{ \frac{d^2}{d\xi^2} + \frac{2\tilde{\omega}\Omega_p}{D}\frac{d}{d\xi} + \frac{2\Omega_p^3}{DA} - \frac{\Omega_p^2}{4A^2} - \frac{\Omega_p^2 D}{4A^2 k_y^2 c^2}\left(1 - \frac{\lambda_n \Omega_p^2}{\tilde{\omega}^2}\right) \right\} P_n(\xi) = \Psi_n(\xi), \tag{5.18}$$

$$\left\{ \frac{d^2}{d\zeta^2} + \zeta\frac{d}{d\zeta} + 1 + \lambda_n \right\} Z_n(\zeta) = 0, \tag{5.19}$$

where λ_n is constant. Similar equations for the polytropic gas disk are derived by Okazaki & Kato (1985).

5.1.3. Solution for vertical direction

To solve equation (5.19), we need the appropriate boundary conditions. We require that kinetic energy density per unit volume, $\rho_0(u_1^2 + v_1^2 + w_1^2)$, approaches zero as ζ approaches infinity. To satisfy this condition, λ_n should be zero or positive integer, otherwise Z_n diverges exponentially for large $|\zeta|$. We set

$$\lambda_n = n. \tag{5.20}$$

The solution of equation (5.19) becomes

$$Z_n(\zeta) = \rho_{00} \exp\left(-\frac{\zeta^2}{2}\right) H_n(\zeta), \tag{5.21}$$

where H_n is Hermite polynomial. The nth-order Hermite polynomial has n nodes. Hermite polynomials with even n are even functions, and those with odd n are odd functions. We take only the even functions in ζ, i.e. functions with $n = 0$ or even n, because the potential of the protoplanet is symmetrical with regard to the equatorial plane. Figure 5-1 shows the functional forms of Z_n for several n.

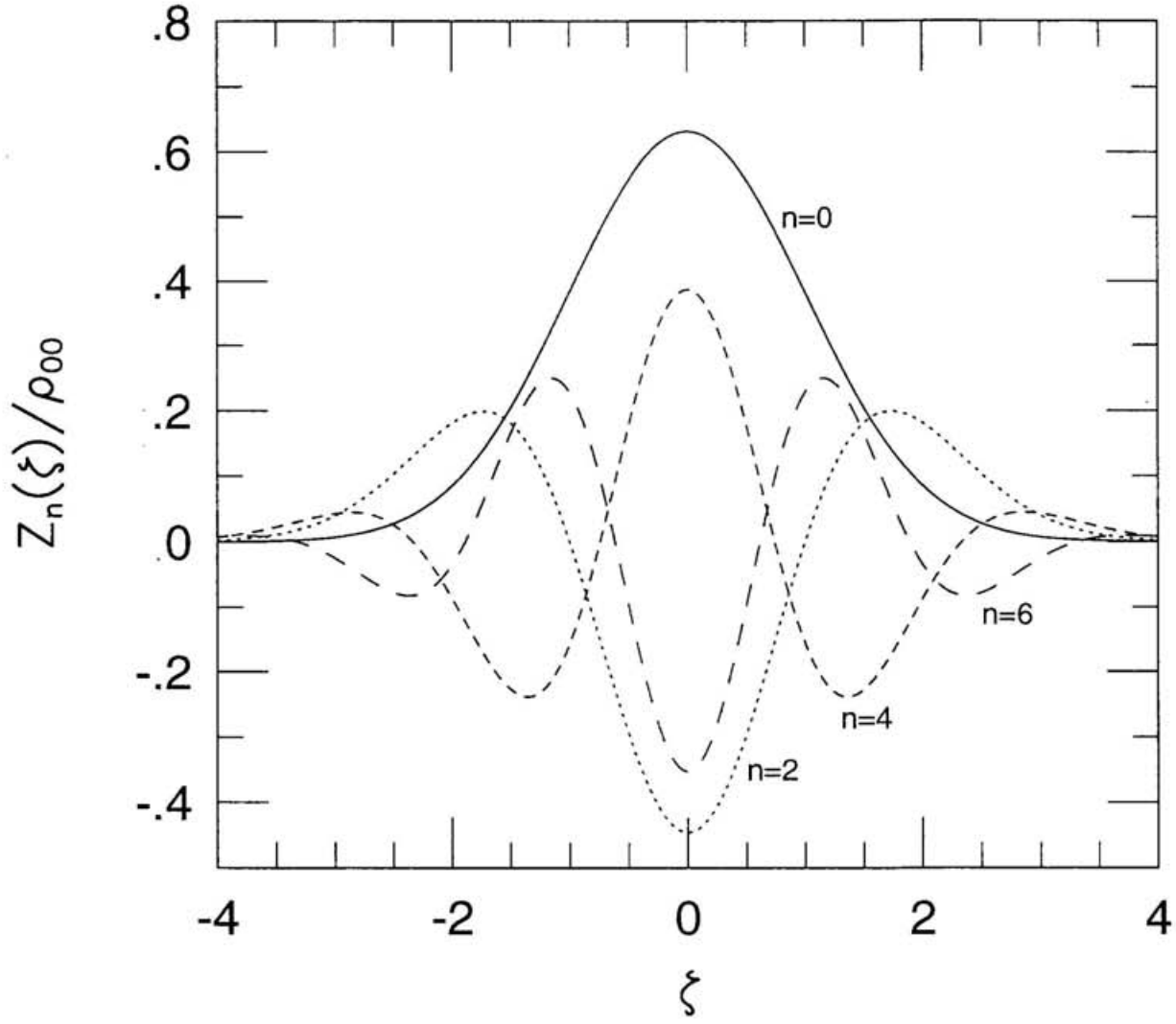

Fig. 5-1.— Functional forms of $Z_n(\zeta)$.

5.1.4. WKB solution for radial direction

Integration of equation (5.18) needs numerical calculation. Before numerical integration, we solve the homogeneous version of equation (5.18) using the WKB approximation. The WKB solution will help us to understand the nature of waves, and will be used in determining the boundary condition in the numerical integration.

We write P_n in the form

$$P_n(\xi) = \Pi(\xi) \exp\left[i \int^{\xi} k_\xi d\xi' \right]. \tag{5.22}$$

Substituting above expression into equation (5.18) and remaining only the highest terms of $k_\xi \gg 1$ and $\Omega_p / k_y c \gg 1$, we obtain

$$k_\xi^2 = -\frac{\Omega_p^2 D}{4A^2 k_y^2 c^2} \left(1 - \frac{n}{\xi^2} \right), \tag{5.23}$$

where we used $\omega = 0$ for the forced oscillation. The wave number k_ξ^2 is plotted for various n in Figure 5-2. The waves can propagate only where $k_\xi^2 > 0$. The region of $k_\xi^2 < 0$ is the evanescent region, where the perturbations grow or damp exponentially in the radial direction. If the wavelength is much shorter than the length scale of the variation of the potential of the protoplanet, then the effect of the potential of the protoplanet would cancel when it is integrated over the one wavelength. The protoplanet's potential affects the waves most effectively where the wavelength is largest. Thus, the waves are considered to be excited at where $k_\xi = 0$ and propagate toward where $k_\xi^2 > 0$.[1]

First, we consider the $n = 0$ waves. From equation (5.6), it is seen that the vertical component of the velocity is zero. Thus $n = 0$ waves represent the two-dimensional waves. Figure 5-2 shows that $n = 0$ waves can exist only where $|\xi| \geq 1$, i.e. outside of the LRs. These waves are excited at LRs and propagate away from the protoplanet.

---

[1] At $k_\xi = 0$ the validity of WKB approximation is lost. However, more careful calculation also shows the wave excitation at $k_\xi = 0$ (see Goldreich & Tremaine 1978).

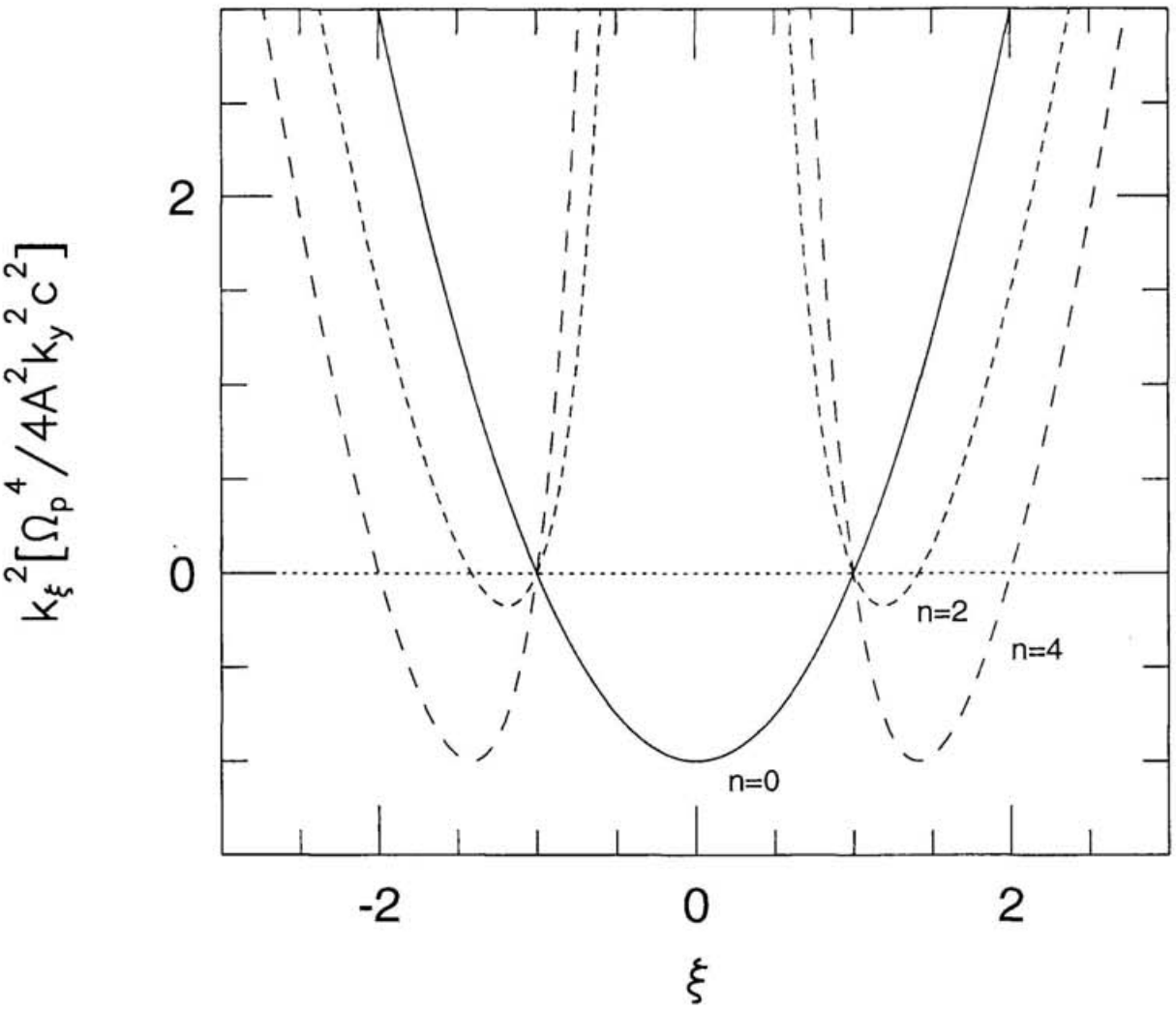

Fig. 5-2.— WKB wave number for various n. The waves propagate only where $k_\xi^2 > 0$.

For $n \geq 2$ waves, they have the non-zero vertical component of the velocity, and thus represent the three-dimensional waves. They can propagate where $|\xi| \leq 1$ or $|\xi| \geq \sqrt{n}$. Thus, there are two types of three-dimensional waves. One is excited at LR ($\xi = \pm 1$) and propagates toward the protoplanet. The other is excited at $\xi = \pm\sqrt{n}$ and propagates away from the protoplanet. The former waves cannot propagate outside the LRs, because there are the evanescent regions just outside the LRs. Therefore, these waves cannot contribute to broaden the gap. The latter waves are excited at $\xi = \pm\sqrt{n}$, that are farther from the protoplanet than the location where the $n = 0$ waves are excited. Because the gravity of the protoplanet decreases with the distance, the amplitude of the three-dimensional waves are smaller than the two-dimensional waves. Therefore, the effect of the three-dimensional waves on the gap size can be neglected.

5.1.5. Angular momentum flux

In this subsection equation (5.18) is integrated numerically and the angular momentum carried by the three-dimensional waves is calculated. The boundary condition is that only out-going waves exist at infinity, because there is no source of the waves except the protoplanet. This condition requires that the solution approaches the WKB solution (5.22) with negative k_ξ at large $|\xi|$. Equation (5.18) has the singular point at $\xi = 0$ (co-rotation resonance). According to Lin's rule (Lin 1955, chap.8), we took the path of integral in the complex ξ plane passing below this singular point to treat the singularity. This procedure is equivalent to introducing a small viscosity around the singular point. The solutions for the two-dimensional waves ($n = 0$) are shown in Figure 5-3, where the real and imaginary parts of P_0 are plotted as a function of ξ for various wave number in y direction, k_y. Figure 5-4 shows solutions for the three-dimensional waves ($n = 2$). For $k_y = 2$, the solutions are plotted only for $|\xi| \leq 5$. In these figures we adopt the sound speed as $c = 5 \times 10^{-2} r_p \Omega_p$.

The angular momentum flux is calculated by (Lynden-Bell & Kalnajs 1972;

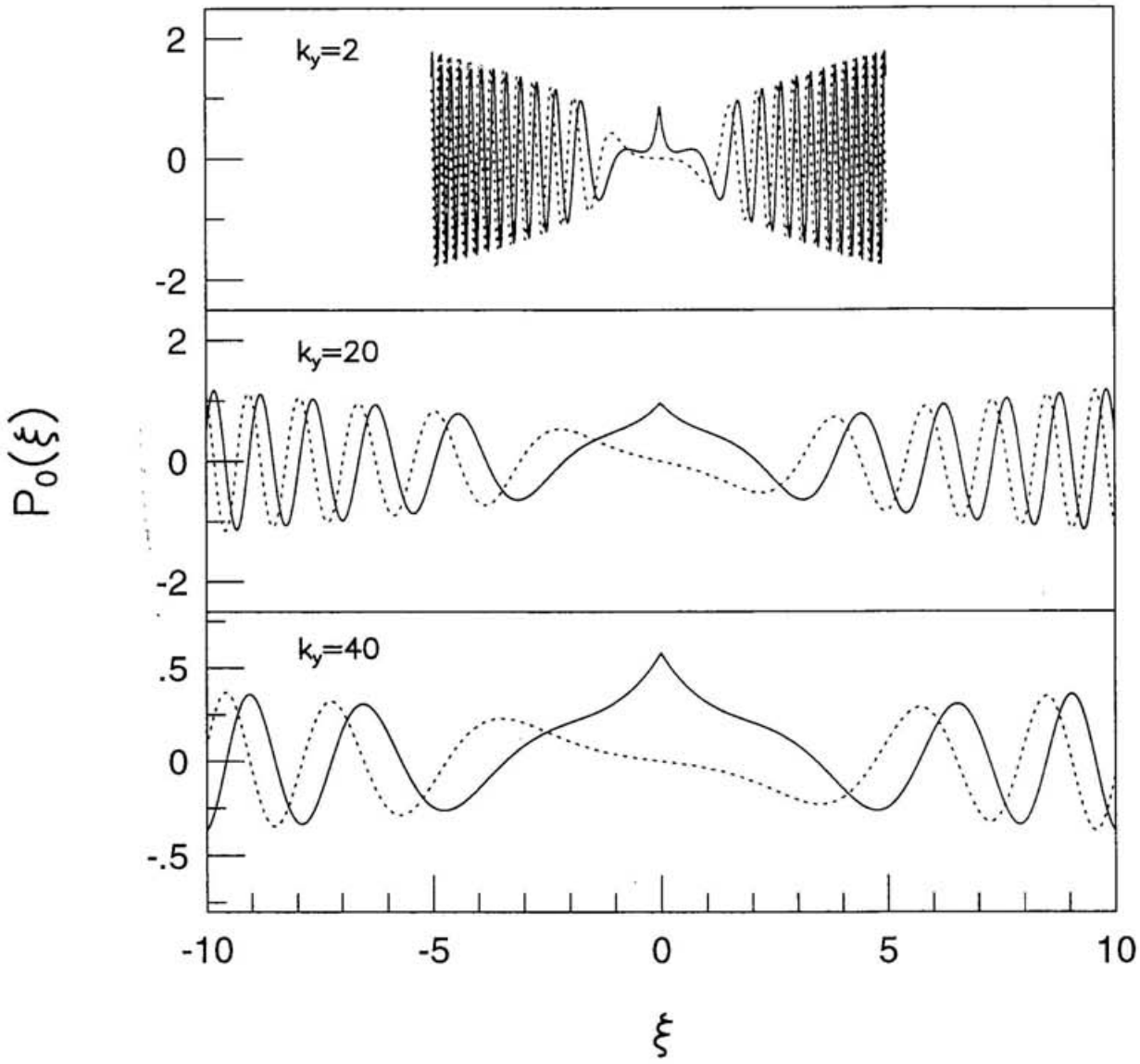

Fig. 5-3.— Wave functions for $n = 0$ two-dimensional waves. Solid lines show the real part of the functions, and dotted lines show the imaginary part. For $k_y = 2$, the function is plotted only for $|\xi| \leq 5$.

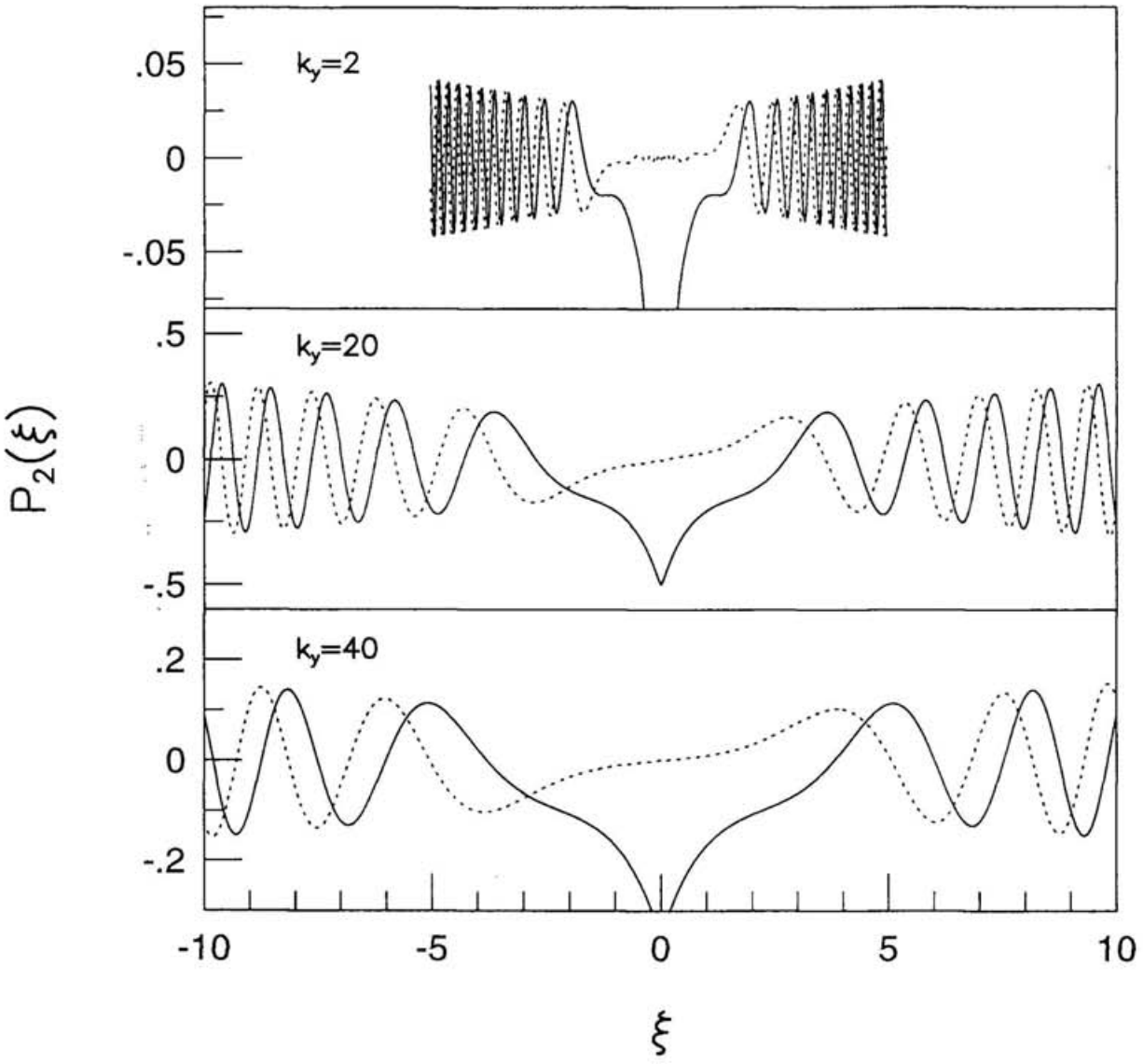

Fig. 5-4.— Wave functions for $n = 2$ three-dimensional waves. Solid lines show the real part of the functions, and dotted lines show the imaginary part. For $k_y = 2$, the function is plotted only for $|\xi| \leq 5$.

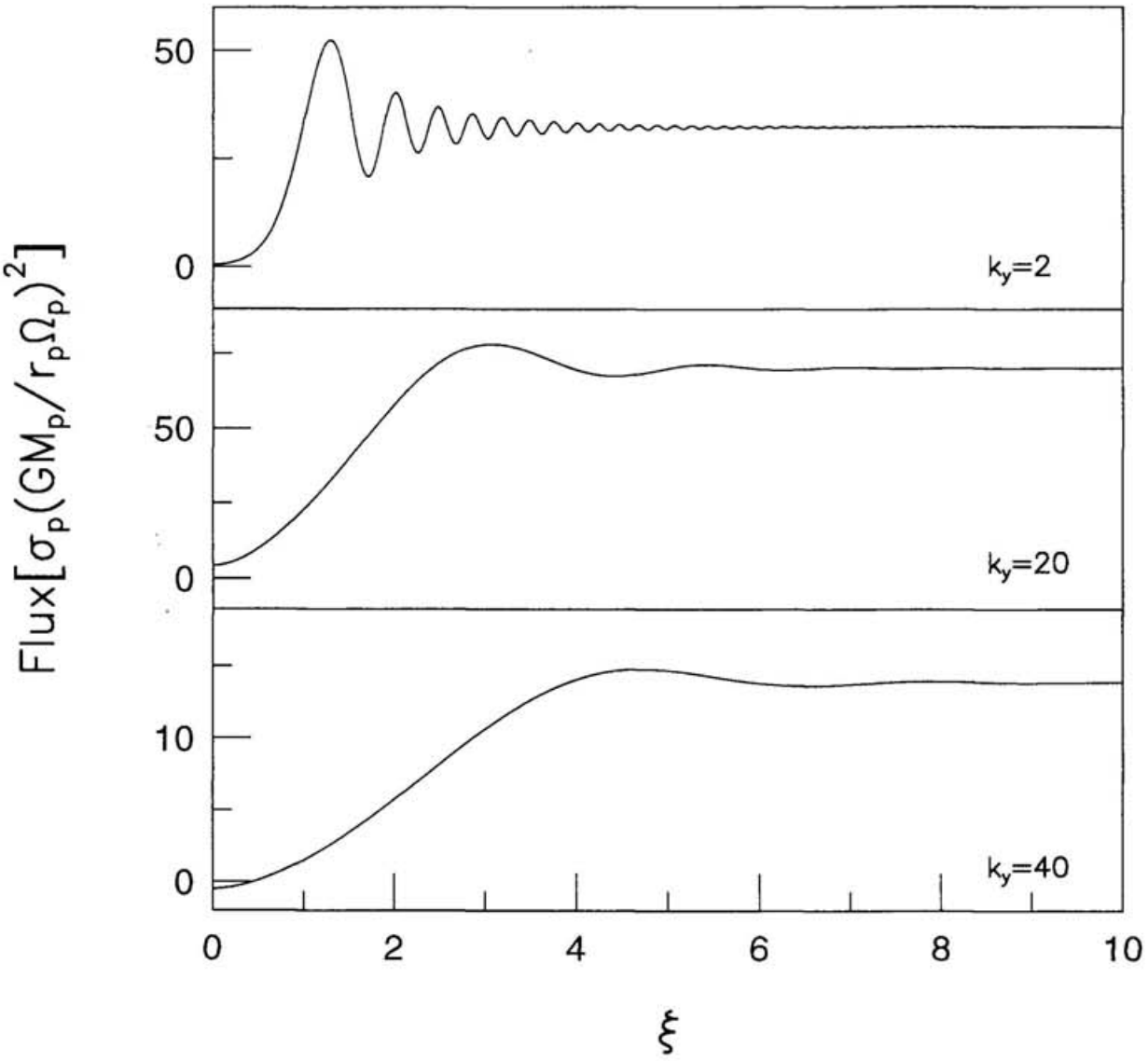

Fig. 5-5.— Angular momentum flux as a function of ξ for $n = 0$ two-dimensional waves.

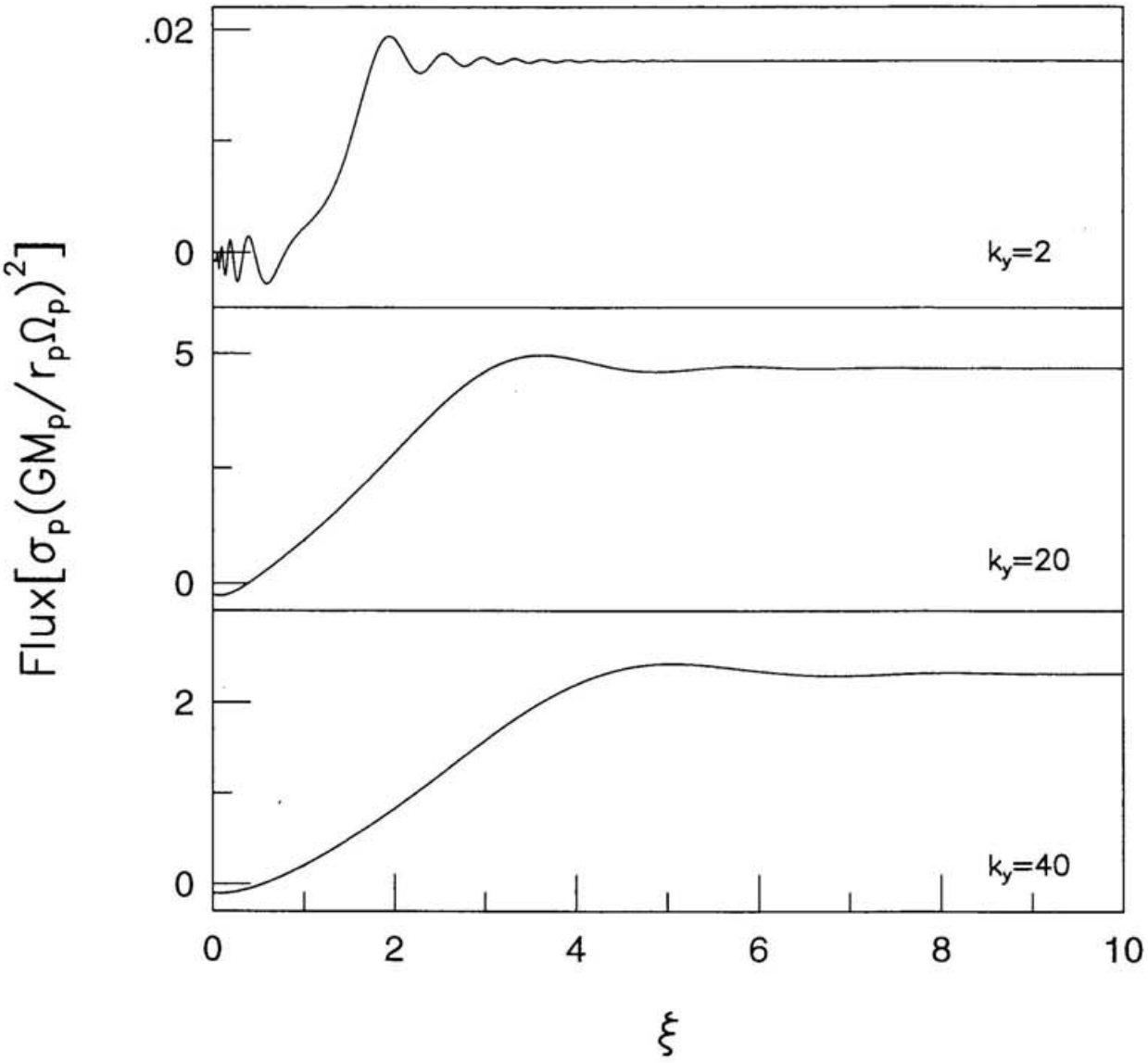

Fig. 5-6.— Angular momentum flux as a function of ξ for $n = 2$ three-dimensional waves.

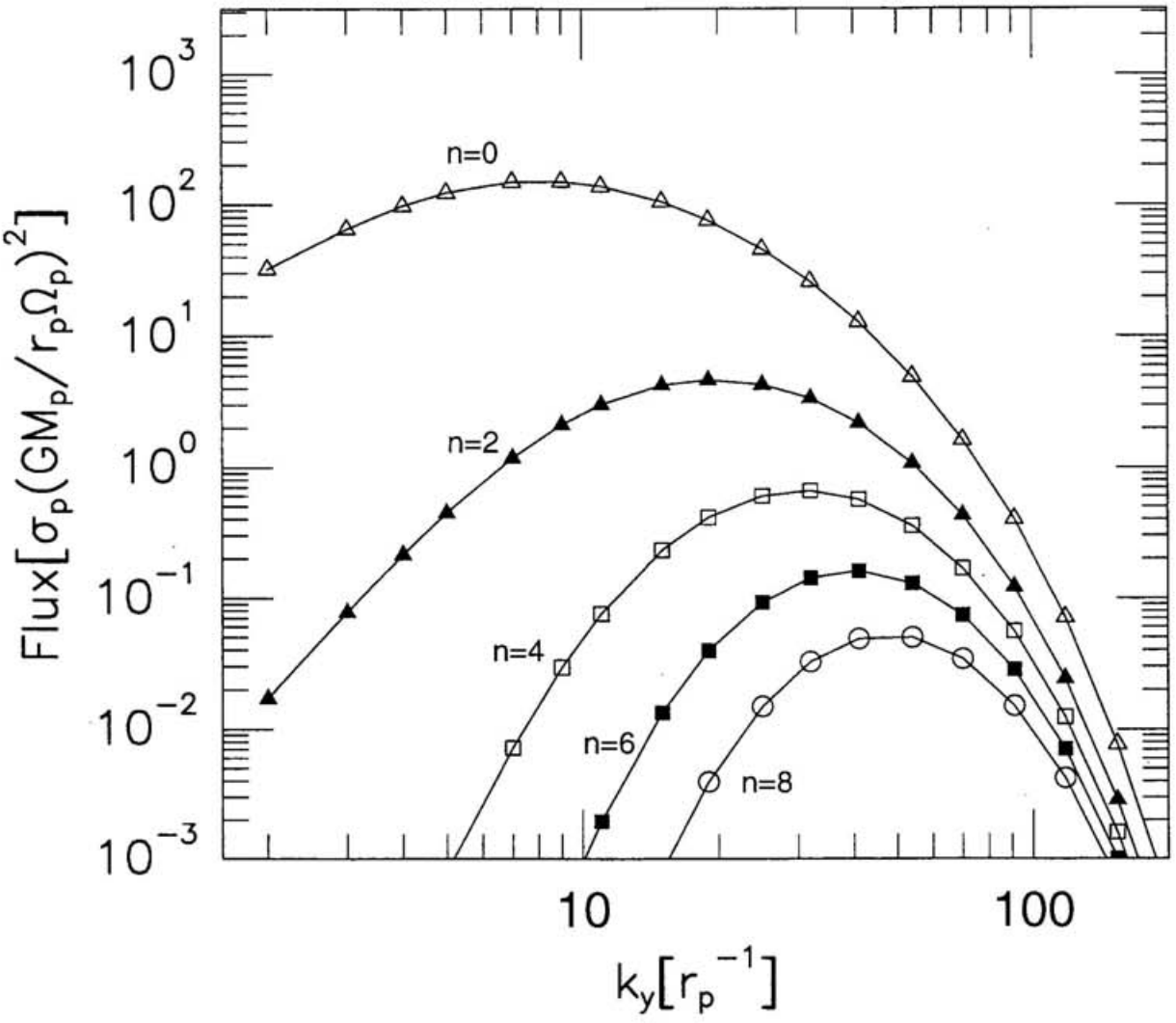

Fig. 5-7.— Angular momentum flux carried by waves to infinity. The two-dimensional waves have $n = 0$. The three-dimensional waves have $n \geq 0$.

Lin, Papaloizou & Savonije 1990a)

$$F = \frac{\rho_0 r_p^2}{k_y} \int_{\infty}^{\infty} dz \int_0^{2\pi/k_y} dy \mathrm{Re}[u_1]\mathrm{Re}[v_1]. \tag{5.24}$$

Figure 5-5 and 5-6 show the angular momentum flux carried by the two-dimensional waves ($n = 0$) and by the three-dimensional waves ($n = 2$), respectively. Since the functional form of the flux is symmetrical with regard to $\xi = 0$, the flux is plotted only for $\xi \geq 0$. It is seen that the angular momentum flux is constant in ξ for large $|\xi|$. Figure 5-7 shows the angular momentum flux at large $|\xi|$ for various n. The angular momentum carried to infinity by the three-dimensional waves ($n \geq 2$) is quite smaller than by the two-dimensional waves ($n = 0$), as seen from the WKB approximation. Therefore, the three-dimensional waves do not contribute to broaden the gap in the case of the protoplanetary disk.

It should be noted that our analysis is restricted to the isothermal perturbation. If the perturbation is not isothermal, not only the pressure waves discussed here but also the gravity waves would propagate in the disk, and carry additional angular momentum. In this case, however, the perturbation equations are not separable, and hence difficult to solve. Calculating the angular momentum carried by the gravity waves is remained as the future problem.

5.1.6. Wave refraction toward vertical direction

Finally, we discuss the wave refraction due to the temperature gradient in vertical direction. Lin, Papaloizou & Savonije(1990a,b) investigated wave propagation in a disk which has density and temperature structure in vertical direction. They found that vertical temperature gradient causes the wave refraction toward the disk surface. The waves excited at LRs propagate horizontally at first. If the temperature increases vertically toward the midplane, the sound speed also increases toward midplane. Thus, the wave front become progressively more retarded as the vertical distance from the midplane increases. The wave front may tilt until it becomes almost parallel to the plane of the disk. Waves begin to

propagate in the vertical direction after they have propagated a moderate distance beyond the LR in the radial direction. Because the density decreases with height, the amplitude of the waves becomes larger as the waves propagate toward the surface of the disk, and the waves may dissipate through the shock formation. Waves with larger m have larger radial wave number and refract more easily. Waves with $m \sim r\Omega/c$ dissipate through vertical propagation and cannot propagate over a large distance in the radial direction. Only the small m waves can propagate in the radial direction. Hence, the gap size may become smaller than indicated by our calculation.

However, if the disk is isothermal in the vertical direction, then the wave refraction does not occur. As discussed in §5.1.1 the protoplanetary disk is expected to have an isothermal structure at the stage considered in this thesis. Thus, we conclude that the effect of the wave refraction can be neglected.

5.2. Effects of the self-gravity of the protoplanetary disks

In this section, we consider the effect of the self-gravity of the protoplanetary disks on the wave propagation and discuss the validity of the approximation of the non-self-gravitating disks.

The waves excited at LRs propagate toward the orbit of the protoplanet in the disk with self-gravity, while the waves propagate away from the protoplanet if only the pressure force is exist. The wave length of these waves becomes shorter as they propagate, and thus the effect of the pressure force becomes stronger. Before the waves reach at the radius of the protoplanet's orbit, they are reflected by the pressure force and then propagate away from the protoplanet as the pressure waves discussed in the previous chapters. Therefore, if the waves launched to the protoplanet damp before they reflect and return to the LR, the expansion of the gap due to the wave propagation does not occur. We derive the condition for this.

For the disks with self-gravity, the expression for the radial wave number (eqs. [A14] and [A15]) are modified as

$$|\mathrm{Re}[k(r)]| = \frac{\pi G\sigma_0}{c^2} \pm \left[\left(\frac{\pi G\sigma_0}{c^2}\right)^2 - \frac{D}{c^2}\right]^{1/2}, \tag{5.25}$$

$$\begin{aligned}\mathrm{Im}[k(r)] \;=\; & -\frac{1}{m(\Omega-\Omega_p)\{2c^2\mathrm{Re}[k]-\mathrm{sgn}(\mathrm{Re}[k])2\pi G\sigma_0\}} \\ & \times\left\{m^2(\Omega-\Omega_p)^2\left(\zeta+\frac{4}{3}\nu+\frac{\kappa^2}{m^2(\Omega-\Omega_p)^2}\nu\right)\mathrm{Re}[k]^2+2\pi G\sigma_0\nu|\mathrm{Re}[k]|^3\right\}.\end{aligned} \tag{5.26}$$

The waves excited at LRs have positive sign of $\mathrm{Re}[k]$. From equation (5.25), it is seen that the reflection of the waves occurs at

$$\left(\frac{\pi G\sigma_0}{c^2}\right)^2 - \frac{D}{c^2} = 0. \tag{5.27}$$

The distance from the LR to the reflection point is approximately

$$d \approx \frac{r_L}{3m}Q^{-2}, \tag{5.28}$$

where

$$Q = \frac{c\Omega}{\pi G\sigma_0} \tag{5.29}$$

is Toomre's stability parameter. The wave number of the waves having returned at the LR is

$$\mathrm{Re}[k(r_L)] = \frac{2\pi G\sigma_0}{c^2}. \tag{5.30}$$

If $|\mathrm{Im}[k(r_L)]|d \ll 1$, then the waves do not damp before returning to the LR (see eq. [A17]), and then the disk can be treated as non-self-gravitating. From equations (5.26), (5.28), (5.29) and (5.30)

$$|\mathrm{Im}[k(r_L)]|d = \frac{1}{3m}\left(\frac{r_L\Omega}{c}\right)\left(\frac{14}{3}Q^{-3}+8Q^{-5}\right)\alpha, \tag{5.31}$$

where we assume $\zeta = 0$ and $\nu = \alpha c^2/\Omega$ for simplicity. The self-gravity is effective for small m and small c. Even for the disks with a large viscosity as $\alpha = 1$, and a small sound speed as $r\Omega/c = 10^2$, if $Q > 6$, then the waves does not damp before returning to the LR.

For the protoplanetary disks with the minimum-mass adopted in this thesis, Q is as large as 20. Therefore the effect of the self-gravity can be neglected.

Chapter 6

Summary

The evolution of the protoplanetary disks due to the protoplanet's gravity is investigated. In particular the effect of the wave propagation is studied in detail.

The propagation and damping of the density waves excited at LRs are solved using WKB approximation. Our calculation shows that waves can propagate in disks with low viscosity. For $\alpha \lesssim 10^{-3}$, $m = 2$ waves, and for $\alpha \lesssim 10^{-4}$, $m \sim (r\Omega/c)_p \sim 20$ waves can propagate to the inner edge of the disk. The torque exerted through the damping of these waves is spread over the entire disk with such a low viscosity. Thus, for the disks with the low viscosity, whole the disk evolves by the protoplanet's gravity.

The gap sizes are calculated for the various value of the viscosity and the mass of the protoplanet. We found that the gap size is determined by two mechanisms. If the viscosity of the disk is enough large for waves to damp immediately, the gap size is determined by the balance between the protoplanet's torque and the viscous diffusion of the gas, as derived previously by Lin & Papaloizou(1986a). However, for the disk with a low viscosity, the gap size is determined by the propagation distance (damping length) of the waves. Because the damping length increases with decreasing viscosity, the gap size becomes wider for the disk with the lower viscosity. If the mass of the protoplanet is larger than Jupiter, even the lowest m waves can be effective to open a gap. These low m waves propagate large distance even

in the disk with a high viscosity($\alpha \sim 10^{-1}$), and the effect of the wave propagation cannot be neglected. The protoplanet with a Jupiter mass would induce the depletion of the inner disk onto the central star if $\alpha \lesssim 3 \times 10^{-4}$ and the $m = 2$ waves propagate to the inner edge of the disk. The time scale of the depletion of the inner disk is of order 10^5 years.

This removal of the inner disk causes the evolution of the spectral energy distribution of the pre-main-sequence star. Our calculation suggests that some T Tauri stars whose spectrum has a deficit in the near-infrared have unseen companions, i.e. protoplanets.

We derived the conditions for the gap formation. One is the condition for that the protoplanet opens up a gap before the diffusion of the gas closes it, as derived by Goldreich & Tremaine (1980) and Lin & Papaloizou (1979a). The other is for that the protoplanet does not escape from the gap, which is proposed by Hourigan & Ward (1984). We improved these conditions to include the effect of wave propagation.

Our results are applied to the gap sizes derived from the observations of the disks around pre-main-sequence binary stars, GW Ori and GG Tau. We infer that $\alpha \sim 10^{-2}$ in the disks around GW Ori and GG Tau.

Appendix

A. Transport of angular momentum

The disk is assumed to be infinitesimally thin and non-self-gravitating and has small shear viscosity ν, and bulk viscosity ζ. The viscosity may vary with the surface density and the temperature. The uncertainty in the viscous damping of waves arises from the unknown dependence of the viscosity on the surface density or the temperature. Some models of the viscosity promote wave growth rather than a decay of the wave (Kato 1978; Borderies, Goldreich & Tramaine 1985). In this thesis we assume that the variation of the viscosity due to the perturbation is negligible for simplicity.

The basic equations governing the disk are

$$\frac{\partial}{\partial t}\boldsymbol{v} + (\boldsymbol{v}\cdot\nabla)\boldsymbol{v} = -\nabla(\eta+\varphi_0+\varphi_1) + \nu\triangle\boldsymbol{v} + \left(\zeta+\frac{1}{3}\nu\right)\nabla(\nabla\cdot\boldsymbol{v}), \tag{A1}$$

$$\frac{\partial}{\partial t}\sigma + \nabla\cdot(\sigma\boldsymbol{v}) = 0, \tag{A2}$$

where $\boldsymbol{v}$ is the velocity, σ is the surface density, η is the enthalpy, φ_0 is the potential of the central star, and φ_1 is the potential of the protoplanet. In cylindrical coordinates (r,θ), the velocity is written as $\boldsymbol{v}=(u,v)$. The pressure, p, relates to the surface density through polytropic relation,

$$p = K\sigma^{\gamma}. \tag{A3}$$

The enthalpy and sound speed, c, satisfy

$$(\gamma-1)\eta = c^2 = \frac{dp}{d\sigma}. \tag{A4}$$

The viscosity is assumed to be small. Thus, the radial drift of the disk is neglected for the unperturbed state. The unperturbed disk rotates as, $\boldsymbol{v}_0 = (u_0, v_0) = (0, r\Omega(r))$. Considering small perturbation, the variables are

$$\begin{aligned} u(r) &= 0 + \sum_m \mathrm{Re}[u_1^{(m)}(r)\exp\{im(\theta - \Omega_p t\}], \\ v(r) &= r\Omega(r) + \sum_m \mathrm{Re}[v_1^{(m)}(r)\exp\{im(\theta - \Omega_p t\}], \\ \sigma(r) &= \sigma_0(r) + \sum_m \mathrm{Re}[\sigma_1^{(m)}(r)\exp\{im(\theta - \Omega_p t\}], \\ \eta(r) &= \eta_0(r) + \sum_m \mathrm{Re}[\eta_1^{(m)}(r)\exp\{im(\theta - \Omega_p t\}], \end{aligned} \tag{A5}$$

where Ω_p is the angular velocity of the protoplanet. These expressions are substituted into equations (A1) and (A2), and $\sigma_1^{(m)}$ is eliminated using equations (A3) and (A4). We then obtain the following perturbation equations for each Fourier components

$$\begin{aligned} im(\Omega - \Omega_p)u_1 - 2\Omega v_1 &= -\frac{\partial}{\partial r}(\eta_1 + \varphi_m) + \nu\left[\frac{1}{r}\frac{\partial}{\partial r}\left(r\frac{\partial u_1}{\partial r}\right) - \frac{m^2}{r^2}u_1 - \frac{2im}{r^2}v_1 - \frac{u_1}{r^2}\right] \\ &\quad + \left(\zeta + \frac{1}{3}\nu\right)\frac{\partial}{\partial r}\left[\frac{1}{r}\frac{\partial}{\partial r}(ru_1) + \frac{im}{r}v_1\right], \end{aligned} \tag{A6}$$

$$\begin{aligned} 2Bu_1 + im(\Omega - \Omega_p)v_1 &= -\frac{im}{r}(\eta_1 + \varphi_m) + \nu\left[\frac{1}{r}\frac{\partial}{\partial r}\left(r\frac{\partial v_1}{\partial r}\right) - \frac{m^2}{r^2}v_1 + \frac{2im}{r^2}u_1 - \frac{v_1}{r^2}\right] \\ &\quad + \left(\zeta + \frac{1}{3}\nu\right)\frac{im}{r}\left[\frac{1}{r}\frac{\partial}{\partial r}(ru_1) + \frac{im}{r}v_1\right], \end{aligned} \tag{A7}$$

$$\frac{1}{r}\frac{\partial}{\partial r}(r\sigma_0 u_1) + im\frac{\sigma_0 v_1}{r} + im(\Omega - \Omega_p)\frac{\sigma_0\eta_1}{c^2} = 0, \tag{A8}$$

where φ_m is the Fourier component of the protoplanet's potential and given by equation (2.6). We omit superscript "(m)" on perturbation variables. The Oort parameter B is defined by

$$B(r) = \frac{1}{2r}\frac{d}{dr}(r^2\Omega), \tag{A9}$$

and is related to the epicycle frequency $\kappa(r)$ by $\kappa^2 = 4B\Omega$.

The protoplanet's potential, φ_m, excites density waves at LRs (Goldreich & Tremaine 1979). These waves have angular momentum flux, F_{m0}, and propagate far away from the protoplanet. As the waves propagate, the wave length becomes shorter, and the waves tend

not to couple with the slowly varying potential, φ_m. Thus, once the waves are launched from the LR with angular momentum flux, F_{m0}, they propagate as free waves. We consider the homogeneous free wave solutions of equations (A6) - (A8). We look for solutions of the form

$$\begin{aligned} u_1(r) &= U(r)\exp[i\int^r k(r')dr'], \\ v_1(r) &= V(r)\exp[i\int^r k(r')dr'], \\ \eta_1(r) &= H(r)\exp[i\int^r k(r')dr'], \end{aligned} \tag{A10}$$

where the radial wave number, $k(r)$, is complex. Substituting equation (A10) into homogeneous form of equations (A6) - (A8), i.e., setting $\varphi_m = 0$, and assuming $|kr| \gg 1$, we obtain

$$im(\Omega - \Omega_p)U - 2\Omega V + ikH + \left(\zeta + \frac{4}{3}\nu\right)k^2 U = 0, \tag{A11}$$

$$2BU + im(\Omega - \Omega_p)V + \nu k^2 V = 0, \tag{A12}$$

$$ikU + im(\Omega - \Omega_p)\frac{H}{c^2} = 0. \tag{A13}$$

Neglecting quantities quadratic in ν and ζ, the dispersion relation is given by

$$\mathrm{Re}[k(r)]^2 = \frac{m^2(\Omega - \Omega_p)^2 - \kappa^2}{c^2}, \tag{A14}$$

and

$$\mathrm{Im}[k(r)] = -\left[\zeta + \left(\frac{4}{3} + \frac{\kappa^2}{m^2(\Omega - \Omega_p)^2}\right)\nu\right]\frac{m(\Omega - \Omega_p)}{2c^2}\mathrm{Re}[k]. \tag{A15}$$

Similar relation for the planetary rings is derived by Shu (1984). The group velocity of the waves is given by

$$c_g(r) = \frac{d}{d(\mathrm{Re}[k])}(m\Omega_p) = -\frac{\mathrm{Re}[k]c^2}{m(\Omega - \Omega_p)}. \tag{A16}$$

The waves excited at LRs and propagating away from the protoplanet have positive sign of $\mathrm{Re}[k]$.

The angular momentum flux carried by the waves is given by (Lynden-Bell & Kalnajs 1972; Lin et al. 1990a)

$$\begin{aligned} F_m(r) &= r^2\sigma_0\int_0^{2\pi}\mathrm{Re}[u_1\exp\{im(\theta - \Omega_p t\}]\mathrm{Re}[v_1\exp\{im(\theta - \Omega_p t\}]d\theta. \\ &= \pi r^2\sigma_0\mathrm{Re}[UV^*]\exp[-2\int^r \mathrm{Im}[k]dr']. \end{aligned} \tag{A17}$$

For an inviscid disk ($\mathrm{Im}[k] = 0$), the angular momentum flux should be constant with r (Goldreich & Tremaine 1979). Thus,

$$\pi r^2 \sigma_0 \mathrm{Re}[UV^*] = \text{constant}. \tag{A18}$$

Because at LR $F_m(r_L) = F_{m0}$, this constant is F_{m0}. Then, we obtain for $r > r_{OL}$ and $r < r_{IL}$

$$F_m(r) = F_{m0} \exp\left[-\int_{r_L}^{r} \left\{ \zeta + \left(\frac{4}{3} + \frac{\kappa^2}{m^2(\Omega - \Omega_p)^2} \right) \nu \right\} \frac{m(\Omega_p - \Omega)}{c^2} \mathrm{Re}[k] dr' \right]. \tag{A19}$$

For $r_{IL} < r < r_{OL}$, $m^2(\Omega - \Omega_p) - \kappa^2$ in equation (A14) becomes negative. Thus, waves cannot propagate into that region. Then, for $r_{IL} < r < r_{OL}$

$$F_m(r) = 0. \tag{A20}$$

Acknowledgments

The author is grateful to Prof. S. M. Miyama for his continuous encouragement and guidance during this work. He would like to thank Prof. D. N. C. Lin for valuable discussions and encouragement. He also acknowledges to Drs. T. Nakano, R. Ogasawara, T. Kajino, T. Nakamoto, S. Inutsuka, T. Tsuchiya and G. Laughlin and Mrs. K. Kobayashi, N. Kikuchi, T. Sano and Y. Yokono and Ms. Y. Aikawa for useful discussions and advice.

REFERENCES

Adams, F. C., & Shu, F.H. 1986, ApJ, 308, 836

Adams, F. C., Lada, C. J., & Shu, F.H. 1987, ApJ, 312, 788

Adams, F. C., Lada, C. J., & Shu, F.H. 1988, ApJ, 326, 865

Andersen, J., Lindgren, H., Hazen, M. L., & Mayor M. 1989, A&A, 219, 142

Artymowicz, P. 1993a, ApJ, 419, 155

Artymowicz, P. 1993b, ApJ, 419, 166

Artymowicz, P., & Lubow, S. H. 1994, ApJ, 421, 651

Balbus, S. A., & Hawley, J. F. 1991, ApJ, 376, 214

Basri, G., & Bertout, C. 1993, in Protostars and Planets III, ed. E. H. Levy & J. I. Lunine (Tucson:Univ. of Arizona Press), 543

Beckwith, S. V. W., Sargent, A. I., Chini, R. S., & Güsten, R. 1990, AJ, 99, 924

Beckwith, S. V. W., & Sargent, A. I. 1991, ApJ, 381, 250

Beckwith, S. V. W., & Sargent, A. I. 1993, in Protostars and Planets III, ed. E. H. Levy & J. I. Lunine (Tucson:Univ. of Arizona Press), 521

Binney, J., & Tremaine, S. 1987, Galactic Dynamics (Princeton:Princetion Univ. Press)

Bodenheimer, P., & Pollack, J. B. 1986, Icarus, 67, 391

Borderies, N., Goldreich, P., & Tremaine, S. 1985, Icarus, 63, 406

Boss, A. P., & Yorke, H. W. 1993, ApJ, 411, L99

Cameron, A. G. W. 1979, Moon and Planets, 21, 173

Chiueh, T., & Tseng, Y-H. 1994, ApJ, 435, 379

Dutrey, A., Guilloteau, S., & Simon, M. 1994, A&A, 286, 149

Ghez, A. M., Neugebauer, G., & Matthews, K. 1993, AJ, 106, 2005

Goldreich, P., & Lynden-Bell, D. 1965, MNRAS, 130, 125

Goldreich, P., & Tremaine, S. 1978, Icarus, 34, 240

Goldreich, P., & Tremaine, S. 1979, ApJ, 233, 857

Goldreich, P., & Tremaine, S. 1980, ApJ, 241, 425

Goodman, A. A., Benson, P. J., Fuller, G. A., & Myers, P. C. 1993, ApJ, 406, 528

Hayashi, C. 1981, Prog. Theor. Phys. Suppl., 70, 35

Hayashi, C., Nakazawa, K., & Nakagawa, Y. 1985, in Protostars and Planets II, ed. D. C. Black & M. S. Matthews (Tucson:Univ. of Arizona Press), 1100

Hayashi, M., Ohashi, N, & Miyama, S. M. 1993, ApJ, 418, L71

Hourigan, K., & Ward, W. R. 1984, Icarus, 60, 29

Ida, S. 1990, Icarus, 88, 129

Ida, S., & Makino, J. 1993, Icarus, 106, 210

Jensen, E. L. N., Mathieu, R. D., & Fuller, G. A. 1994, ApJ, 429, L29

Jensen, E. L. N., Mathieu, R. D., & Fuller, G. A. 1996, ApJ in press

Kato, S. 1978, MNRAS, 185, 629

Kawabe, R., Ishiguro, M., Omodaka, T., Kitamura, Y., & Miyama, S. M. 1993, ApJ, 404, L63

Kenyon, S. J., & Hartmann, L. 1987, ApJ, 323, 714

Kitamura, Y., Omodaka, T., Kawabe, R., Yamashita, T., & Handa, T. 1993, PASJ, 45, L27

Korycansky, D. G., & Pollack, J. B. 1993, Icarus, 102, 150

Larson, R. B. 1989, in The Formation and Evolution of Planetary Systems, ed. H. A. Weaver & L. Danly (Cambridge: Cambridge Univ. Press)

Larson, R. B. 1990, MNRAS, 243, 588

Leinert, Ch., Haas, M., Richichi, A., Zinnecker, H., & Mundt, R. 1991, A&A, 250, 407

Leinert, Ch., Zinnecker, H., Weitzel, N., Christou, J., Ridgway, S. T., Jameson, R., Haas, M., & Lenzen, R. 1993, A&A, 278, 129

Lin, C. C. 1955, The Theory of Hydrodynamic Stability (Cambridge: Cambridge Univ. Press)

Lin, D. N. C., & Papaloizou, J. C. B. 1979a, MNRAS, 186, 799

Lin, D. N. C., & Papaloizou, J. C. B. 1979b, MNRAS, 188, 191

Lin, D. N. C., & Papaloizou, J. C. B. 1980, MNRAS, 191, 37

Lin, D. N. C., & Papaloizou, J. C. B. 1985, in Protostars and Planets II, ed. D. C. Black & M. S. Matthews (Tucson:Univ. of Arizona Press), 981

Lin, D. N. C., & Papaloizou, J. C. B. 1986a, ApJ, 307, 395

Lin, D. N. C., & Papaloizou, J. C. B. 1986b, ApJ, 309, 846

Lin, D. N. C., & Papaloizou, J. C. B. 1993, in Protostars and Planets III, ed. E. H. Levy & J. I. Lunine (Tucson:Univ. of Arizona Press), 749

Lin, D. N. C., Papaloizou, J. C. B., & Kley W. 1993, ApJ, 416, 689

Lin, D. N. C., Papaloizou, J. C. B., & Savonije, G. J. 1990a, ApJ, 364, 326

Lin, D. N. C., Papaloizou, J. C. B., & Savonije, G. J. 1990b, ApJ, 365, 748

Lissauer, J. J. 1993, ARA&A, 31, 129

Lynden-Bell, D., & Kalnajs, A. J. 1972, MNRAS, 157, 1

Lynden-Bell, D., & Pringle, J. E. 1974, MNRAS, 168, 603

Marsh, K. A., & Mahoney, M. J. 1992, ApJ, 395, L115

Marsh, K. A., & Mahoney, M. J. 1993, ApJ, 405, L71

Mathieu, R. D. 1994, ARA&A, 32, 465

Mathieu, R. D., Adams, F. C., & Latham, D. W. 1991, AJ, 101, 2184

Mathieu, R. D., Adams, F. C., Fuller, G. A., Jensen, E. L. N., Koerner, D. W., & Sargent, A. I. 1995, AJ, 109, 2655

Miki, S. 1982, Prog. Theor. Phys., 67, 1053

Miyake, K., & Nakagawa, Y. 1993, Icarus, 106, 20

Miyake, K., & Nakagawa, Y. 1995, ApJ, 441, 361

Mizuno, H., Nakazawa, K., & Hayashi, C. 1978, Prog. Theor. Phys., 60, 699

Mizuno, H. 1980, Prog. Theor. Phys., 64, 544

Nakagawa, Y., Hayashi, C., & Nakazawa, K. 1983, Icarus, 54, 361

O'Dell, C. R., & Wen, Z. 1994, ApJ, 436, 194

Okazaki, A. T., Kato, S. 1985, PASJ, 37, 683

Osterloh, M., & Beckwith, S. V. W. 1995, ApJ, 439, 288

Ostriker, E. C., Shu, F. H., & Adams, F. C. 1992, ApJ, 399, 192

Paczyński, B. 1977, ApJ, 216, 822

Papaloizou, J. C. B., & Lin, D. N. C. 1984, ApJ, 285, 818

Papaloizou, J. C. B., & Pringle, J. E. 1984, MNRAS, 208, 721

Roddier, C., Roddier, F., Northcott, M. J., Graves, J. E., & Jim, K. 1996, ApJ, in press

Ruden, S. P., & Lin, D. N. C. 1986, ApJ, 308, 883

Ruden, S. P., & Pollack, J. B. 1991, ApJ, 375, 740

Saito, M., Kawabe, R., Ishiguro, M., Miyama, S. M., Hayashi, M., Handa, T., Kitamura, Y., & Omodaka, T. 1995, ApJ, 453, 384

Sargent, A. I. 1995, preprint

Savonije, G. J., Papaloizou, J. C. B.,& Lin, D. N. C. 1994, MNRAS, 268, 13.

Sawada, K., Matsuda, T., Inoue, M., & Hachisu, I. 1987, MNRAS, 224, 307

Sekiya, M., Miyama, S. M., & Hayashi, C. 1987, Earth, Moon, and Planets, 39, 1

Sekiya, M., Miyama, S. M., & Hayashi, C. 1988, Prog. Theor. Phys. Suppl., 96, 274

Shakura, N. I., & Sunyaev, R. A. 1973, A&A, 24,337

Shu, F. H. 1984, in Planetary Rings, ed. R. Greenberg & A. Brahic (Tucson:Univ. of Arizona Press), 513

Shu, F. H., Adams, F. C., & Lizano, S. 1987, ARA&A, 25, 23

Shu, F. H., Johnstone, D., & Hollenbach, D. 1993, Icarus, 106, 92

Simon, M., Chen, W. P., Howell R. R., Benson, J. A., & Slowik, D. 1992, ApJ, 384, 212

Simon, M., Ghez, A. M., Leinert, Ch., Cassar, L., Chen, W. P., Howell, R. R., Jameson, R. F., Matthews, K., Neugebauer, G., & Richichi, A. 1995, ApJ, 443, 625

Spruit, H. C., Matsuda, T. Inoue, M., Sawada, K. 1987, MNRAS, 229, 517

Spruit, H. C., 1989, in Theory of Accretion Disks, ed. F. Meyer, W. J. Duschl, J. Frank, & E. Meyer-Hofmeister (Dordrecht: Kluwer), 325

Strom, S. E., Edwards, S., & Skrutskie, M. F. 1993, in Protostars and Planets III, ed. E. H. Levy & J. I. Lunine (Tucson:Univ. of Arizona Press), 837

Takeuchi, T., Miyama, S. M., & Lin, D. N. C. 1995, ApJ in press

Ward, W. R. 1986, Icarus, 67, 164

Ward, W. R. 1989, ApJ, 336, 526

Ward, W. R., & Hourigan, K. 1989, ApJ, 347, 490

Watanabe, S., Nakagawa, Y., & Nakazawa, K. 1990, ApJ, 358, 282

This preprint was prepared with the AAS LaTeX macros v4.0.